

REFERENCES

- Antonio Castro Neto, F.G. and Nuno Miguel Peres (2006) Drawing conclusions from graphene. Physics World, 19(11):33–7.
- Atieh, M.A., Nazir, N., Yusof, F., Fettouhi, M., Ratnam, C.T., Alharthi, M., Abu-Ilaiwi, F.A., Mohammed, K., and Al-Amer, A. (2010) Radiation vulcanization of natural rubber latex loaded with carbon nanotubes. Fullerenes, Nanotubes and Carbon Nanostructures, 18(1), 56-71.
- Banerjee, P. and Mandal, B.M. (1995) Conducting polyaniline nanoparticle blends with extremely low percolation thresholds. Macromolecules, 28(11), 3940-3943.
- Becerril, H.A., Mao, J., Liu, Z., Stoltenberg, R.M., Bao, Z., and Chen, Y. (2008) Evaluation of solution-processed reduced graphene oxide films as transparent conductors. ACS Nano, 2(3), 463-470.
- Berger, C., Song, Z., Li, T., Li, X., Ogbazghi, A.Y., Feng, R., Dai, Z., Marchenkov, A.N., Conrad, E.H., First, P.N., and de Heer, W.A. (2004) Ultrathin epitaxial graphite: 2D electron gas properties and a route toward graphene-based nanoelectronics. Journal of Physical Chemistry B, 108(52), 19912-19916.
- Chodak, I. and Krupa, I. (1999) “Percolation effect” and mechanical behavior of carbon black filled polyethylene. Journal of Materials Science Letters, 18(18), 1457-1459.
- Ciofani, G., Raffa, V., Pensabene, V., Menciassi, A., and Dario, P. (2008) Dispersion of multi-walled carbon nanotubes in aqueous pluronic F127 solutions for biological applications. Fullerenes, Nanotubes and Carbon Nanostructures, 17(1), 11-25.
- Deiters, J., Böhnstedt, W., Boesler, J., and Ihmels, K. (2006) A new polyethylene separator for heavy-duty traction batteries. Journal of Power Sources, 158(2), 1069-1072.
- Delille, R., Urdaneta, M., Hsieh, K., and Smela, E. (2006) Novel compliant electrodes based on platinum salt reduction. Smart Structures and Materials

- 2006: Electroactive Polymer Actuators and Devices (EAPAD), San Diego, CA, Volume 6168, 61681Q-61681Q.
- Fernández-Merino, M.J., Guardia, L., Paredes, J.I., Villar-Rodil, S., Solís-Fernández, P., Martínez-Alonso, A., and Tascón, J.M.D. (2010) Vitamin C is an ideal substitute for hydrazine in the reduction of graphene oxide suspensions. The Journal of Physical Chemistry C, 114(14), 6426-6432.
- Fiske, T.J., Gokturk, H.S., and Kalyon, D.M. (1997) Percolation in magnetic composites. Journal of Materials Science, 32(20), 5551-5560.
- Göktürk, H.S., Fiske, T.J., and Kalyon, D.M. (1993) Effects of particle shape and size distributions on the electrical and magnetic properties of nickel/polyethylene composites. Journal of Applied Polymer Science, 50(11), 1891-1901.
- Grossiord, N., Loos, J., Regev, O., and Koning, C.E. (2006) Toolbox for dispersing carbon nanotubes into polymers to get conductive nanocomposites. Chemistry of Materials, 18(5), 1089-1099.
- Haque, M.E., Dafader, N.C., Akhtar, F., and Ahmad, M.U. (1996) Radiation dose required for the vulcanization of natural rubber latex. Radiation Physics and Chemistry, 48(4), 505-510.
- Hernández, M., Bernal, M.d.M., Verdejo, R., Ezquerro, T.A., and López-Manchado, M.A. (2012) Overall performance of natural rubber/graphene nanocomposites. Composites Science and Technology, 73(0), 40-46.
- Hummers, W.S., and Offeman, R.E. (1958) Preparation of graphitic oxide. Journal of the American Chemical Society, 80(6), 1339-1339.
- Iijima, S. (1991). Helical microtubules of graphitic carbon. Nature, 354(6348), 56-58.
- Jing, X., Zhao, W., and Lan, L. (2000) The effect of particle size on electric conducting percolation threshold in polymer/conducting particle composites. Journal of Materials Science Letters, 19(5), 377-379.
- Kalaitzidou, K., Fukushima, H., and Drzal, L.T. (2007) A new compounding method for exfoliated graphite–polypropylene nanocomposites with enhanced flexural properties and lower percolation threshold. Composites Science and Technology, 67(10), 2045-2051.

- Keller, L., Decker, C., Zahouily, K., Benfarhi, S., Le Meins, J.M., and Miehe-Brendle, J. (2004) Synthesis of polymer nanocomposites by UV-curing of organoclay–acrylic resins. Polymer, 45(22), 7437-7447.
- Khamput, P., and Suweero, K. (2011) Properties of mortar mixing with medium ammonia concentrated latex. Energy Procedia, 9(0), 559-567.
- Kim, T.A., Kim, H.S., Lee, S.S., and Park, M. (2012) Single-walled carbon nanotube/silicone rubber composites for compliant electrodes. Carbon, 50(2), 444-449.
- Kosynkin, D.V.H., Amanda L. Sinitskii, Alexander, Lomeda, Jay R., and Dimiev, Ayrat (2009) Longitudinal unzipping of carbon nanotubes to form graphene nanoribbons. Nature, 458(7240), 872 - 876.
- Krishnamoorthy, K., Kim, G.-S., and Kim, S.J. (2013) Graphene nanosheets: Ultrasound assisted synthesis and characterization. Ultrasonics Sonochemistry, 20(2), 644-649.
- Kueseng, P., Sae-oui, P., and Rattanasom, N. (2013) Mechanical and electrical properties of natural rubber and nitrile rubber blends filled with multi-wall carbon nanotube: Effect of preparation methods. Polymer Testing, 32(4), 731-738.
- Kujawski, M., Pearse, J.D., and Smela, E. (2010) Elastomers filled with exfoliated graphite as compliant electrodes. Carbon, 48(9), 2409-2417.
- Lee, S., Lee, K., and Zhong, Z. (2010) Wafer scale homogeneous bilayer graphene films by chemical vapor deposition. Nano Letters, 10(11), 4702-4707.
- Ma, P.-C., Siddiqui, N.A., Marom, G., and Kim, J.-K. (2010) Dispersion and functionalization of carbon nanotubes for polymer-based nanocomposites: A review. Composites Part A: Applied Science and Manufacturing, 41(10), 1345-1367.
- Manmoun, S. (2013) Para rubber with Asean Economics Community Para Rubber (Rubber Research Institute of Thailand), 34(1), 1-33.
- Martin-Gallego, M., Bernal, M.M., Hernandez, M., Verdejo, R., and Lopez-Manchado, M.A. (2013) Comparison of filler percolation and mechanical properties in graphene and carbon nanotubes filled epoxy nanocomposites. European Polymer Journal, 49(6), 1347-1353.

- Matos, C.F., Galembeck, F., and Zarbin, A.J.G. (2012) Multifunctional materials based on iron/iron oxide-filled carbon nanotubes/natural rubber composites. Carbon, 50(12), 4685-4695.
- McAllister, M.J., Li, J.-L., Adamson, D.H., Schniepp, H.C., Abdala, A.A., Liu, J., Herrera-Alonso, M., Milius, D.L., Car, R., Prud'homme, R.K., and Aksay, I.A. (2007) Single sheet functionalized graphene by oxidation and thermal expansion of graphite. Chemistry of Materials, 19(18), 4396-4404.
- Moisala, A., Li, Q., Kinloch, I.A., and Windle, A.H. (2006) Thermal and electrical conductivity of single- and multi-walled carbon nanotube-epoxy composites. Composites Science and Technology, 66(10), 1285-1288.
- Moniruzzaman, M., and Winey, K.I. (2006) Polymer nanocomposites containing carbon nanotubes. Macromolecules, 39(16), 5194-5205.
- Mustafa, L., Yenny, H., J, K.P., J, S.R., Valeria, N., S, K.L., M, B.F., Sukanta, D.E., Zhiming, W., McGovern I, T., S, D.G., and N, C.J. (2009) Liquid phase production of graphene by exfoliation of graphite in surfactant/water solutions. Journal of the American Chemical Society, 131(10), 3611-3620.
- Nethravathi, C., Rajamathi, J.T., Ravishankar, N., Shivakumara, C., and Rajamathi, M. (2008) Graphite oxide-intercalated anionic clay and its decomposition to graphene–inorganic material nanocomposites. Langmuir, 24(15), 8240-8244.
- Novoselov, K.S., Geim, A.K., Morozov, S.V., Jiang, D., Zhang, Y., Dubonos, S.V., Grigorieva, I.V., and Firsov, A.A. (2004) Electric field effect in atomically thin carbon films. Science, 306(5696), 666-669.
- Pang, H., Chen, T., Zhang, G., Zeng, B., and Li, Z.-M. (2010) An electrically conducting polymer/graphene composite with a very low percolation threshold. Materials Letters, 64(20), 2226-2229.
- Paradise, M. and Goswami, T. (2007) Carbon nanotubes – Production and industrial applications. Materials & Design, 28(5), 1477-1489.
- Pelrine, R., Kornbluh, R., Pei, Q., and Joseph, J. (2000) High-Speed electrically actuated elastomers with strain greater than 100%. Science, 287(5454), 836-839.

- Piya-areetham, P., Prasassarakich, P., and Rempel, G.L. (2013) Organic solvent-free hydrogenation of natural rubber latex and synthetic polyisoprene emulsion catalyzed by water-soluble rhodium complexes. Journal of Molecular Catalysis A: Chemical, 372(0), 151-159.
- Preetha Nair, K., Thomas, P., and Joseph, R. (2012) Latex stage blending of multiwalled carbon nanotube in carboxylated acrylonitrile butadiene rubber: Mechanical and electrical properties. Materials & Design, 41(0), 23-30.
- Rastogi, R., Kaushal, R., Tripathi, S.K., Sharma, A.L., Kaur, I., and Bharadwaj, L.M. (2008) Comparative study of carbon nanotube dispersion using surfactants. Journal of Colloid and Interface Science, 328(2), 421-428.
- Rosset, S. and Shea, H. (2013) Flexible and stretchable electrodes for dielectric elastomer actuators. Applied Physics A, 110(2), 281-307.
- Schlaak, H.F., Jungmann, M., Matysek, M., and Lotz, P. (2005, March) Novel multilayer electrostatic solid state actuators with elastic dielectric (Invited Paper). Progres present at Smart Structures and Materials 2006: Electroactive Polymer Actuators and Devices (EAPAD), San Diego, CA.
- Sekitani, T., Noguchi, Y., Hata, K., Fukushima, T., Aida, T., and Someya, T. (2008) A rubberlike stretchable active matrix using elastic conductors. Science, 321(5895), 1468-1472.
- Sengupta, R., Bhattacharya, M., Bandyopadhyay, S., and Bhowmick, A.K. (2011) A review on the mechanical and electrical properties of graphite and modified graphite reinforced polymer composites. Progress in Polymer Science, 36(5), 638-670.
- Simien, D., Fagan, J.A., Luo, W., Douglas, J.F., Migler, K., and Obrzut, J. (2008) Influence of nanotube length on the optical and conductivity properties of thin single-wall carbon nanotube networks. ACS Nano, 2(9), 1879-1884.
- Sincharoenkul, C.R.A.O.T. (2012) "Para rubber situation in 2013." Retrieved december,2012.
- Someya, T. and Sekitani, T. (2009) Printed skin-like large-area flexible sensors and actuators. Procedia Chemistry, 1(1), 9-12.
- Sohil, A., Tushar, G., and John, M. (2007) Dielectric elastomer based prototype fiber actuators. Sensors and Actuators A: Physical, 136(1), 321-328.

- Spitalsky, Z., Tasis, D., Papagelis, K., and Galiotis, C. (2010) Carbon nanotube–polymer composites: Chemistry, processing, mechanical and electrical properties. Progress in Polymer Science, 35(3), 357-401.
- Stankovich, S., Dikin, Dmitriy A., Dommett, Geoffrey H. B., Kohlhaas, Kevin M., Zimney, Eric J., and Stach, Eric A. (2006) Graphene-based composite materials. Nature, 442(7100), 282 - 286.
- Su, X., Wang, G., Li, W., Bai, J., and Wang, H. (2013) A simple method for preparing graphene nano-sheets at low temperature. Advanced Powder Technology, 24(1), 317-323.
- Szabó, T., Szeri, A., and Dékány, I. (2005) Composite graphitic nanolayers prepared by self-assembly between finely dispersed graphite oxide and a cationic polymer. Carbon, 43(1), 87-94.
- Tkalya, E.E., Ghislandi, M., de With, G., and Koning, C.E. (2012) The use of surfactants for dispersing carbon nanotubes and graphene to make conductive nanocomposites. Current Opinion in Colloid & Interface Science, 17(4), 225-232.
- Tsuchiya, K., Sakai, A., Nagaoka, T., Uchida, K., Furukawa, T., and Yajima, H. (2011) High electrical performance of carbon nanotubes/rubber composites with low percolation threshold prepared with a rotation–revolution mixing technique. Composites Science and Technology, 71(8), 1098-1104.
- Wang, J.Z.Y. and Bogner, R.H. (1995) Techniques to monitor the UV curing of potential solvent-free film-coating polymers. International Journal of Pharmaceutics, 113(1), 113-122.
- Wang, X., Zhi, L., and Mullen, K. (2007) transparent, conductive graphene electrodes for dye-sensitized solar cells. Nano Letters, 8(1), 323-327.
- Yigit, S., Hacaloglu, J., Akbulut, U., and Toppare, L. (1996) Conducting polymer composites of polythiophene with natural and synthetic rubbers. Synthetic Metals, 79(1), 11-16.
- Yuan, Y. and Shi, W. (2012) A novel LDH nanofiller intercalated by silsesquioxane for preparing organic/inorganic hybrid composites. Applied Clay Science, 67–68(0), 83-90.

- Zhang, Q.-H. and Chen, D.-J. (2004) Percolation threshold and morphology of composites of conducting carbon black/polypropylene/EVA. Journal of Materials Science, 39(5), 1751-1757.
- Zhou, T., Chen, F., Tang, C., Bai, H., Zhang, Q., Deng, H., and Fu, Q. (2011) The preparation of high performance and conductive poly (vinyl alcohol)/graphene nanocomposite via reducing graphite oxide with sodium hydrosulfite. Composites Science and Technology, 71(9), 1266-1270.

APPENDICES

Appendix A Raman Spectra of The Synthesized Graphene

Raman spectroscopy was used to verify graphite and graphene due to the ability to identify and characterize all the members of the carbon family. The characterizations were nondestructive, fast, with high resolution and give the maximum structural and electronic information. The indications of graphite raw material and synthesized graphene were measured by the Raman spectroscopy (NT-MDT, NTEGRA Spectra) with 632.8 nm excitation laser, objective lens 100x and accumulate time 60s from National Nanotechnology Center.

The main features in the Raman spectra of carbons are called G and D peaks, which lie at around 1560 and 1360 cm^{-1} , respectively, for visible excitation. The G peak represents the bond stretching of all pairs of sp^2 atoms in both rings and chains. The D peak refers to the breathing modes of sp^2 atoms in the rings. Another peak is 2D, at 2700 cm^{-1} , which is the second order of D peak. A significant change in the shape and intensity of the 2D peak of graphene compared to bulk graphite is that the 2D peak in bulk graphite consists of two components (2D_1 and 2D_2), while graphene has only one peak (2D). Moreover, graphene has a single, sharp 2D peak, roughly four times more intense than the G peak (Ferrari, 2007).

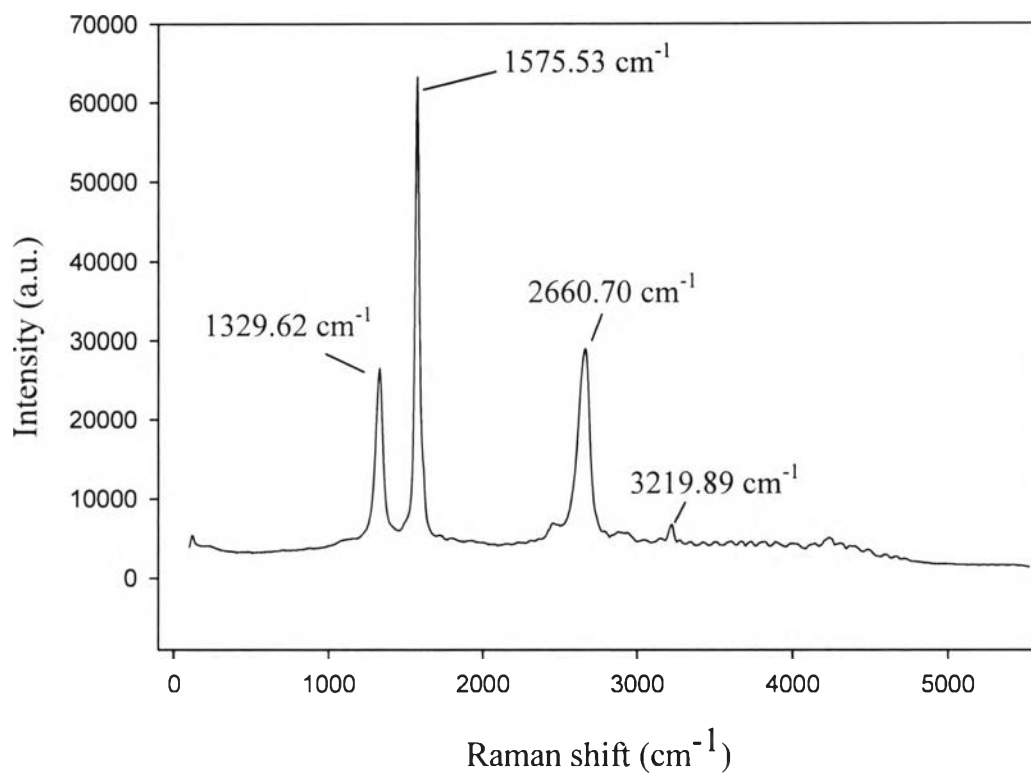


Figure A1 Raman spectrum of the raw graphite.

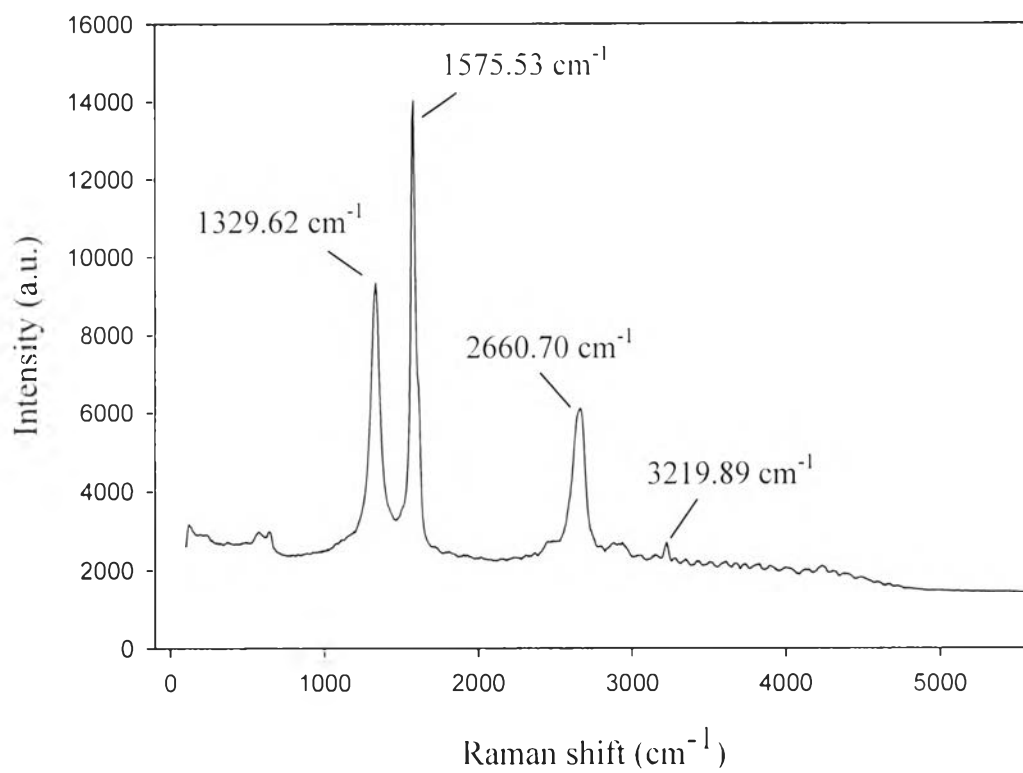


Figure A2 Raman spectrum of the graphene multilayers.

Appendix B XRD Pattern of The Synthesized Graphene

The wide angle X-ray diffraction microscope (XRD) was used to study the crystal structure below the nanometer scale. The CuK-alpha radiation source was operated at 40 kV/30 mA. K-beta filter was used to eliminate interference peak. Divergence slit and scattering slit 0.5 deg together with 0.3 mm of receiving slit were set on the instrument. The graphene powder was placed into a sample holder and the measurement was continuously run. The experiments were recorded by monitoring the diffraction appearing in the diffraction angle (2θ) range from 10 to 80 with a scan speed 5 deg/min and a scan step 0.02 deg.

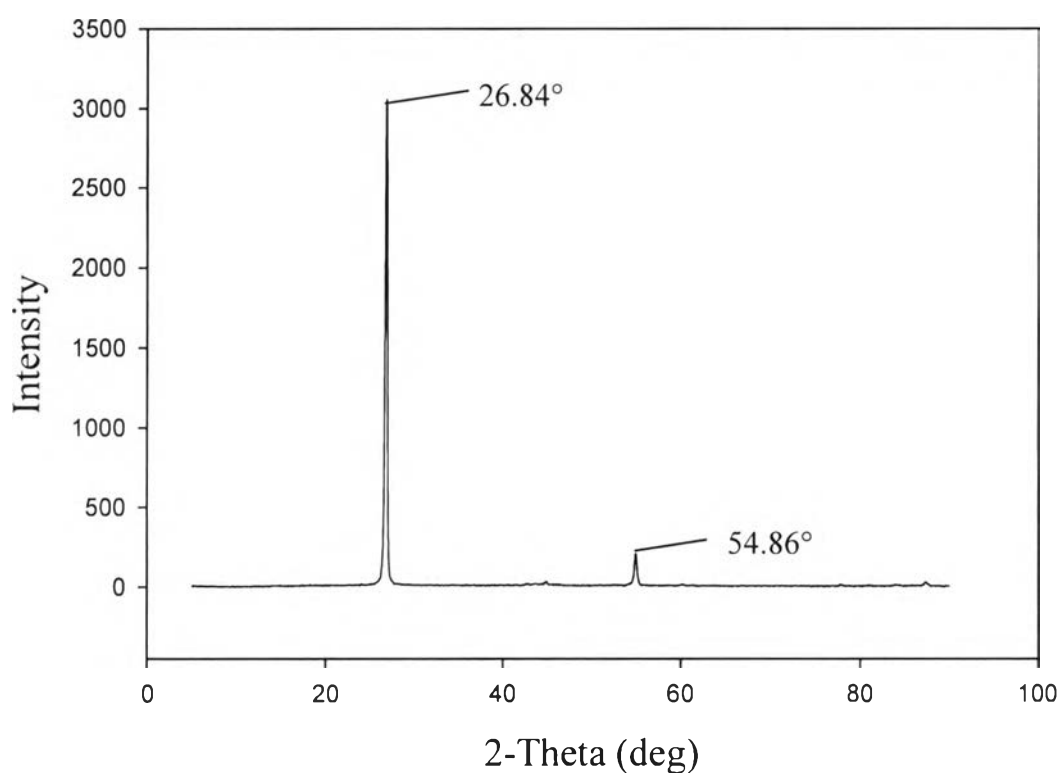


Figure B1 XRD pattern of the raw graphite.

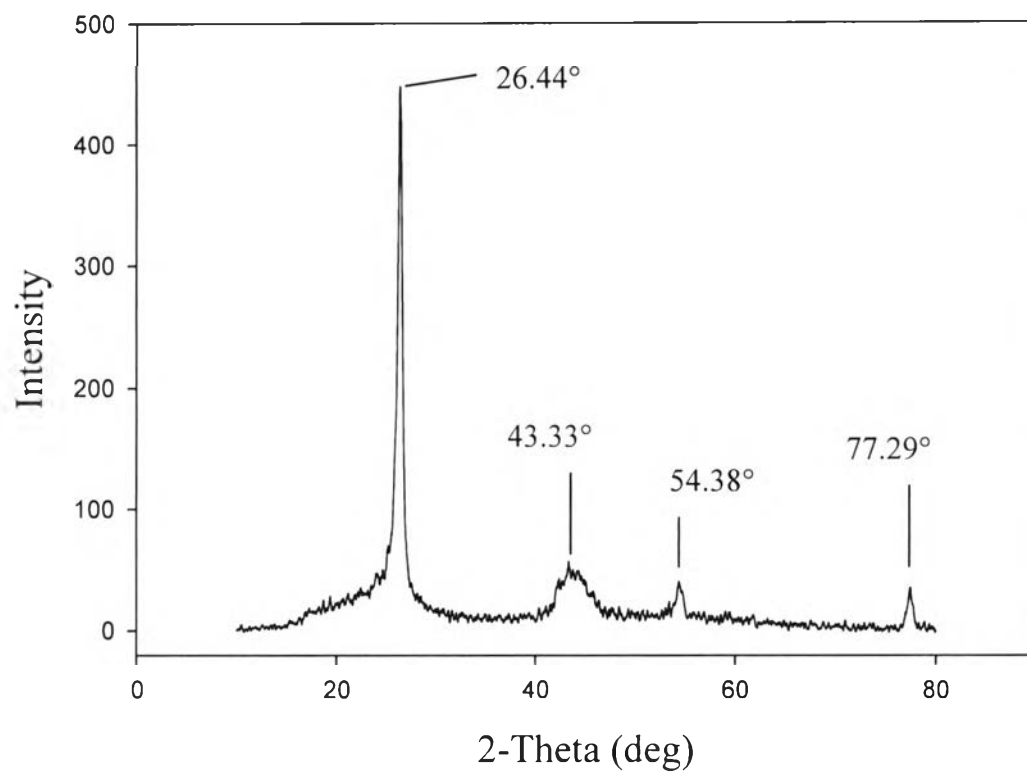


Figure B2 XRD pattern of the graphene multilayers.

Appendix C FT-IR Spectra of The Synthesized Graphene and Natural Rubber (NR)

Fourier Transform Infrared Spectroscopy (FT-IR) was used to investigate the characteristic vibration frequencies of the molecules in order to determine the molecular structure of the samples. This technique employed the absorption mode with 32 scans a resolution of $\pm 4 \text{ cm}^{-1}$, covering a wavelength range of $400\text{-}4000 \text{ cm}^{-1}$, using deuterated triglycine sulfate as a detector. Optical grade KBr powder was used as a background material to characterize the synthesized graphene and the graphite raw material. The sample powder was ground with KBr and pressed to form pallets before testing. In addition, NR films were characterized for the functional groups by using the Attenuated total reflectance (ATR) mode.

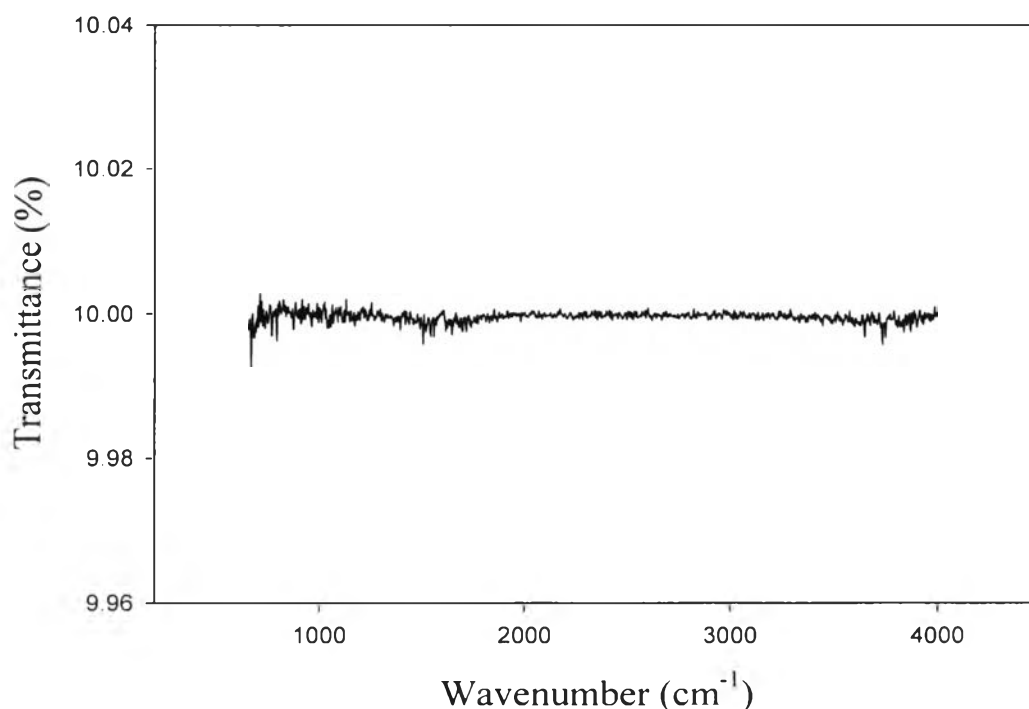


Figure C1 FT-IR spectrum of the raw graphite.

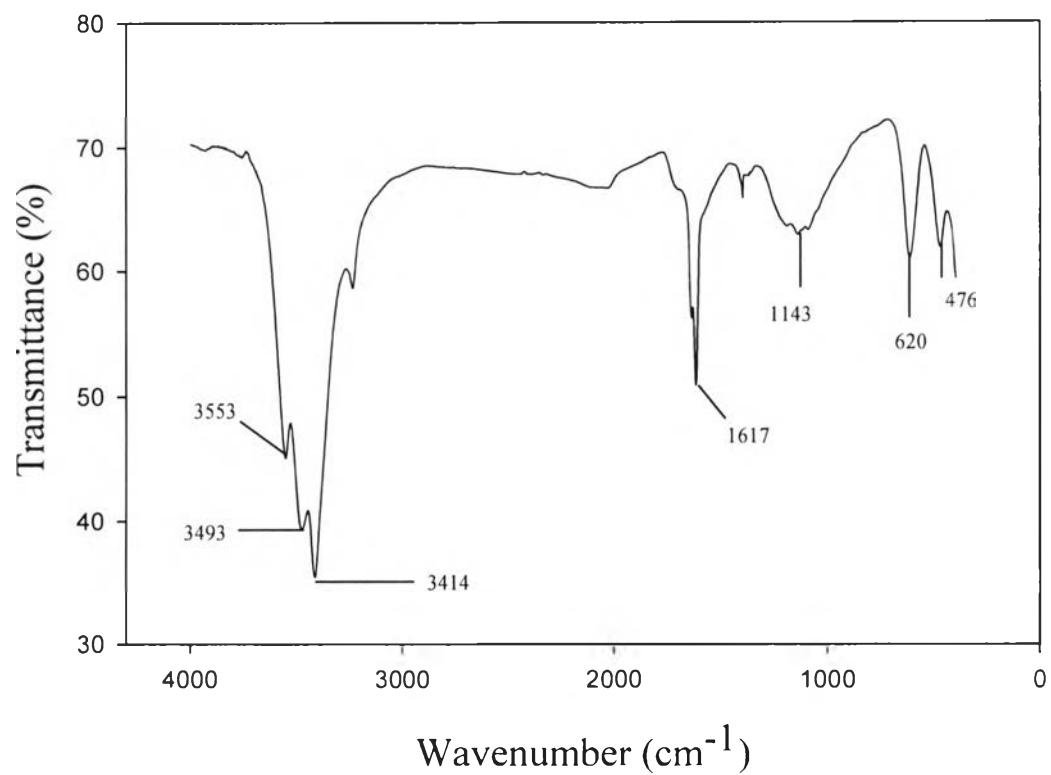


Figure C2 FT-IR spectrum of the synthesized graphite oxide.

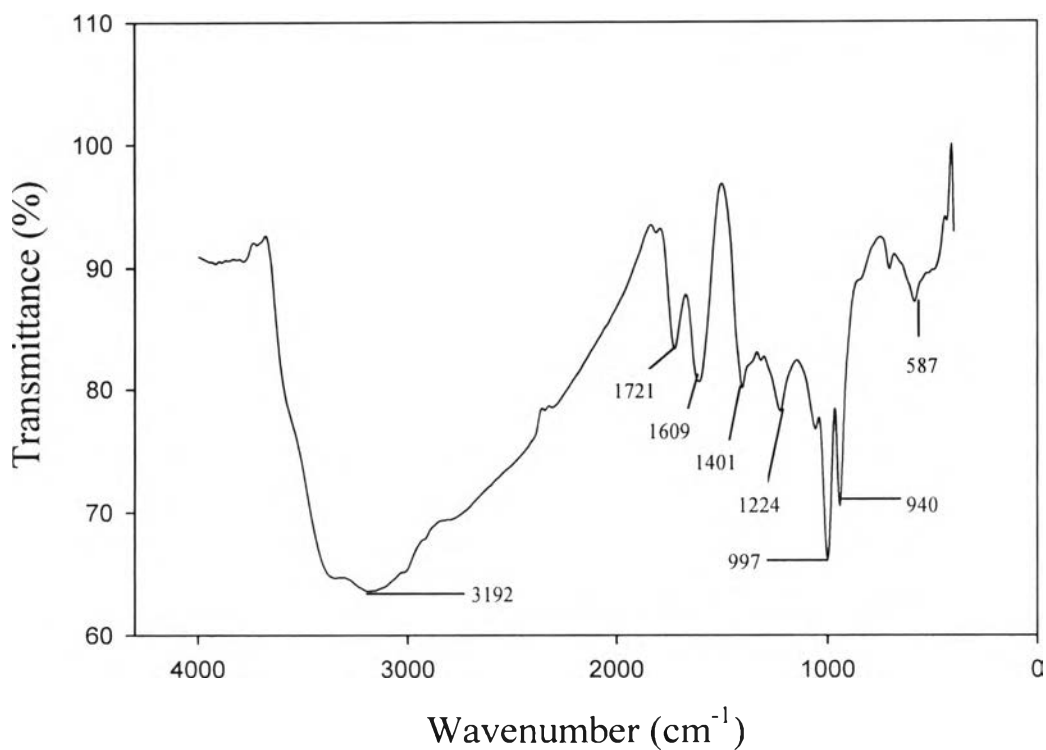


Figure C3 FT-IR spectrum of the synthesized graphene oxide.

Table C1 Assignments of the fundamental vibration modes for graphene oxide (Krishnamoorthy, 2013)

| Assignment | Wavenumber (cm ⁻¹) |
|----------------|--------------------------------|
| OH stretching | 3260 |
| C=O stretching | 1728 |
| C-C vibration | 1600 |
| C-OH bending | 1413 |
| C-O stretching | 1250 |
| C-O stretching | 1050 |

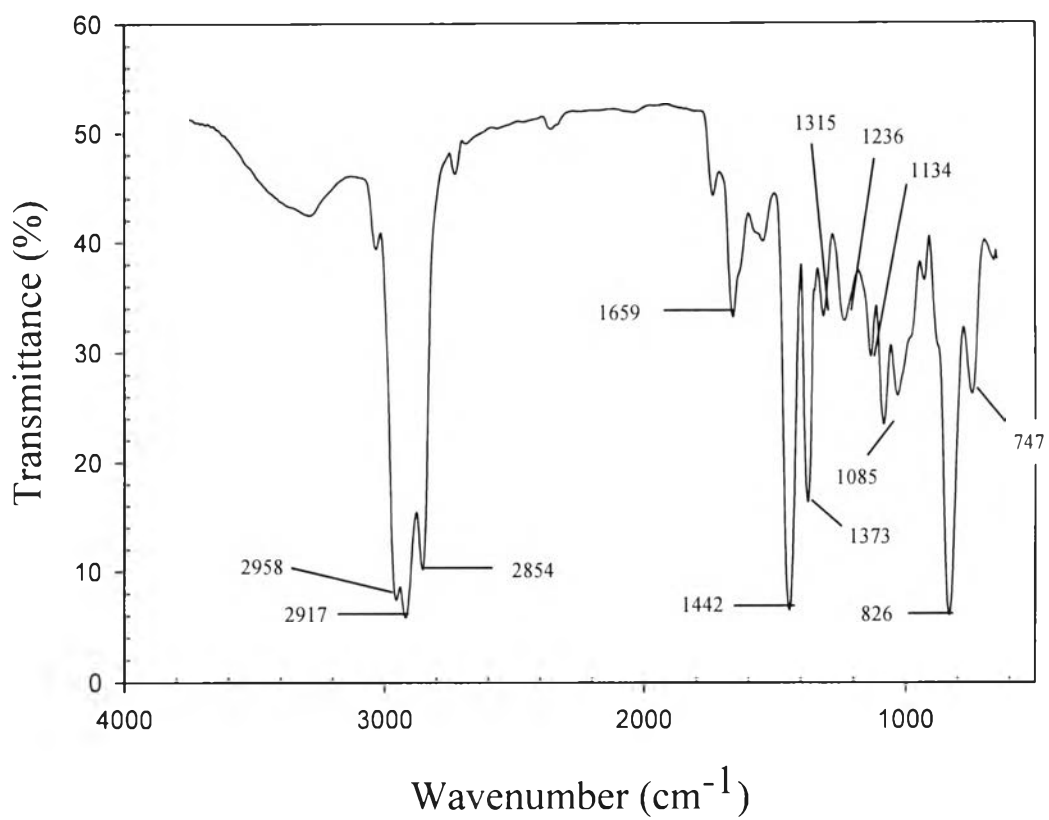


Figure C4 FT-IR spectrum of pure natural rubber.

Table C2 Assignments of the fundamental vibration modes for pure NR (Guidelli, 2011)

| Assignment | Wavenumber (cm ⁻¹) |
|--------------------------------------|--------------------------------|
| CH ₃ stretching | 2960 |
| CH ₂ asymmetry stretching | 2920 |
| CH ₂ symmetry stretching | 2855 |
| C=O symmetric stretching | 1667 |
| CH ₂ bending | 1447 |
| C-H asymmetric bending | 1376 |
| CH ₂ wagging | 1126 |
| C-CH ₂ stretching | 1086 |
| C=C-H bending | 838 |

Appendix D TGA Themogram of The Natural Rubber Film and Its Composites

A thermogravimetric analyzer (Thermo, TGA Q 50) was used to determine the thermal behavior of the NR film. The thermal behavior was examined by weighting sample of 4-5 mg and loaded into a platinum pan. The mass change under the temperature scan from 30 to 550 °C at a heating rate of 10 °C/min and under the nitrogen flow was monitored and recorded.

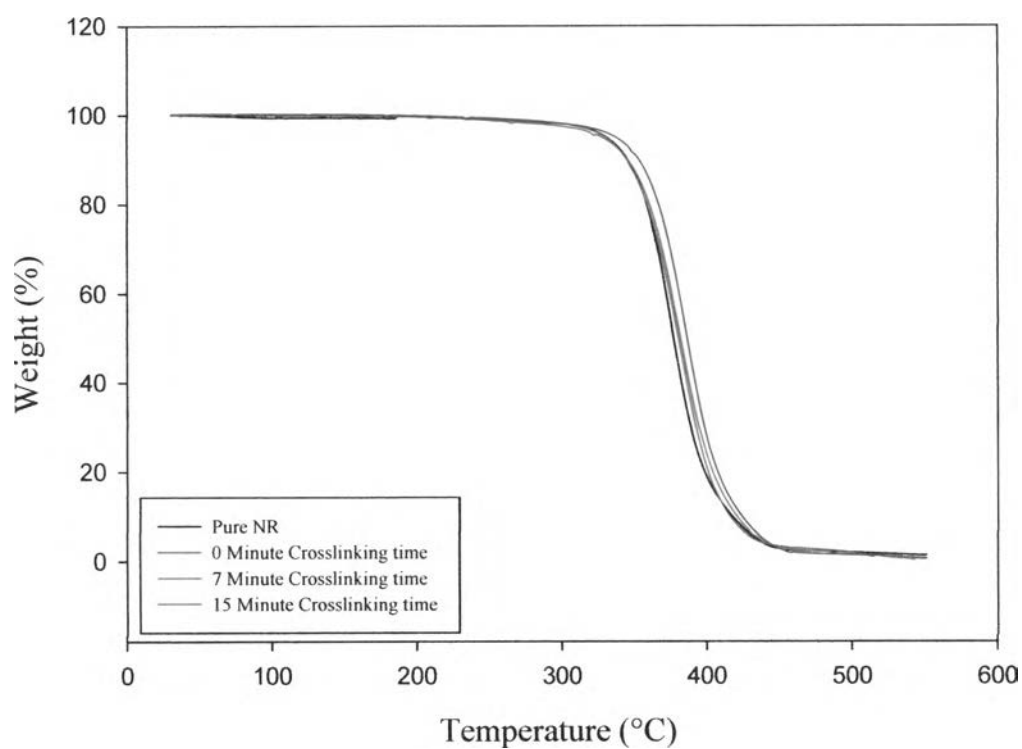


Figure D1 TGA themogram of the crosslinked NR with various crosslink times and a fixed crosslinking ratio of 2.0 %v/v.

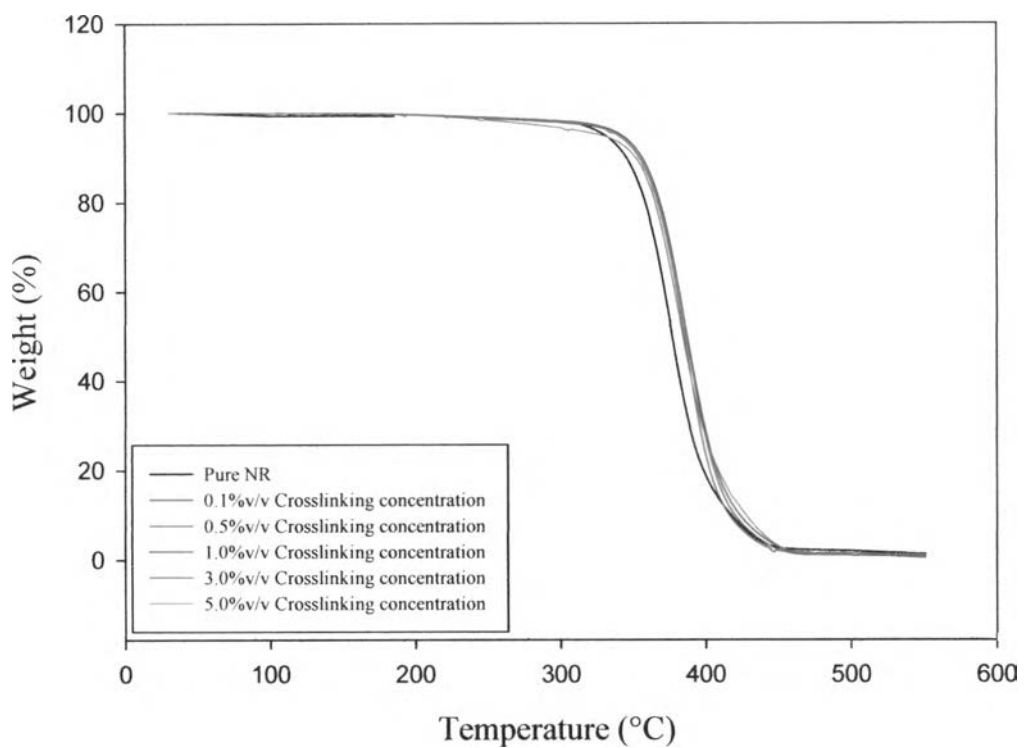


Figure D2 TGA themogram of the crosslinked NR with various crosslinking concentrations and a fixed crosslinking time of 7 minute.

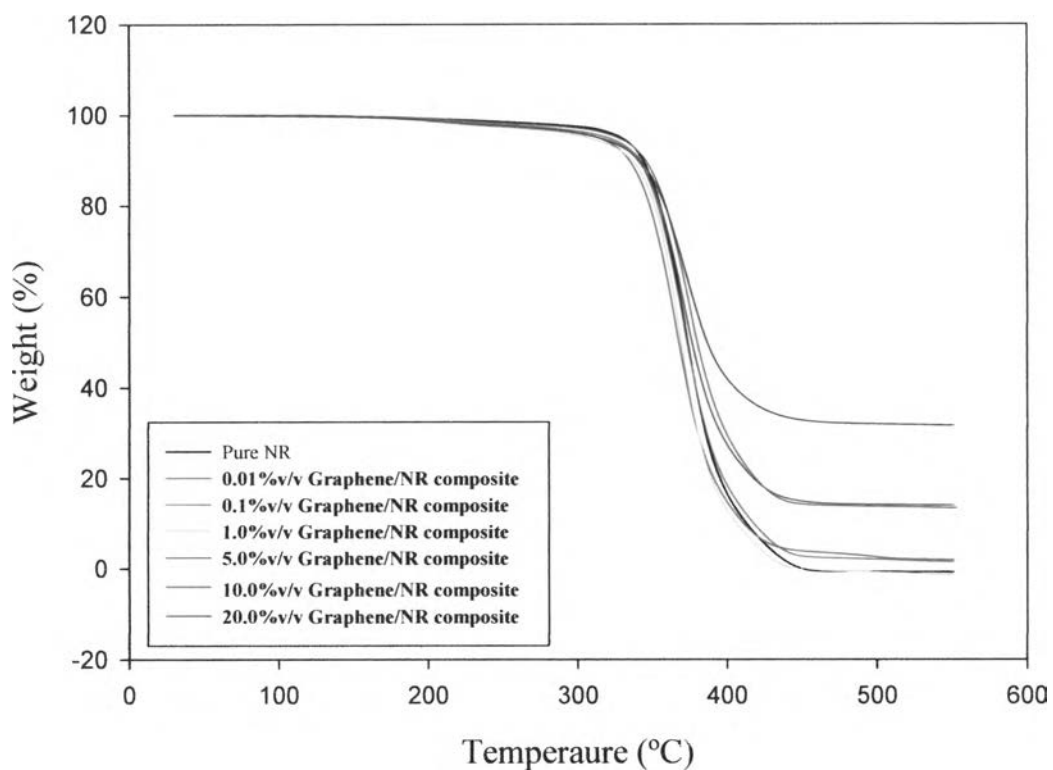


Figure D3 TGA themogram of the crosslinked NR with various concentrations of commercial graphene, a fixed crosslinking time of 7 minute and crosslinking concentration of 5.0 % v/v.

Table D1 Summary of the thermal behavior of NR film

| Sample | | Onset Temperature, T_o , (°C) | Derivative Peak Temperature, T_p , (°C) |
|--|------|------------------------------------|---|
| Pure NR | | 223.77 | 352.29 |
| Crosslinking times (min) | 0 | 229.16 | 353.24 |
| | 7 | 208.90 | 355.66 |
| | 15 | 210.42 | 360.68 |
| Crosslinking concentrations (%v/v) | 0.1 | 231.95 | 363.22 |
| | 0.5 | 231.95 | 363.45 |
| | 1.0 | 240.51 | 361.99 |
| | 3.0 | 243.40 | 362.52 |
| | 5.0 | 249.61 | 359.91 |
| Graphene concentrations (%v/v) | 0 | 273.55 | 372.33 |
| | 0.01 | 265.01 | 366.32 |
| | 0.1 | 260.11 | 371.26 |
| | 1.0 | 251.17 | 368.05 |
| | 5.0 | 245.07 | 370.68 |
| | 10.0 | 255.13 | 374.43 |
| | 20.0 | 258.04 | 372.73 |

Table D2 Thermal behavior assignments for TGA behavior of NR film

| Behavior | Temperature (°C) | References |
|--|------------------|-----------------------------|
| Removal of adsorbed water on the surface | below 200 | Lu <i>et al.</i> , 2006 |
| Decomposition of C-C linkages | 200 - 270 | Yahya <i>et al.</i> , 2011 |
| Degradation of carbon backbone | Above 350 | Sharif <i>et al.</i> , 2005 |

Appendix E Mole Percent Uptake of Solvent, Weight Loss, and Crosslink Density Determined by Swelling Method

Dried rubber sheets were prepared by casting the latex on glass plates and cured under UV radiation with various UV irradiation times and concentration of crosslinker. The thin films were cut into small pieces (1 cm²) and then immersed in toluene (150 mL) until the swelling reaches the equilibrium (3 days). The mole percent uptake of solvent, weight loss, and crosslinking density of crosslinked NR were calculated from the following equations;

$$\text{Mole percent uptake of solvent} = \frac{\frac{W_t - W_0}{W_0}}{M_w} \times 100 \quad (\text{E1})$$

where W_0 and W_t are the weights of dried and swollen samples, respectively. M_w is the molar mass of toluene (92.14 g mol⁻¹).

$$\% \text{ Weight loss} = \frac{M_i - M_d}{M_i} \times 100 \quad (\text{E2})$$

where M_i and M_d are the weight of dried rubber before and after soaking in toluene.

$$v_e = \frac{-[\ln(1 - V_r) + V_r + \chi_1 V_r^2]}{[V_1(V_r^{\frac{1}{3}} - V_r)/2]} \quad (\text{E3})$$

where v_e is effective number of chains in a real network per unit volume, V_r is volume fraction of polymer in a swollen network in equilibrium with pure solvent and is calculated as:

$$V_r = \frac{\text{Weight of dry rubber/density of dry rubber}}{\frac{\text{Weight of dry rubber}}{\text{Density of dry rubber}} + \frac{\text{Weight of solvent absorbed by sample}}{\text{Density of solvent}}} \quad (\text{E4})$$

χ_1 is polymer-solvent interaction parameter (0.391) and V_1 is molecular volume of solvent.

Table E1 Swelling results of crosslinked NR films at various UV irradiation times, fixed crosslinking ratio 2.0 %v/v

| UV irradiation times (min) | No. | Weight before swelling (g) | Weight after swelling (g) | Dried weight (g) | Mole % uptake of toluene | Weight loss (%) | Crosslink density (mole/cm ³) |
|----------------------------|-----|----------------------------|---------------------------|------------------|--------------------------|-----------------|---|
| 0 | 1 | 0.0396 | - | - | - | 100.00 | - |
| | 2 | 0.0508 | - | - | - | 100.00 | - |
| | 3 | 0.0494 | - | - | - | 100.00 | - |
| 3 | 1 | 0.0599 | 1.2140 | 0.0329 | 1.0318 | 45.08 | 4.38E-08 |
| | 2 | 0.0514 | 1.0042 | 0.0263 | 1.0298 | 48.83 | 1.62E-07 |
| | 3 | 0.0481 | 0.7913 | 0.0226 | 1.0193 | 53.01 | 9.14E-07 |
| 5 | 1 | 0.0405 | 0.6020 | 0.0313 | 1.0123 | 22.72 | 3.15E-07 |
| | 2 | 0.0355 | 0.4509 | 0.0167 | 0.9999 | 52.96 | 1.62E-06 |
| | 3 | 0.0442 | 0.6746 | 0.0254 | 1.0142 | 42.54 | 3.58E-07 |
| 7 | 1 | 0.0298 | 0.2775 | 0.0278 | 0.9688 | 6.71 | 1.10E-06 |
| | 2 | 0.0383 | 0.3489 | 0.0345 | 0.9662 | 9.92 | 1.52E-06 |
| | 3 | 0.0393 | 0.3802 | 0.0346 | 0.9731 | 11.96 | 4.22E-07 |
| 10 | 1 | 0.0401 | 0.2790 | 0.0371 | 0.9293 | 7.48 | 2.70E-06 |
| | 2 | 0.0360 | 0.2607 | 0.0334 | 0.9354 | 7.22 | 3.17E-06 |
| | 3 | 0.0357 | 0.2610 | 0.0325 | 0.9369 | 8.96 | 2.39E-06 |
| 12 | 1 | 0.0276 | 0.1685 | 0.0257 | 0.9075 | 6.88 | 8.74E-06 |
| | 2 | 0.0287 | 0.1883 | 0.0277 | 0.9199 | 3.48 | 2.91E-05 |
| | 3 | 0.0267 | 0.1702 | 0.0257 | 0.9150 | 3.74 | 2.17E-06 |

Table E1 Swelling results of crosslinked NR films at various UV irradiation times, fixed concentration of crosslinker 2.0 %v/v (continue 1)

| UV irradiation times (min) | No. | Weight before swelling (g) | Weight after swelling (g) | Dried weight (g) | Mole % uptake of toluene | Weight loss (%) | Crosslink density (mole/cm ³) |
|----------------------------|-----|----------------------------|---------------------------|------------------|--------------------------|-----------------|---|
| 15 | 1 | 0.0402 | 0.6858 | 0.0246 | 1.0217 | 38.81 | 6.69E-06 |
| | 2 | 0.0388 | 0.6236 | 0.0227 | 1.0178 | 41.50 | 2.37E-07 |
| | 3 | 0.0331 | 0.5281 | 0.0207 | 1.0173 | 37.46 | 1.57E-06 |

Table E2 Swelling results of crosslinked NR films at various concentrations of crosslinker, fixed UV irradiation time 7 min

| Concentration of crosslinker (%v/v) | No. | Weight before swelling (g) | Weight after swelling (g) | Dried weight (g) | Mole uptake of toluene (%) | Weight loss (%) | Crosslink density (mole/cm ³) |
|-------------------------------------|-----|----------------------------|---------------------------|------------------|----------------------------|-----------------|---|
| 0 | 1 | 0.0396 | - | - | - | 100.00 | - |
| | 2 | 0.0508 | - | - | - | 100.00 | - |
| | 3 | 0.0494 | - | - | - | 100.00 | - |
| 0.1 | 1 | 0.0393 | - | - | - | 100.00 | - |
| | 2 | 0.0322 | - | - | - | 100.00 | - |
| | 3 | 0.0289 | - | - | - | 100.00 | - |
| 0.5 | 1 | 0.0442 | 1.1931 | 0.0195 | 1.0451 | 55.88 | 3.00E-04 |
| | 2 | 0.0326 | 0.8192 | 0.0183 | 1.0421 | 43.86 | 2.82E-05 |
| | 3 | 0.0386 | 0.9982 | 0.0171 | 1.0433 | 55.70 | 3.90E-05 |

Table E2 Swelling results of crosslinked NR films at various concentrations of crosslinker, fixed UV irradiation time 7 min (continue 1)

| Concentration of crosslinker (%v/v) | NO. | Weight before swelling (g) | Weight after swelling (g) | Dried weight (g) | Mole uptake of toluene (%) | Weight loss (%) | Crosslink density (mole/cm ³) |
|-------------------------------------|-----|----------------------------|---------------------------|------------------|----------------------------|-----------------|---|
| 1.0 | 1 | 0.0269 | 0.6444 | 0.0145 | 2.4910 | 46.09 | 0.29E-05 |
| | 2 | 0.0280 | 0.6448 | 0.0159 | 2.3900 | 43.21 | 0.31E-05 |
| | 3 | 0.0254 | 0.3167 | 0.0080 | 1.2440 | 68.50 | 0.89E-05 |
| 2.0 | 1 | 0.0283 | 0.3424 | 0.0241 | 1.2040 | 14.84 | 0.94E-05 |
| | 2 | 0.0311 | 0.3518 | 0.0265 | 1.1190 | 14.79 | 1.05E-05 |
| | 3 | 0.0284 | 0.3063 | 0.0248 | 1.0610 | 12.67 | 1.14E-05 |
| 3.0 | 1 | 0.0255 | 0.2044 | 0.0242 | 0.9499 | 5.09 | 1.99E-05 |
| | 2 | 0.0259 | 0.2006 | 0.0240 | 0.9451 | 7.33 | 1.94E-05 |
| | 3 | 0.0292 | 0.2247 | 0.0266 | 0.9443 | 8.90 | 1.00E-04 |
| 5.0 | 1 | 0.0468 | 0.2470 | 0.0445 | 0.8797 | 4.91 | 2.00 E-04 |
| | 2 | 0.0322 | 0.1577 | 0.0313 | 0.8637 | 2.79 | 9.11E-06 |
| | 3 | 0.0419 | 0.2184 | 0.0410 | 0.8771 | 2.14 | 2.18E-05 |
| 7.0 | 1 | 0.0273 | 0.1453 | 0.0253 | 0.8814 | 7.32 | 7.50E-05 |
| | 2 | 0.0231 | 0.1135 | 0.0225 | 0.8644 | 2.59 | 1.00E-04 |
| | 3 | 0.0383 | 0.2614 | 0.0346 | 0.9263 | 9.66 | 3.37E-05 |
| 10.0 | 1 | 0.0239 | 0.1092 | 0.0211 | 0.8478 | 11.71 | 7.53E-06 |
| | 2 | 0.0343 | 0.1816 | 0.0313 | 0.8803 | 8.74 | 2.85E-05 |
| | 3 | 0.0409 | 0.2263 | 0.0381 | 0.8891 | 6.84 | 2.74E-05 |

Table E2 Swelling results of crosslinked NR films at various concentrations of crosslinker, fixed UV irradiation time 7 min (continue 2)

| concentration of crosslinker (%v/v) | NO. | Weight before swelling (g) | Weight after swelling (g) | Dried weight (g) | Mole uptake of toluene (%) | Weight loss (%) | Crosslink density (mole/cm ³) |
|-------------------------------------|-----|----------------------------|---------------------------|------------------|----------------------------|-----------------|---|
| 15.0 | 1 | 0.0233 | 0.1085 | 0.0200 | 0.8522 | 14.16 | 1.00E-04 |
| | 2 | 0.0268 | 0.0972 | 0.0237 | 0.7861 | 11.57 | 6.58E-05 |
| | 3 | 0.0379 | 0.1838 | 0.0306 | 0.8615 | 19.26 | 1.00E-04 |
| 20.0 | 1 | 0.0208 | 0.0850 | 0.0175 | 0.8197 | 15.87 | 2.00E-04 |
| | 2 | 0.0583 | 0.3730 | 0.0457 | 0.9157 | 21.61 | 1.32E-05 |
| | 3 | 0.0331 | 0.1505 | 0.0265 | 0.8466 | 19.94 | 6.06E-05 |

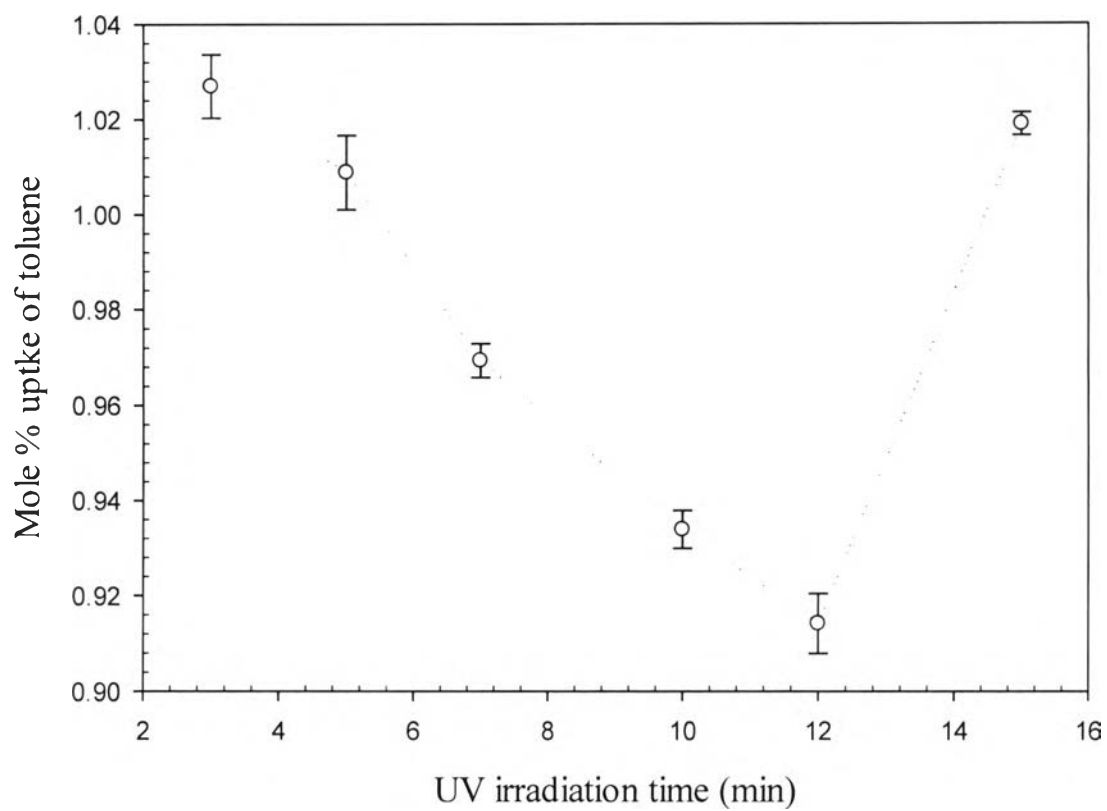


Figure E1 Mole uptake of toluene of crosslinked NR films at various UV irradiation times, a fixed concentration of crosslinker of 2.0 %v/v.

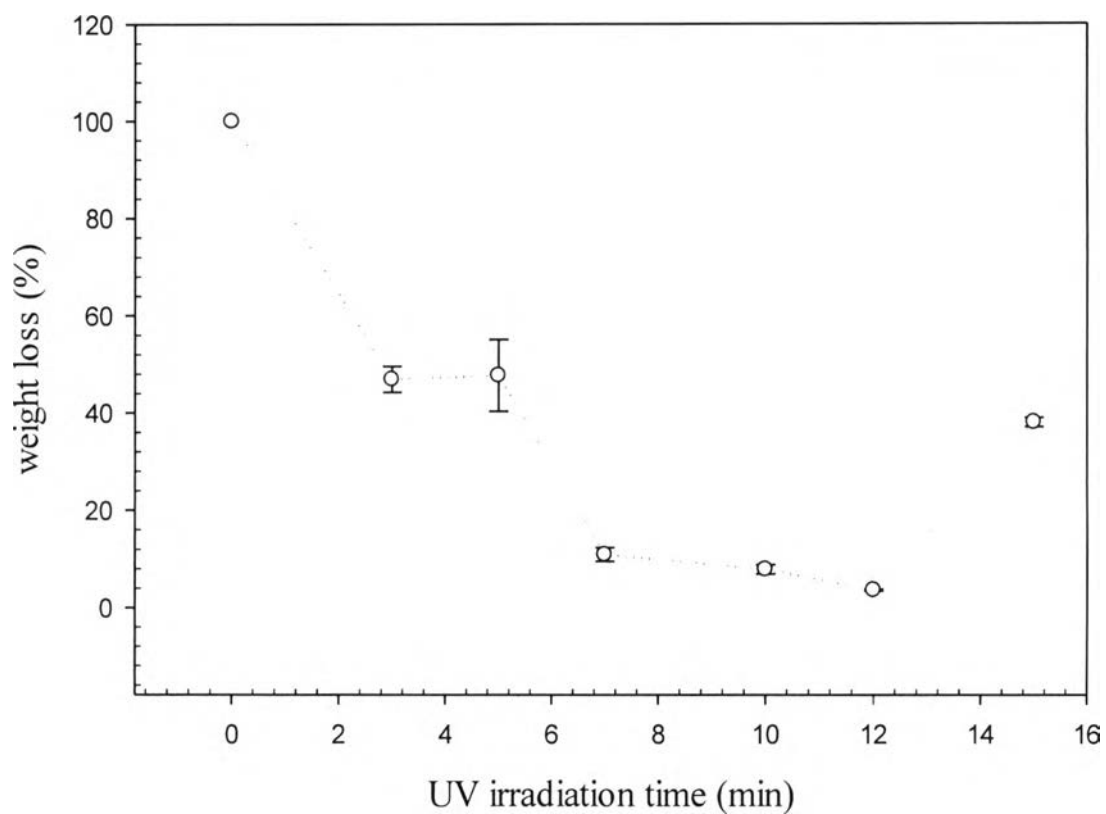


Figure E2 Weight loss of crosslinked NR films at various UV irradiation times, a fixed concentration of crosslinker of 2.0 %v/v.

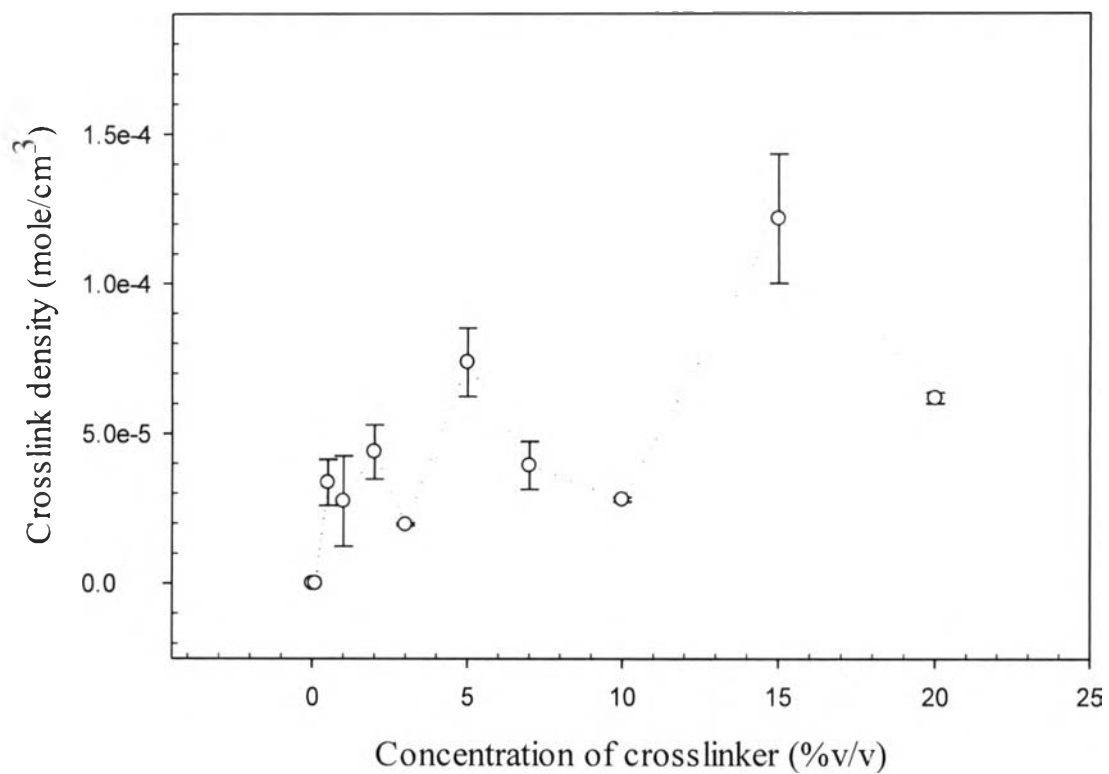


Figure E3 Crosslinking density of crosslinked NR films at various UV irradiation times, a fixed concentration of crosslinker of 2.0 %v/v.

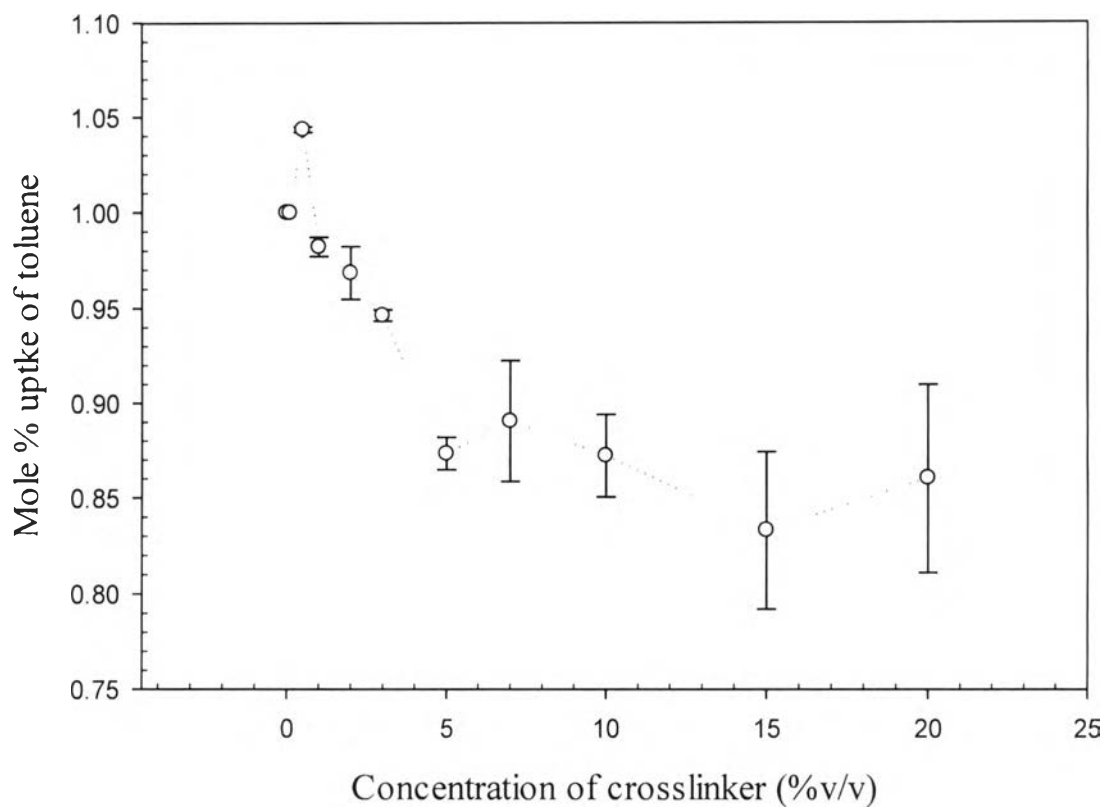


Figure E4 Mole uptake of toluene of crosslinked NR films at various concentrations of crosslinker, a fixed crosslinking time of 7 min.

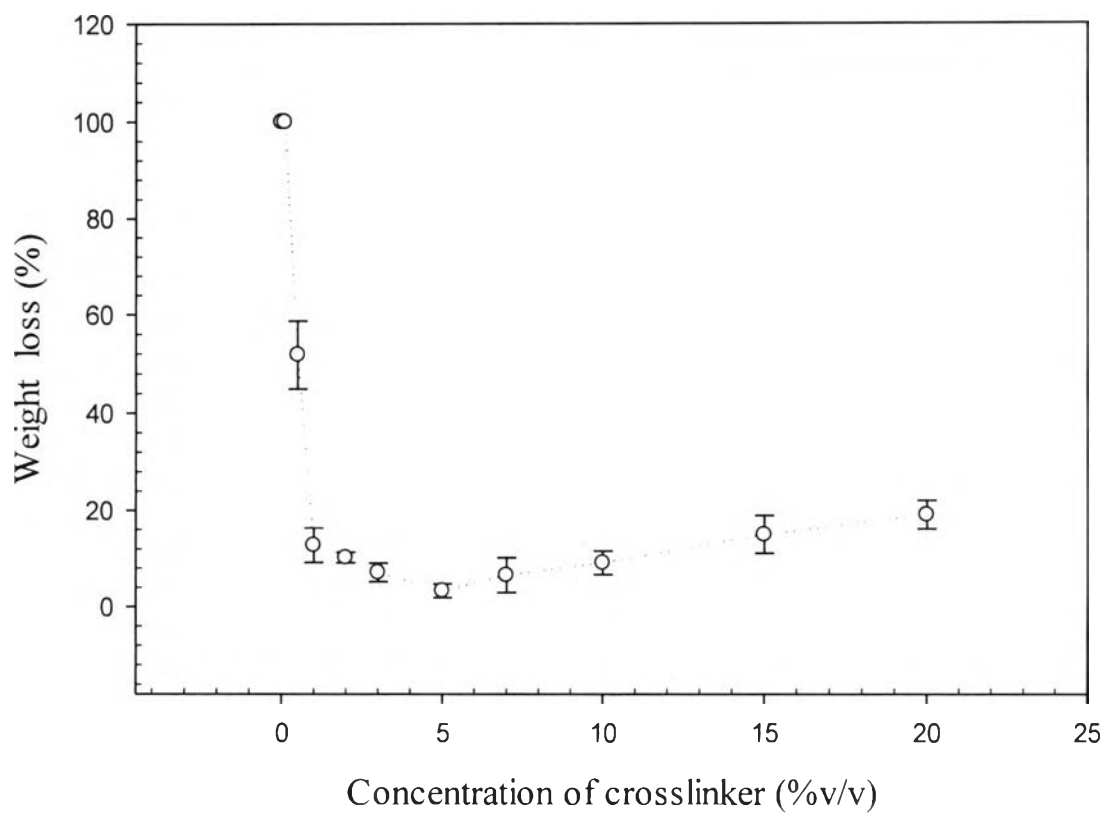


Figure E5 Weight loss of crosslinked NR films at various concentrations of crosslinker, a fixed UV irradiation time of 7 min.

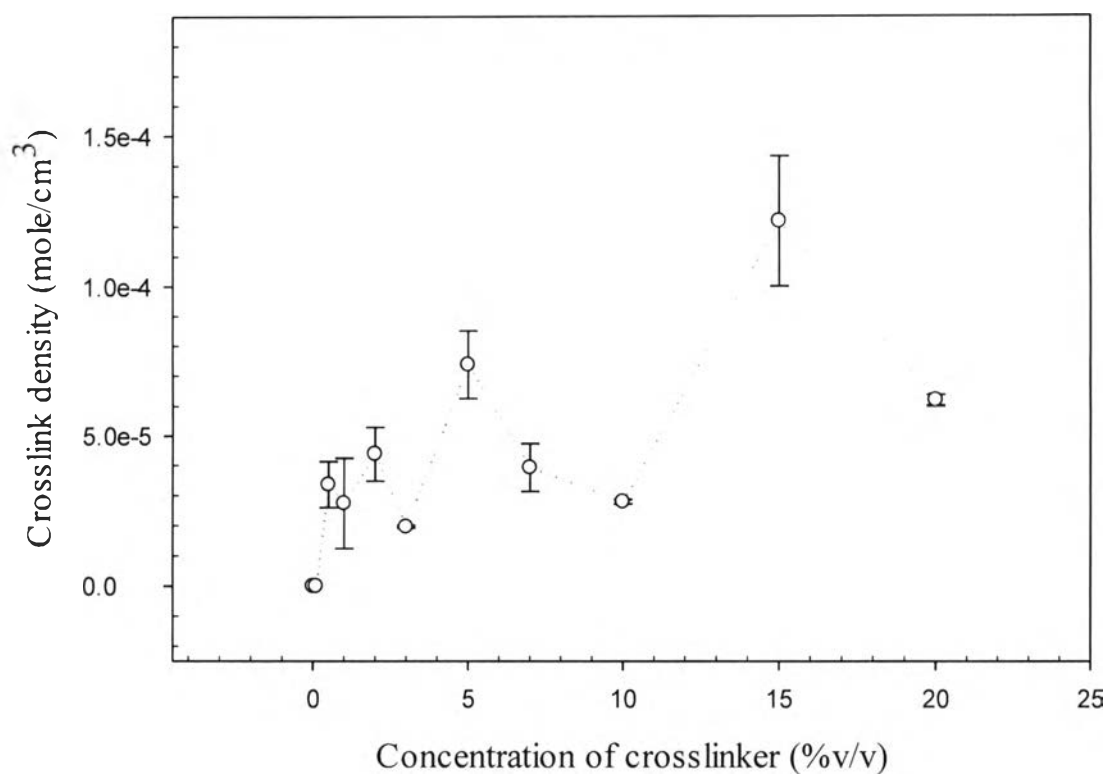


Figure E6 Crosslinking density of crosslinked NR films at various concentrations of crosslinker, a fixed UV irradiation time of 7 min.

Appendix F Mechanical Properties of Natural Rubber Film

The mechanical properties of NR film were measured by the melt rheometer (Rheometric scientific, Ares) with the extensional fixture at room temperature. In this experiment, the transient mode was applied and the stress was monitored during stretching, as a function of strain, at strain rate 0.01s^{-1} . From the results, stress vs. strain was obtained. An evaluation of the mechanical properties of the film was focus on the modulus, the yield point, and the yield strain. The mechanical properties of NR were studied in terms of UV-irradiation time and concentration of crosslinker.

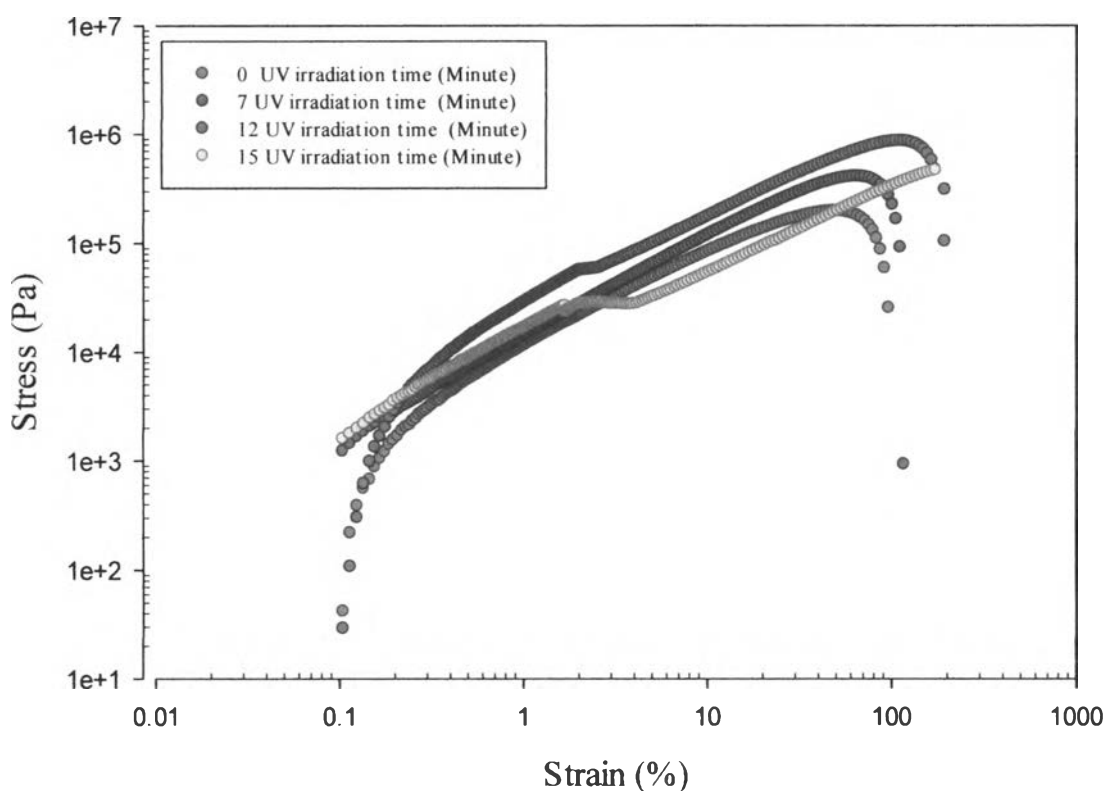


Figure F1 Stress-strain curve of NR films at various UV irradiation times, a fixed concentration of crosslinker of 2.0 %v/v, by using the melt rheometer in the tension mode with a strain rate 0.01 s^{-1} and temperature of 300 K.

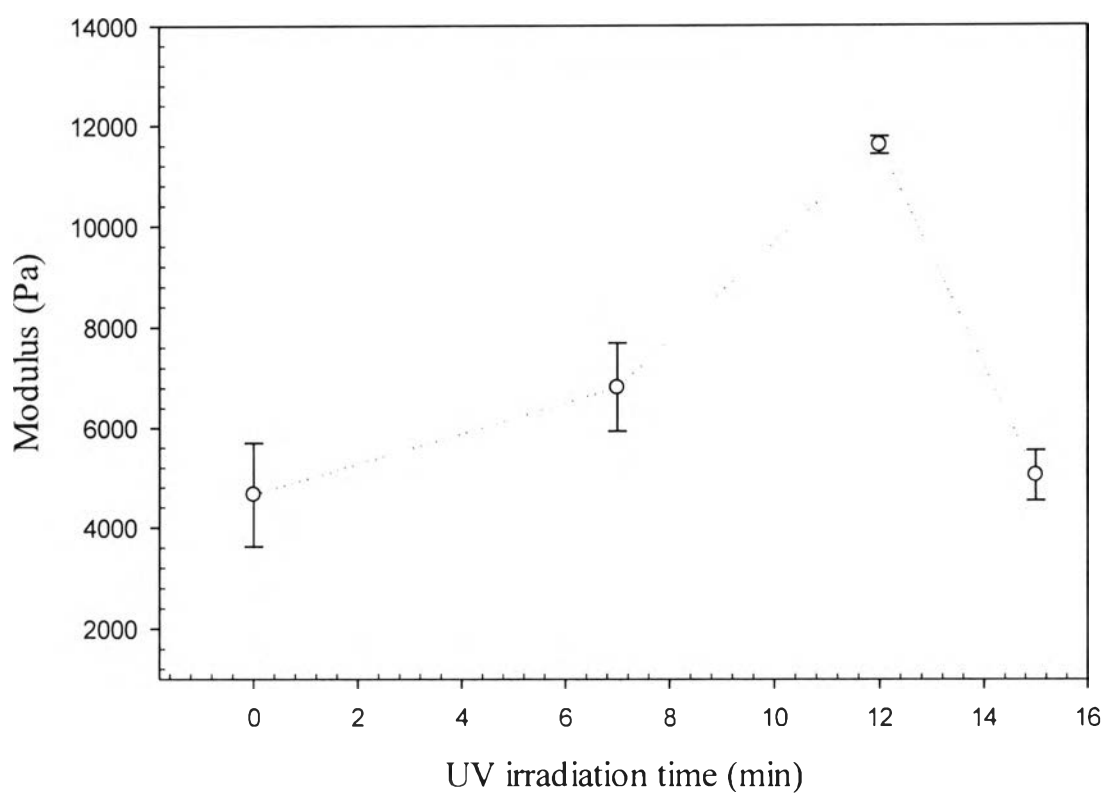


Figure F2 Modulus of NR films at various UV irradiation times, a fixed concentration of crosslinker of 2.0 %v/v, by using the melt rheometer in the tension mode with a strain rate 0.01 s^{-1} and temperature of 300 K.

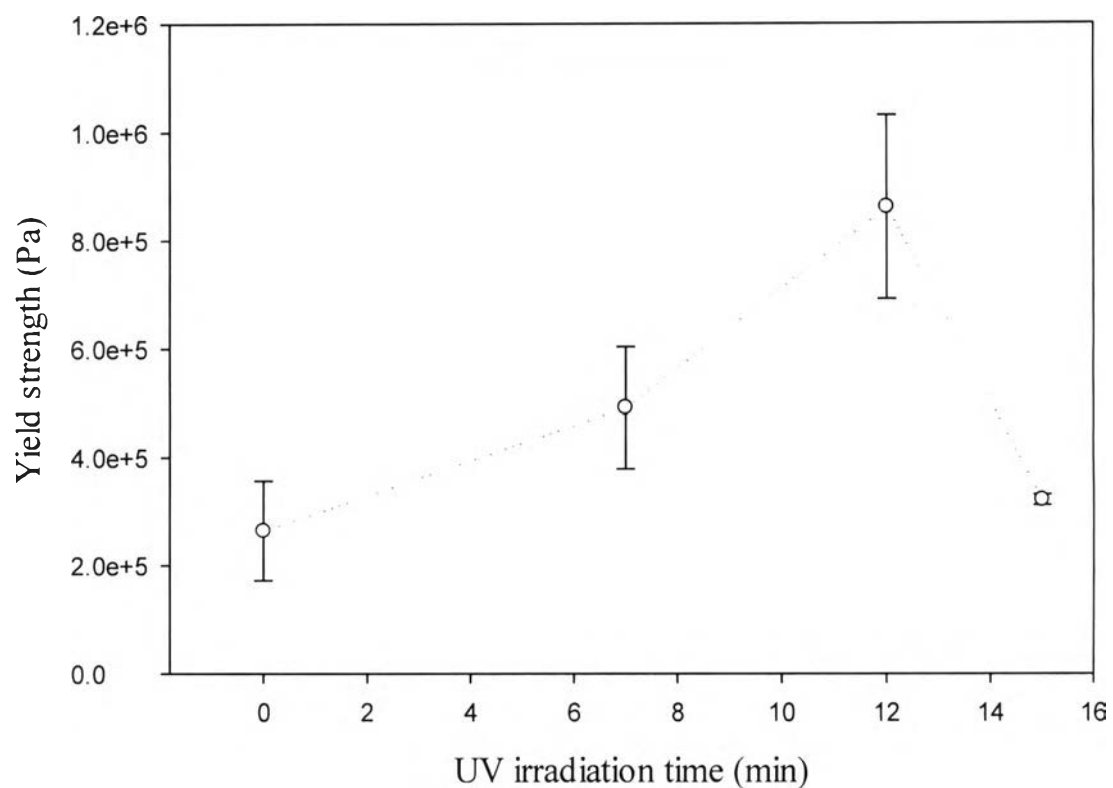


Figure F3 Yield strength of NR films at various UV irradiation times, a fixed concentration of crosslinker of 2.0 %v/v, by using the melt rheometer in the tension mode with a strain rate 0.01 s^{-1} and temperature of 300 K.

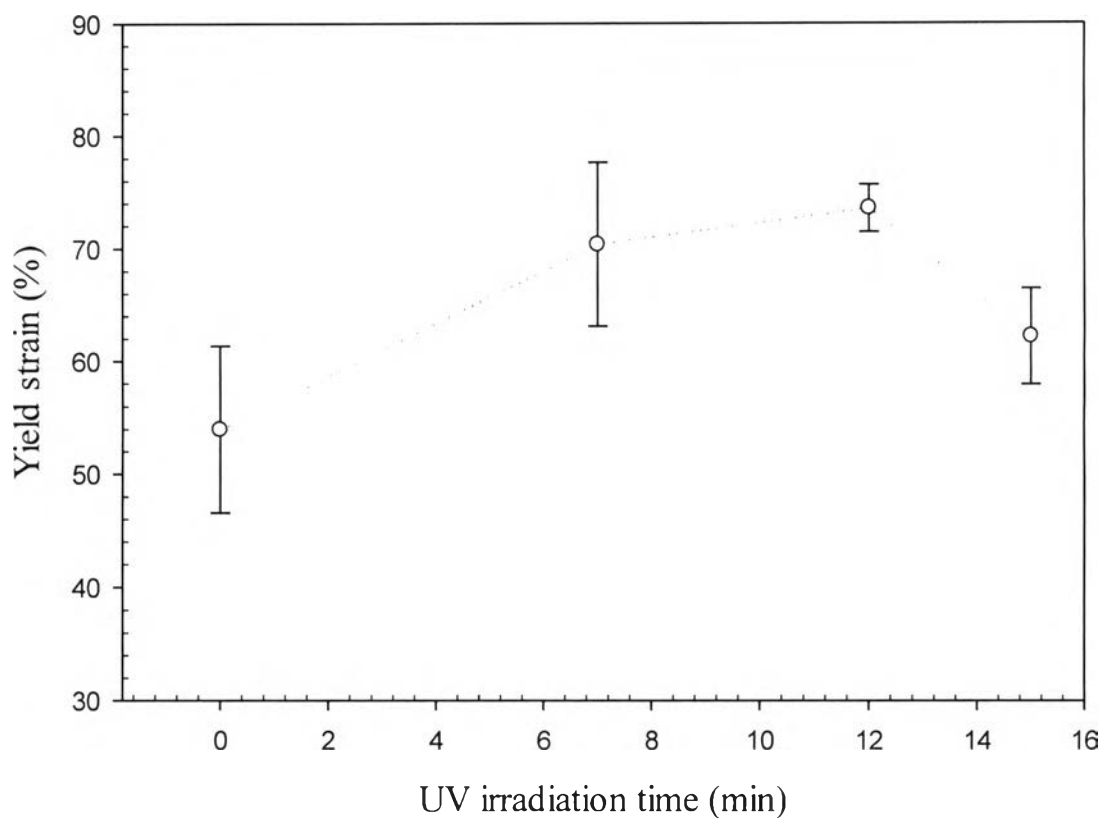


Figure F4 Yield strain of NR films at various UV irradiation times, a fixed concentration of crosslinker of 2.0 %v/v, by using the melt rheometer in the tension mode with a strain rate 0.01 s^{-1} and temperature of 300 K.

Table F1 Mechanical properties of NR films at various UV irradiation times, a fixed concentration of crosslinker of 2.0 %v/v, by using the melt rheometer in the tension mode with a strain rate 0.01 s^{-1} and temperature of 300 K

| Crosslinking time (min) | Yield strength (Pa) | Yield strain (%) | Modulus (Pa) |
|-------------------------|-------------------------------------|------------------|-------------------------------------|
| 0 | $2.65\text{E}+5 \pm 9.27\text{E}+4$ | 53.97 ± 7.39 | $4.67\text{E}+3 \pm 1.0\text{E}+3$ |
| 7 | $4.92\text{E}+5 \pm 1.12\text{E}+5$ | 70.39 ± 7.26 | $6.82\text{E}+3 \pm 8.74\text{E}+2$ |
| 12 | $8.62\text{E}+5 \pm 1.70\text{E}+5$ | 73.61 ± 2.09 | $1.16\text{E}+4 \pm 1.75\text{E}+2$ |
| 15 | $3.23\text{E}+5 \pm 9.67\text{E}+3$ | 62.23 ± 4.28 | $5.05\text{E}+3 \pm 5.06\text{E}+2$ |

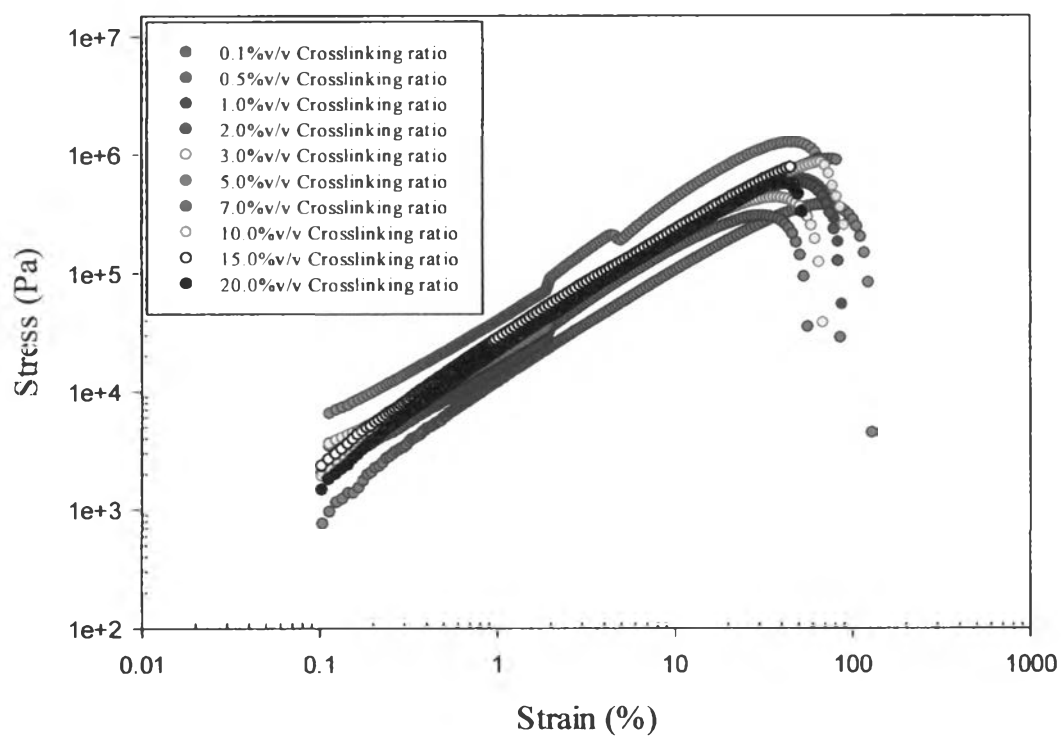


Figure F5 Stress-strain curve of NR films at various concentrations of crosslinker, a fixed UV irradiation time of 7 min, by using the melt rheometer in the tension mode with a strain rate 0.01 s^{-1} and temperature of 300 K.

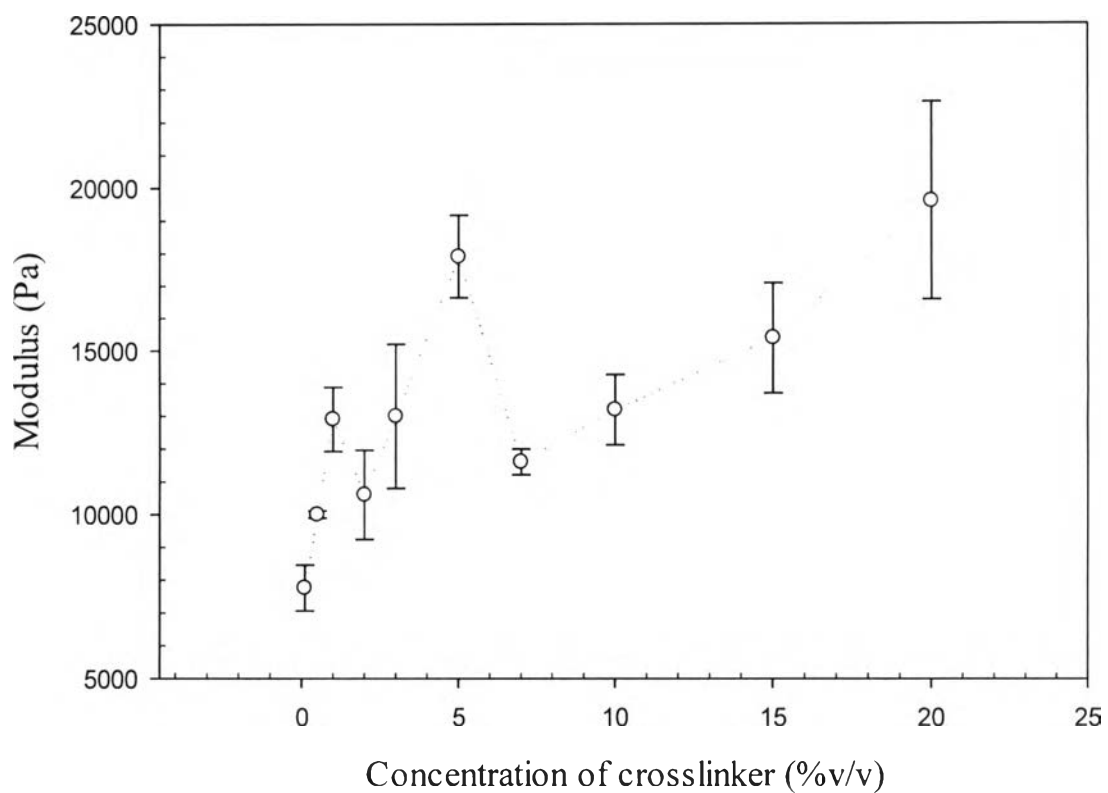


Figure F6 Modulus of NR films at various concentrations of crosslinker, a fixed UV irradiation time of 7 min, by using the melt rheometer in the tension mode with a strain rate 0.01 s^{-1} and temperature of 300 K.

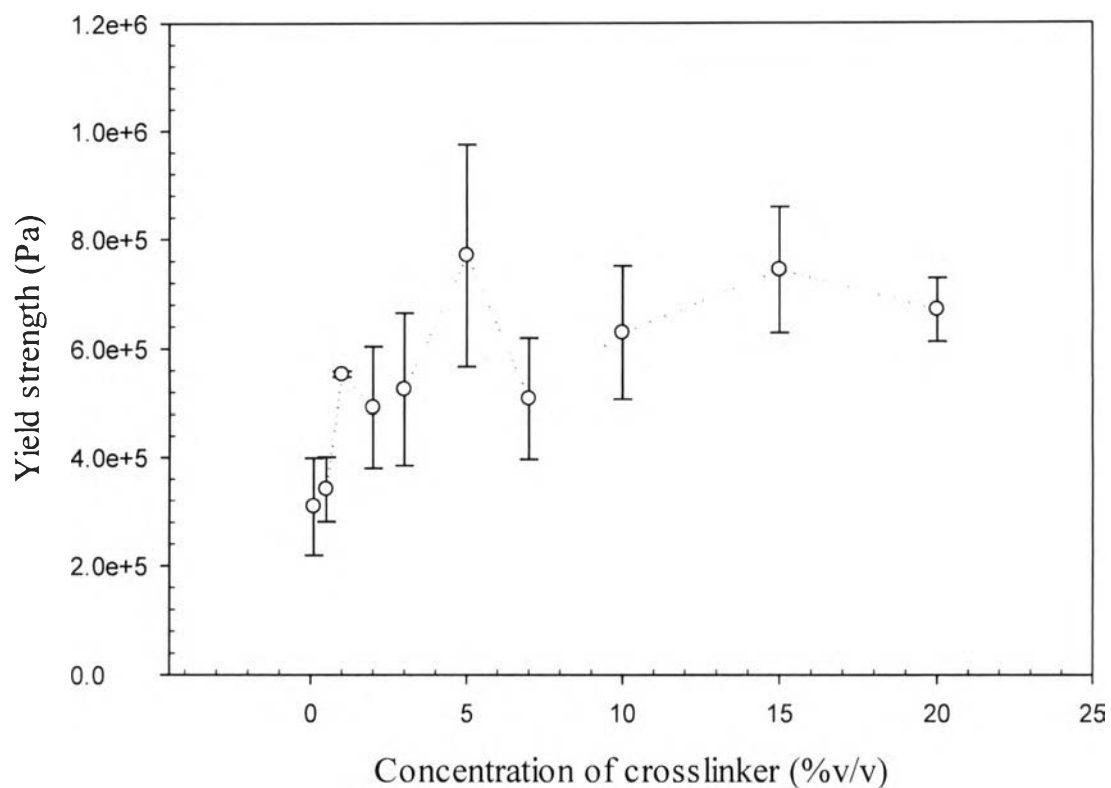


Figure F7 Yield strength of NR films at various concentrations of crosslinker, a fixed UV irradiation time of 7 min, by using the melt rheometer in the tension mode with a strain rate 0.01 s^{-1} and temperature of 300 K.

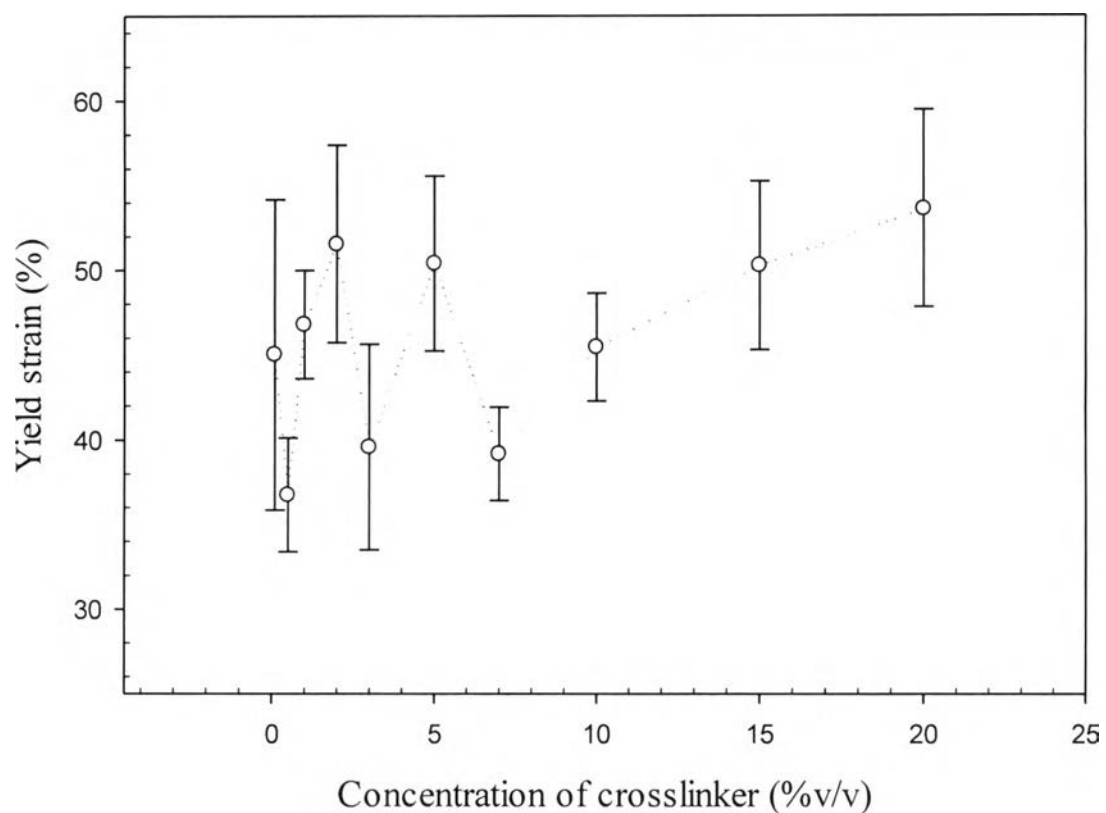


Figure F8 Yield strain of NR films at various concentrations of crosslinker, a fixed UV irradiation time of 7 min, by using the melt rheometer in the tension mode with a strain rate 0.01 s^{-1} and temperature of 300 K.

Table F2 Mechanical properties of NR films at various concentrations of crosslinker, a fixed UV irradiation time of 7 min, by using the melt rheometer in the tension mode with a strain rate 0.01 s^{-1} and temperature of 300 K

| Concentrations of crosslinker (%v/v) | Yield strength (Pa) | Yield strain (%) | Modulus (Pa) |
|--------------------------------------|-------------------------------------|------------------|-------------------------------------|
| 0.1 | $3.09\text{E}+5 \pm 9.00\text{E}+4$ | 45.02 ± 9.17 | $7.76\text{E}+3 \pm 7.00\text{E}+2$ |
| 0.5 | $3.41\text{E}+5 \pm 6.00\text{E}+4$ | 36.76 ± 3.37 | $1.00\text{E}+4 \pm 1.09\text{E}+2$ |
| 1.0 | $5.53\text{E}+5 \pm 5.37\text{E}+3$ | 46.80 ± 3.20 | $1.29\text{E}+4 \pm 9.82\text{E}+2$ |
| 2.0 | $4.92\text{E}+5 \pm 1.12\text{E}+5$ | 51.57 ± 5.84 | $1.06\text{E}+4 \pm 1.36\text{E}+3$ |
| 3.0 | $5.25\text{E}+5 \pm 1.40\text{E}+5$ | 39.58 ± 6.07 | $1.30\text{E}+4 \pm 2.20\text{E}+3$ |
| 5.0 | $7.71\text{E}+5 \pm 2.04\text{E}+5$ | 50.41 ± 5.18 | $1.79\text{E}+4 \pm 1.27\text{E}+3$ |
| 7.0 | $5.08\text{E}+5 \pm 1.11\text{E}+5$ | 39.18 ± 2.74 | $1.16\text{E}+4 \pm 3.93\text{E}+2$ |
| 10.0 | $6.29\text{E}+5 \pm 1.22\text{E}+5$ | 45.46 ± 3.18 | $1.32\text{E}+4 \pm 1.08\text{E}+3$ |
| 15.0 | $7.44\text{E}+5 \pm 1.15\text{E}+5$ | 50.30 ± 4.98 | $1.54\text{E}+4 \pm 1.69\text{E}+3$ |
| 20.0 | $6.71\text{E}+5 \pm 5.81\text{E}+4$ | 53.66 ± 5.82 | $1.96\text{E}+4 \pm 3.02\text{E}+3$ |

Appendix G Mechanical properties of natural rubber and graphene composite film under the effect of commercial graphene multilayers with UV irradiation time of 7 min. and concentration of crosslinker 5.0 %v/v

The mechanical properties of graphene/NR composites were measured by the melt rheometer (Rheometric scientific, Ares) with the extensional fixture at room temperature. In this experiment, the transient mode was applied and the stress was monitored during stretching, at strain rate 0.01s^{-1} , as a function of strain. From the results, stress vs. strain was obtained. An evaluation of the mechanical properties of the film was focus on the modulus, the yield strength, and the yield strain.

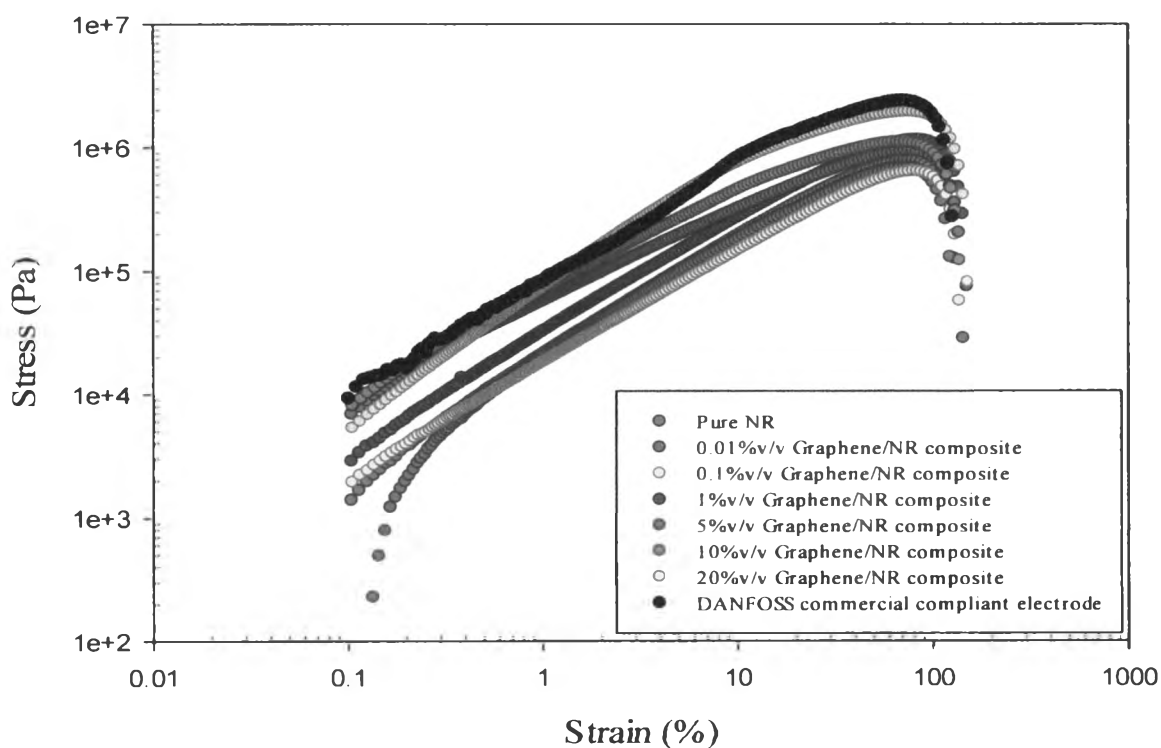


Figure G1 Stress-strain curve of graphene/NR composites at various concentrations of graphene multilayers as measured by the melt rheometer in the tension mode with a strain rate of 0.01 s^{-1} and temperature of 300 K.

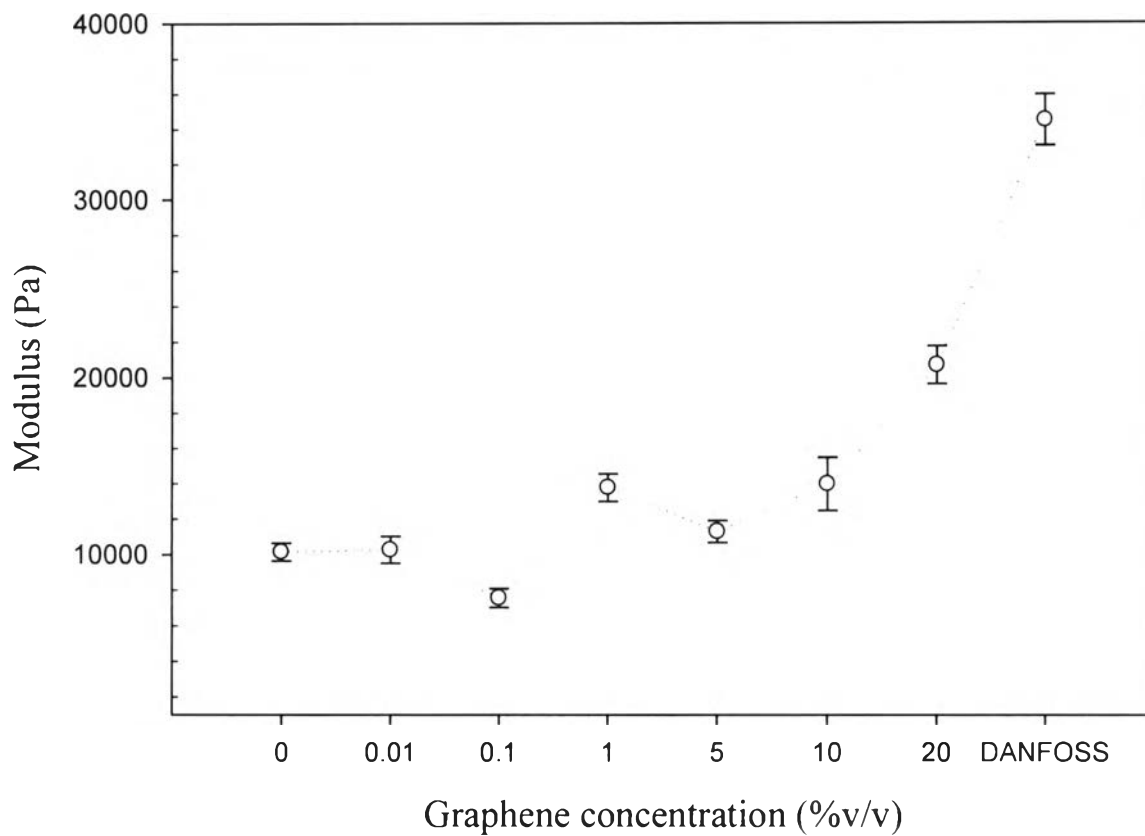


Figure G2 Modulus of graphene/NR composites at various concentrations of graphene multilayers as measured by the melt rheometer in the tension mode with a strain rate of 0.01 s^{-1} and temperature of 300 K.

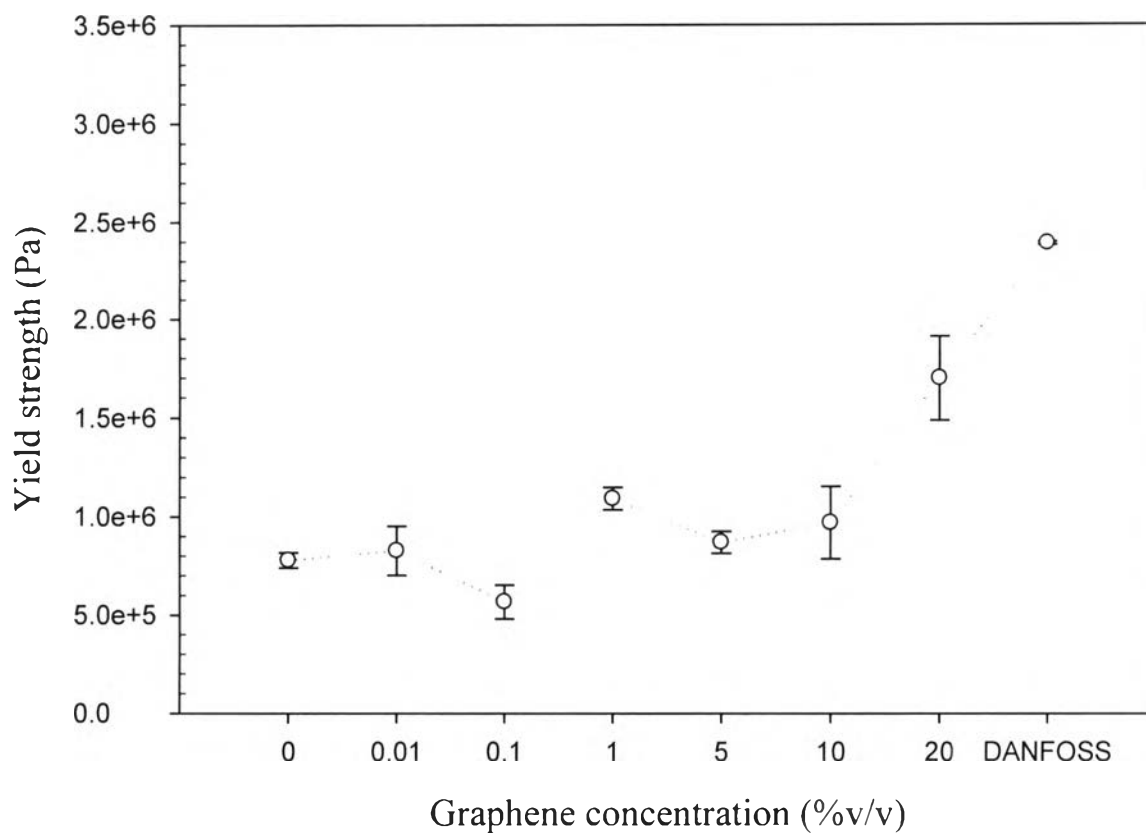


Figure G3 Yield strength of graphene/NR composites at various concentrations of graphene multilayers as measured by the melt rheometer in the tension mode with a strain rate of 0.01 s^{-1} and temperature of 300 K.

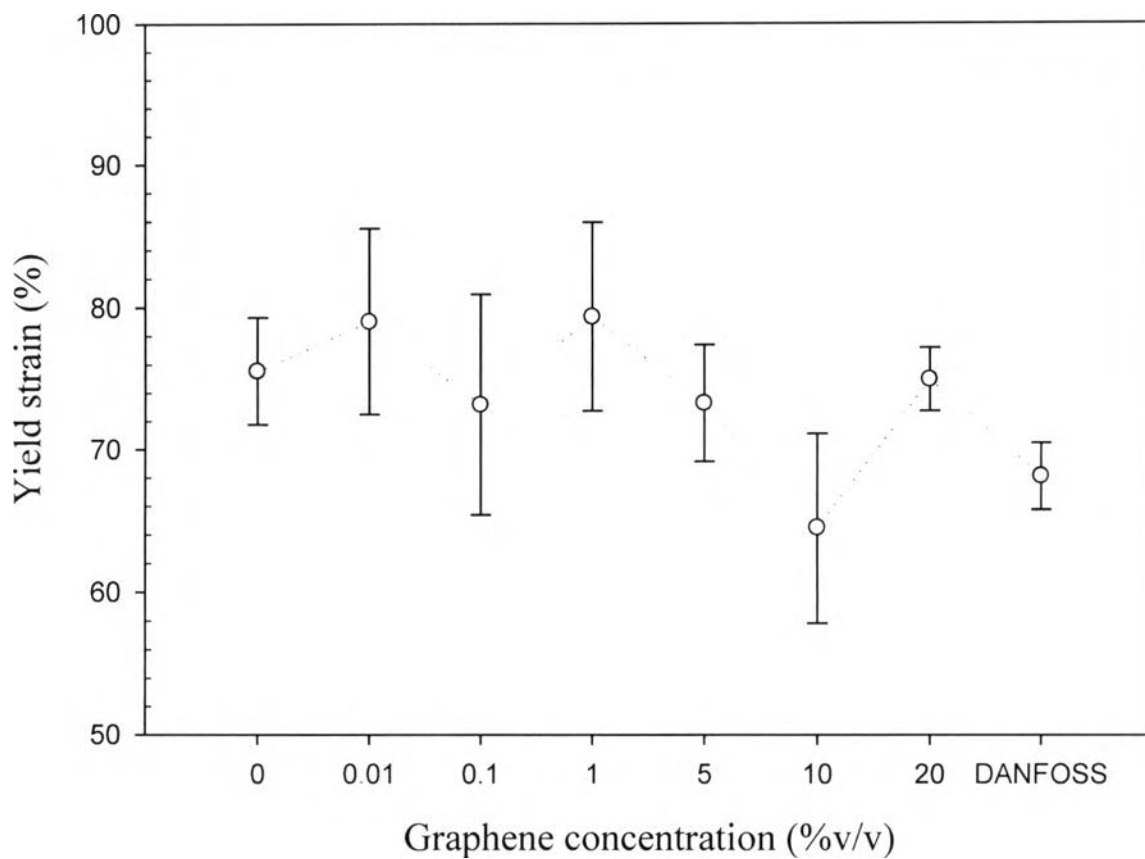


Figure G4 Yield strain of graphene/NR composites at various concentrations of graphene multilayers as measured by the melt rheometer in the tension mode with a strain rate of 0.01 s^{-1} and temperature of 300 K.

Table G1 Mechanical properties of graphene/NR composites at various concentrations of graphene multilayers as measured by the melt rheometer in the tension mode with a strain rate of 0.01 s^{-1} and temperature of 300 K

| Graphene concentration (%v/v) | Yield strength (Pa) | Yield strain (%) | Modulus (Pa) |
|-------------------------------|-------------------------------------|------------------|------------------------------|
| 0.0 | $7.78\text{E}+5 \pm 3.89\text{E}+4$ | 75.54 ± 3.77 | $1.01\text{E}+4 \pm 507.25$ |
| 0.01 | $8.26\text{E}+5 \pm 1.25\text{E}+5$ | 79.01 ± 6.51 | $1.03\text{E}+4 \pm 757.46$ |
| 0.1 | $5.67\text{E}+5 \pm 8.62\text{E}+4$ | 73.16 ± 7.77 | $7.57\text{E}+3 \pm 527.50$ |
| 1.0 | $1.10\text{E}+6 \pm 5.70\text{E}+4$ | 79.34 ± 6.61 | $1.38\text{E}+4 \pm 782.71$ |
| 5.0 | $8.70\text{E}+5 \pm 5.61\text{E}+4$ | 73.28 ± 4.12 | $1.13\text{E}+4 \pm 620.69$ |
| 10.0 | $9.70\text{E}+5 \pm 1.84\text{E}+5$ | 64.48 ± 6.64 | $1.40\text{E}+4 \pm 1507.49$ |
| 20.0 | $1.70\text{E}+6 \pm 2.12\text{E}+5$ | 74.97 ± 2.22 | $2.07\text{E}+4 \pm 1068.84$ |
| DANFOSS | $2.39\text{E}+6 \pm 8.34\text{E}+3$ | 68.10 ± 2.35 | $3.45\text{E}+4 \pm 1445.84$ |

Appendix H Mechanical Properties and Electrical Conductivity of Natural Rubber and Graphene Composite Film under The Effect of Graphene Multilayers with UV Irradiation Time of 7 min. and Concentration of Crosslinker of 5.0 %v/v with Applied Electric Field of 5 volt

The mechanical properties of graphene/NR composites were measured by the melt rheometer (Rheometric scientific, Ares) with the extensional fixture at room temperature. In this experiment, the transient mode was applied and the stress was monitored during stretching, at strain rate $0.01s^{-1}$, as a function of strain. From the results, stress versus strain was obtained. An evaluation of the mechanical properties of the film was focused on the modulus, the yield strength, and the yield strain.

Table H1 Preparation conditions of graphene/NR composite films

| Graphene content (%v/v) | TWEEN80 (surfactant) (%v/v) | Natural rubber latex (ml) | Water (ml) | TWEEN80/graphene volume ratio |
|-------------------------|-----------------------------|---------------------------|------------|-------------------------------|
| 0.0 | - | 20 | - | - |
| 0.01 | 1 | 20 | 20 | 100 |
| 0.1 | 1 | 20 | 20 | 10 |
| 1.0 | 1 | 20 | 20 | 1 |
| 5.0 | 1 | 20 | 20 | 0.2 |
| 10.0 | 2 | 20 | 20 | 0.2 |
| 20.0 | 8 | 20 | 40 | 0.4 |
| 30.0 | 12 | 20 | 60 | 0.4 |
| 35.0 | 14 | 20 | 70 | 0.4 |
| 40.0 | 16 | 20 | 80 | 0.4 |
| 45.0 | 18 | 20 | 90 | 0.4 |

*Crosslink under UV irradiation time of 7 minute and crosslink concentration of 5.0

%v/v

The electrical conductivity of graphene/NR composites was investigated with the same fixture as mechanical testing and then the DC voltage was applied with DC power supply (Instek, GFG 8216A) connected with a digital multimeter (Tektronix, CDM 250) to monitor the voltage input. The electrical conductivity during stretching was calculated through the following equation:

$$\sigma = \frac{1}{R} \times \frac{l}{A} = \frac{I}{V} \times \frac{l}{A} \quad (\text{H1})$$

where, σ is the electrical conductivity (S/cm), R is the resistivity ($\Omega \times \text{cm}$), l is the length of specimen (cm), A is the cross-section area of specimen (cm^2), I is the current (Ampere), and V is the applied voltage (Volt).

In addition, the length and area of specimen depend on the stretching which was calculated based on the incompressible material via the following equations:

$$\gamma = -\frac{\epsilon_{22}}{\epsilon_{11}} = -\frac{\epsilon_{33}}{\epsilon_{11}} = 0.5 \quad (\text{H2})$$

$$t_x = t_0(1 - \epsilon_{33}) = t_0(1 + 0.5\epsilon_{11}) \quad (\text{H3})$$

$$w_x = w_0(1 - \epsilon_{33}) = w_0(1 + 0.5\epsilon_{11}) \quad (\text{H4})$$

$$l_x = l_0(1 + \epsilon_{11}) \quad (\text{H5})$$

$$\epsilon_{11} = \frac{\Delta l}{l_0} = \frac{l_x - l_0}{l_0} \quad (\text{H6})$$

where γ is the Poisson ratio (for rubber = 0.5), $\epsilon_{11,22,33}$ is the strain in x, y, z axis, t is the thickness of specimen (cm), w is the width of specimen (cm), l is the length of specimen (cm). Subscript x means the value at any strain, and subscript 0 means at strain = 0.

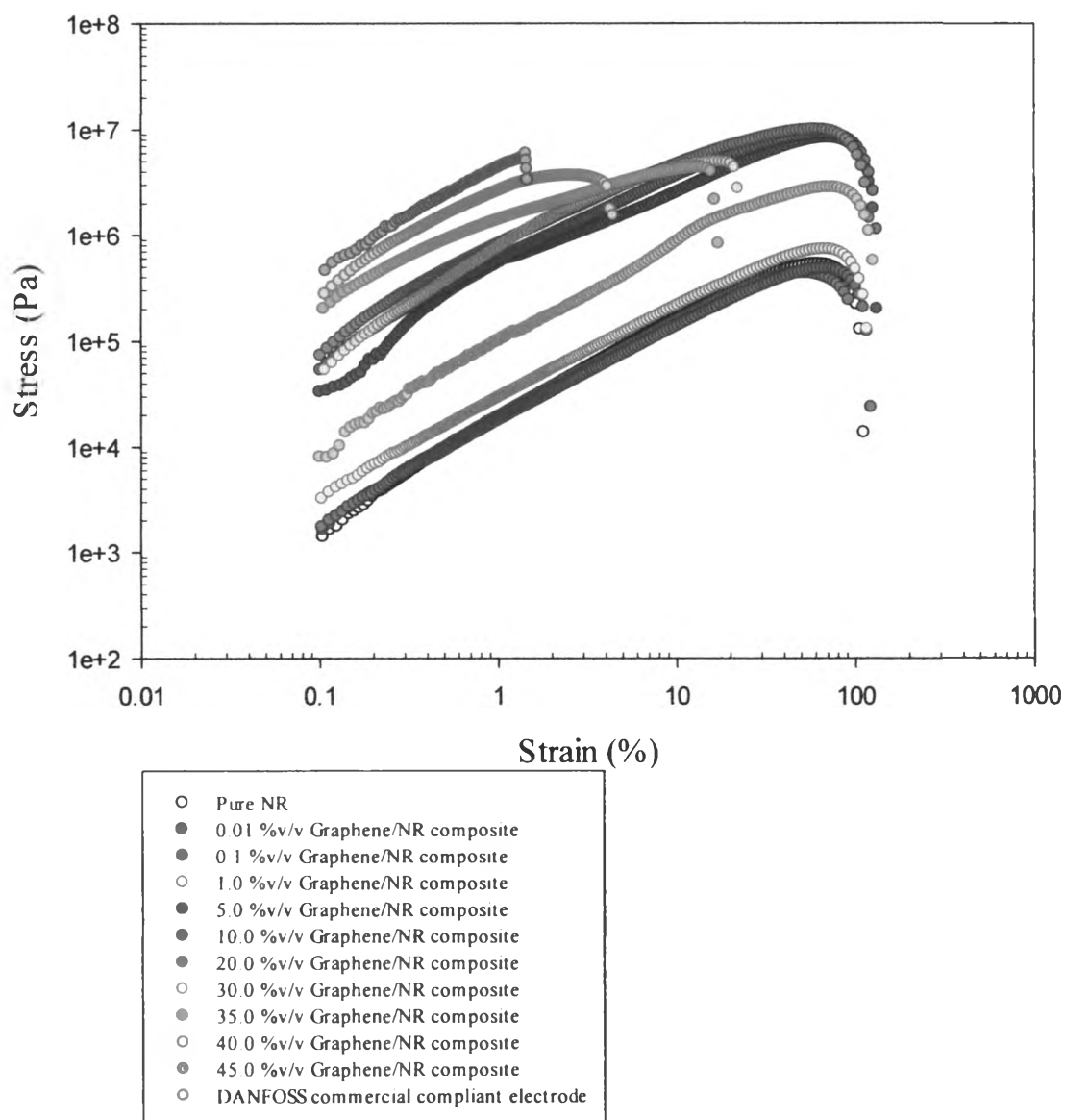


Figure H1 Stress-strain curve of graphene/NR composites at various concentrations of the graphene multilayers measured by the melt rheometer in the tension mode with a strain rate of 0.01s^{-1} , temperature of 300 K, and applied electric field of 5 volt.

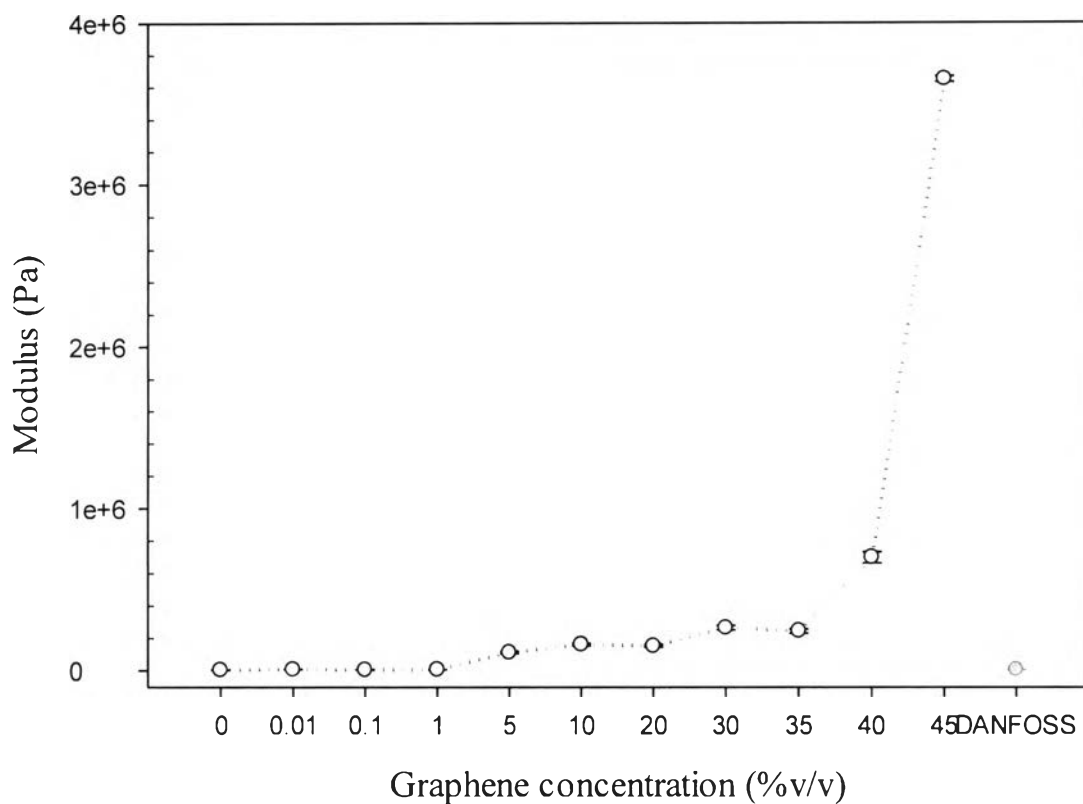


Figure H2 Modulus of graphene/NR composites at various concentrations of the graphene multilayers as measured by the melt rheometer in the tension mode with a strain rate of 0.01 s^{-1} , temperature of 300 K, and applied electric field of 5 volt.

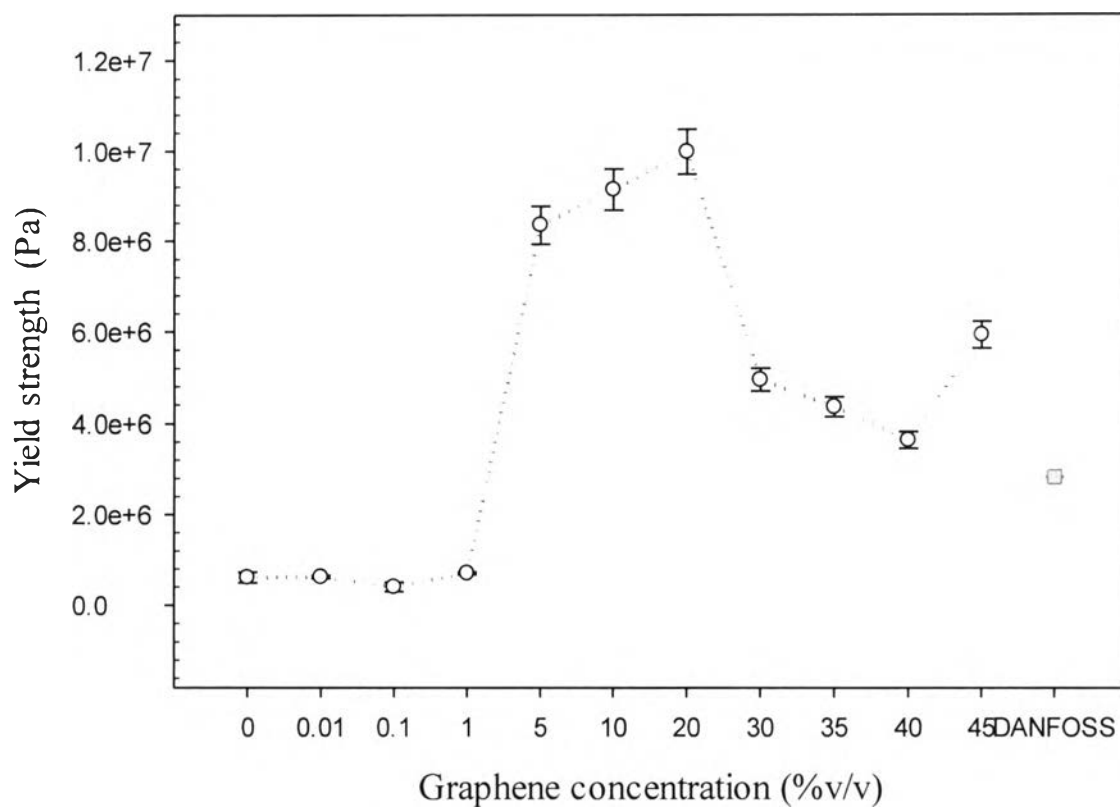


Figure H3 Yield strength of graphene/NR composites at various concentrations of the graphene multilayers as measured by the melt rheometer in the tension mode with a strain rate of 0.01 s^{-1} , temperature of 300 K, and applied electric field of 5 volt.

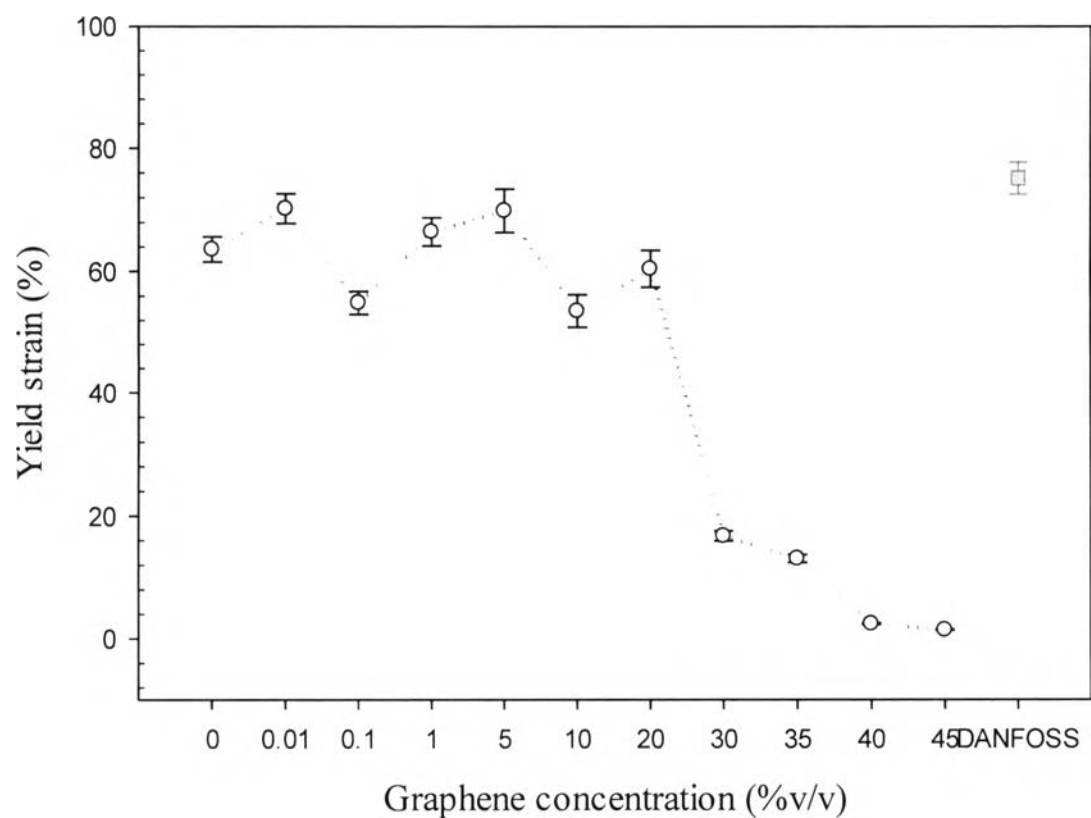


Figure H4 Yield strain of graphene/NR composites at various concentrations of the graphene multilayers as measured by the melt rheometer in the tension mode with a strain rate of 0.01 s^{-1} , temperature of 300 K, and applied electric field of 5 volt.

Table H2 Mechanical properties of graphene/NR composites at various concentrations of the graphene multilayers as measured by the melt rheometer in the tension mode with a strain rate of 0.01 s^{-1} , temperature of 300 K, and applied electric field of 5 volt

| Graphene concentration (%v/v) | Yield strength (Pa) | Yield strain (%) | Modulus (Pa) |
|-------------------------------|-------------------------------------|------------------|------------------------------|
| 0.0 | $6.14\text{E}+5 \pm 1.18\text{E}+5$ | 63.60 ± 2.04 | $4.75\text{E}+4 \pm 399.45$ |
| 0.01 | $6.26\text{E}+5 \pm 3.28\text{E}+4$ | 70.23 ± 2.42 | $8.48\text{E}+3 \pm 497.65$ |
| 0.1 | $4.07\text{E}+5 \pm 1.04\text{E}+5$ | 54.87 ± 1.88 | $5.95\text{E}+3 \pm 401.56$ |
| 1.0 | $7.11\text{E}+5 \pm 2.76\text{E}+4$ | 66.46 ± 2.29 | $7.12\text{E}+3 \pm 356.10$ |
| 5.0 | $8.36\text{E}+6 \pm 4.18\text{E}+5$ | 69.86 ± 3.49 | $1.13\text{E}+5 \pm 5670.71$ |
| 10.0 | $9.15\text{E}+6 \pm 4.57\text{E}+5$ | 53.53 ± 2.67 | $1.63\text{E}+5 \pm 8148.37$ |
| 20.0 | $9.99\text{E}+6 \pm 4.99\text{E}+5$ | 60.42 ± 3.00 | $1.54\text{E}+5 \pm 7709.10$ |
| 30.0 | $4.95\text{E}+6 \pm 2.47\text{E}+5$ | 16.75 ± 0.84 | $2.66\text{E}+5 \pm 1330.54$ |
| 35.0 | $4.36\text{E}+6 \pm 2.18\text{E}+5$ | 13.06 ± 0.65 | $2.46\text{E}+5 \pm 1234.12$ |
| 40.0 | $3.65\text{E}+6 \pm 1.82\text{E}+5$ | 2.46 ± 0.12 | $6.99\text{E}+5 \pm 3506.67$ |
| 45.0 | $5.94\text{E}+6 \pm 2.97\text{E}+5$ | 1.44 ± 0.07 | $3.65\text{E}+6 \pm 1834.23$ |
| DANFOSS | $2.84\text{E}+6 \pm 1.78\text{E}+4$ | 75.12 ± 2.60 | $8.15\text{E}+3 \pm 1893.50$ |

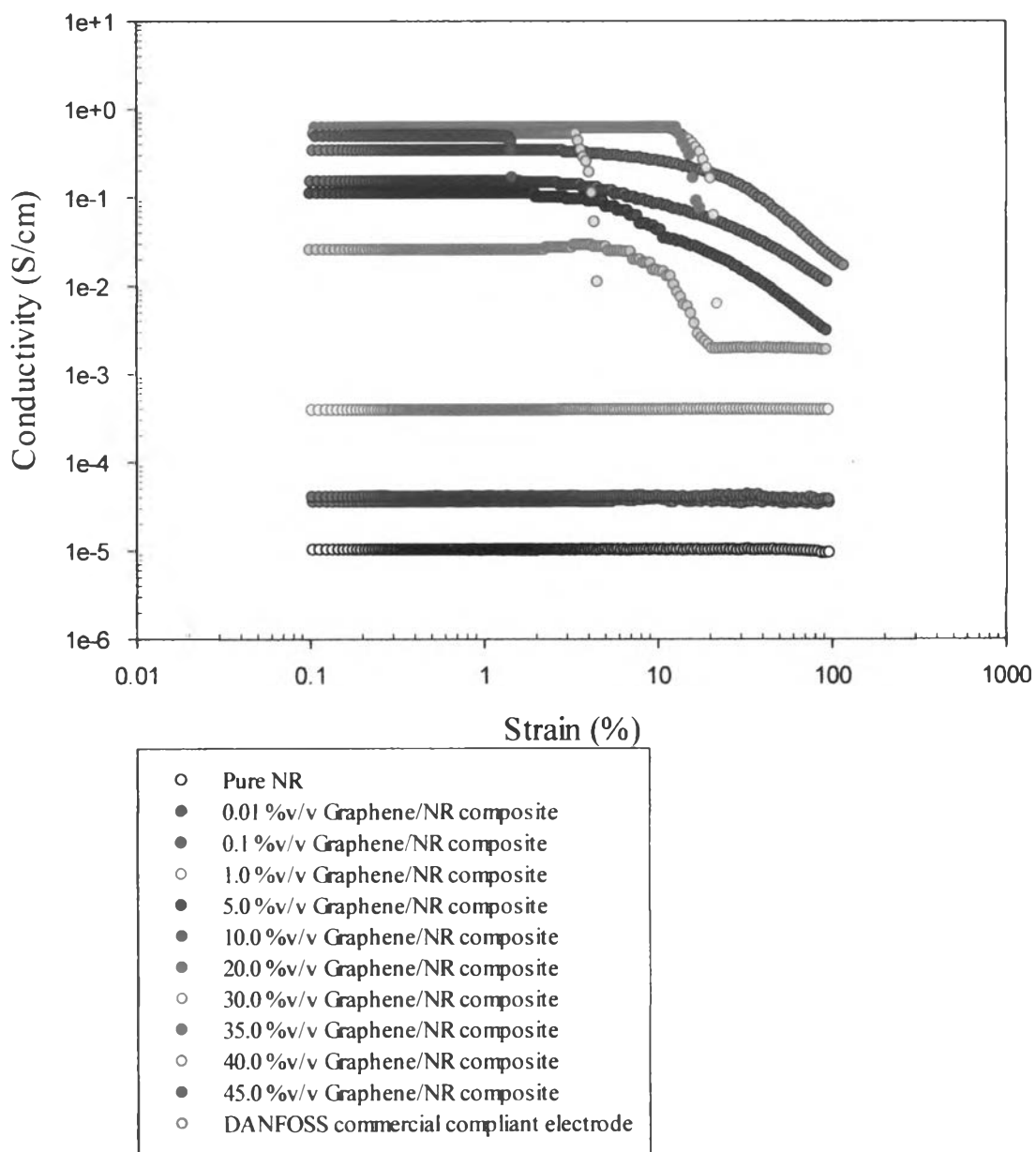


Figure H5 Conductivity of graphene/NR composites at various concentrations of the graphene multilayers as measured by the melt rheometer in the tension mode with a strain rate of 0.01 s^{-1} , temperature of 300 K, and applied electric field of 5 volt.

Table H3 Electrical conductivity of graphene/NR composites at various concentrations of the graphene multilayers as measured by the melt rheometer in the tension mode with a strain rate of 0.01 s^{-1} , temperature of 300 K, and applied electric field of 5 volt.

| Graphene concentration (%v/v) | Conductivity before stretching (S/cm) | Critical strain* (%) |
|-------------------------------|---------------------------------------|----------------------|
| 0.0 | $1.41\text{E-}5 \pm 5.47\text{E-}6$ | > 100 |
| 0.01 | $3.55\text{E-}5 \pm 1.77\text{E-}6$ | > 100 |
| 0.1 | $4.05\text{E-}5 \pm 2.03\text{E-}6$ | > 100 |
| 1.0 | $3.84\text{E-}4 \pm 2.23\text{E-}4$ | > 100 |
| 5.0 | $1.10\text{E-}1 \pm 5.50\text{E-}3$ | 2.01 ± 0.11 |
| 10.0 | $1.50\text{E-}1 \pm 5.07\text{E-}2$ | 3.11 ± 0.51 |
| 20.0 | $3.36\text{E-}1 \pm 1.90\text{E-}2$ | 5.02 ± 0.67 |
| 30.0 | $6.04\text{E-}1 \pm 1.00\text{E-}2$ | 12.70 ± 0.92 |
| 35.0 | $6.12\text{E-}1 \pm 3.06\text{E-}2$ | 12.74 ± 0.67 |
| 40.0 | $5.22\text{E-}1 \pm 2.61\text{E-}2$ | 3.38 ± 0.17 |
| 45.0 | $4.86\text{E-}1 \pm 2.43\text{E-}2$ | 1.38 ± 0.07 |
| DANFOSS | $2.54\text{E-}2 \pm 1.27\text{E-}3$ | 6.45 ± 0.32 |

* Critical strain refers to 5% conductivity drop. Beyond this critical strain point, the material's behavior is non-linear and the conductivity declines.

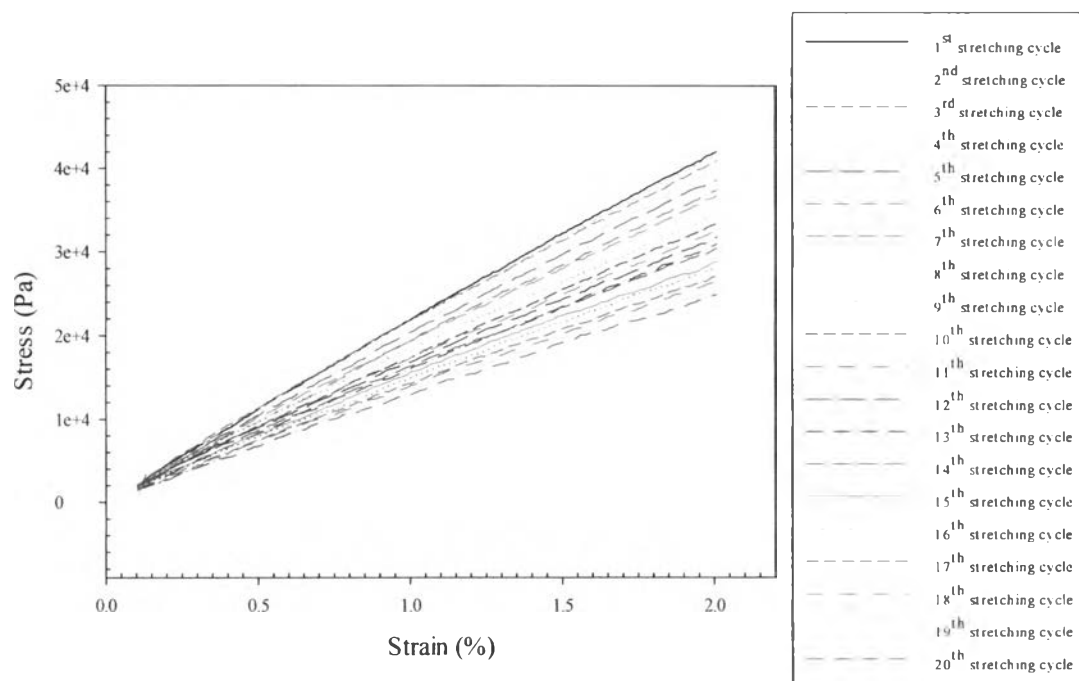


Figure H6 Stress-strain curve for 20 stretching cycles of 0.01%v/v graphene/NR composite as measured by the melt rheometer in the tension mode with a strain rate of 0.01s^{-1} , temperature of 300 K, and applied electric field of 5 volt.

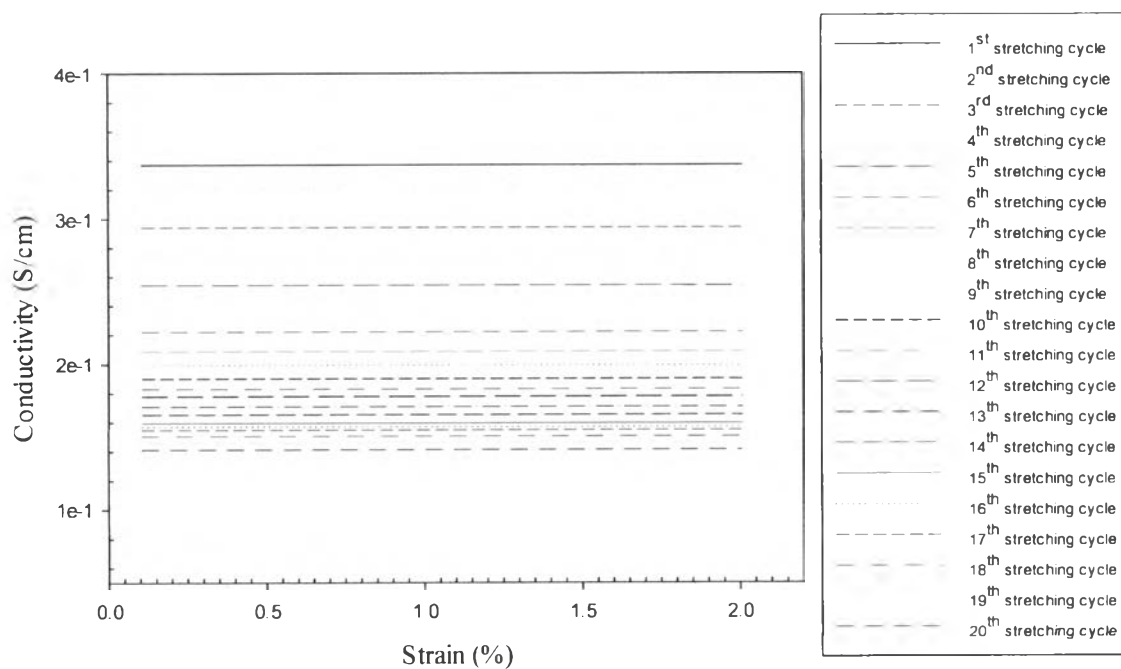


Figure H7 Conductivity for 20 stretching cycles of 0.01%v/v graphene/NR composite as measured by the melt rheometer in the tension mode with a strain rate of 0.01 s^{-1} , temperature of 300 K, and applied electric field of 5 volt.

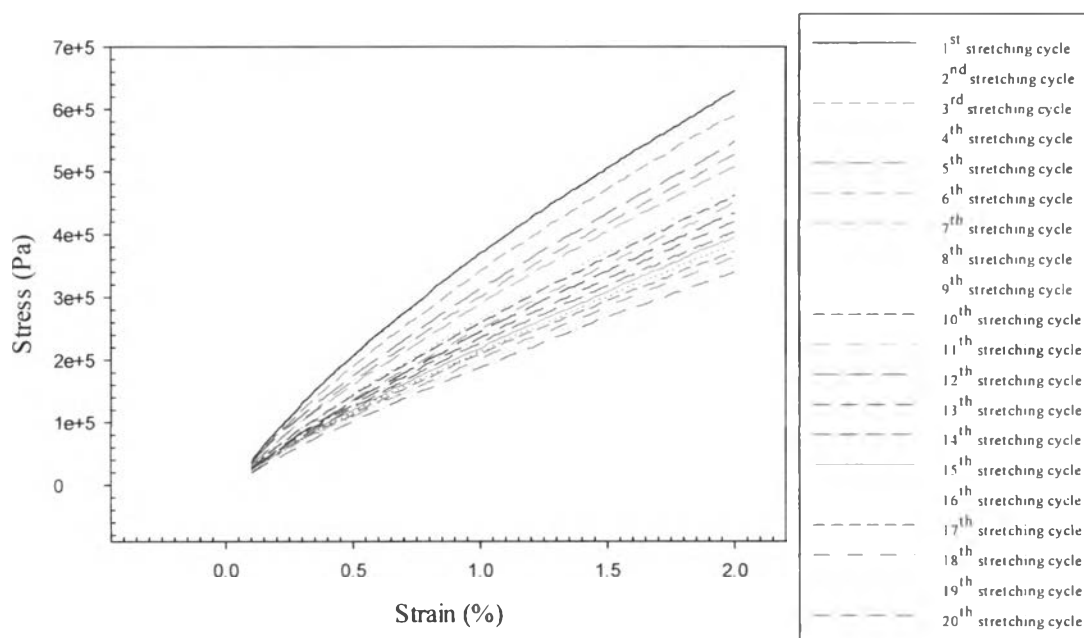


Figure H8 Stress-strain curve for 20 stretching cycles of 5.0%v/v graphene/NR composite as measured by the melt rheometer in the tension mode with a strain rate of 0.01s^{-1} , temperature of 300 K, and applied electric field of 5 volt.

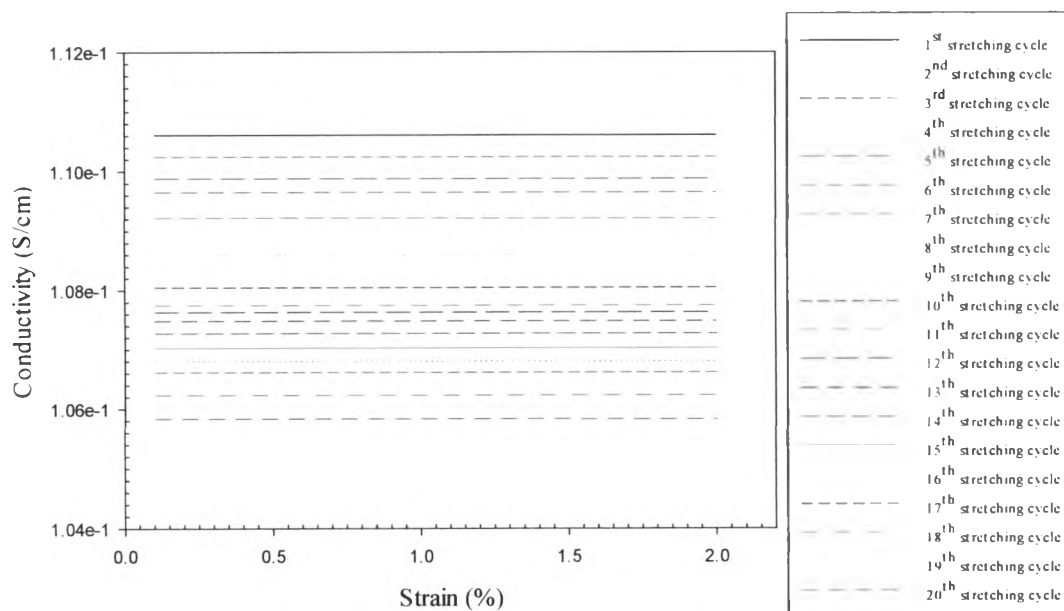


Figure H9 Conductivity for 20 stretching cycles of 5.0%v/v graphene/NR composite as measured by the melt rheometer in the tension mode with a strain rate of 0.01s^{-1} , temperature of 300 K, and applied electric field of 5 volt.

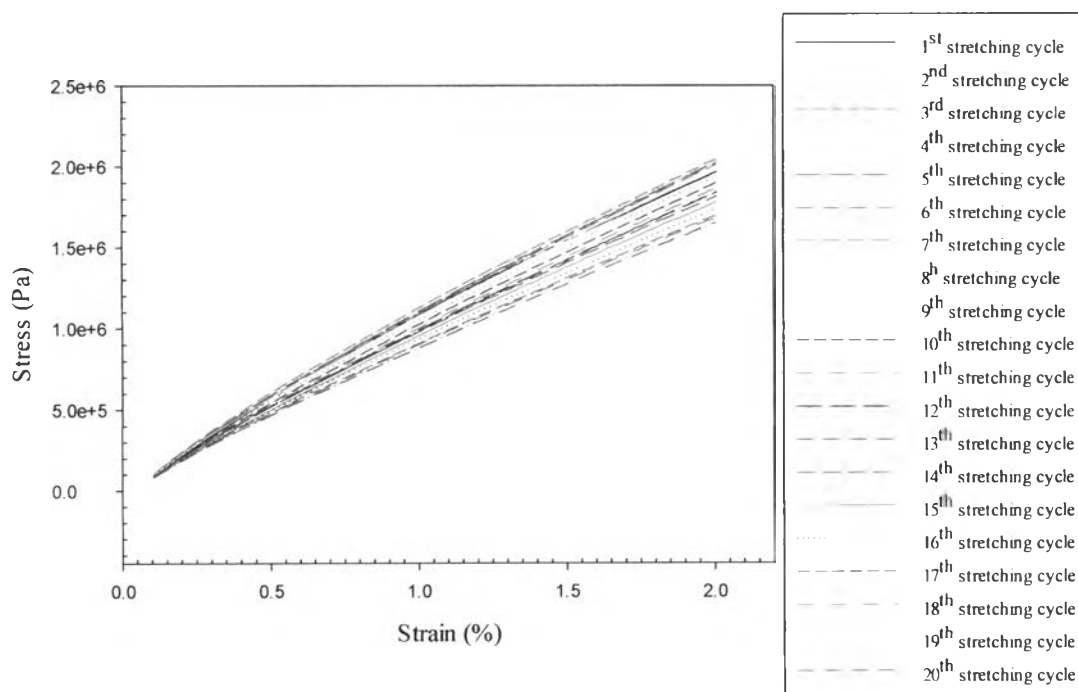


Figure H10 Stress-strain curve for 20 stretching cycles of 20.0%v/v graphene/NR composite as measured by the melt rheometer in the tension mode with a strain rate of 0.01s^{-1} , temperature of 300 K, and applied electric field of 5 volt.

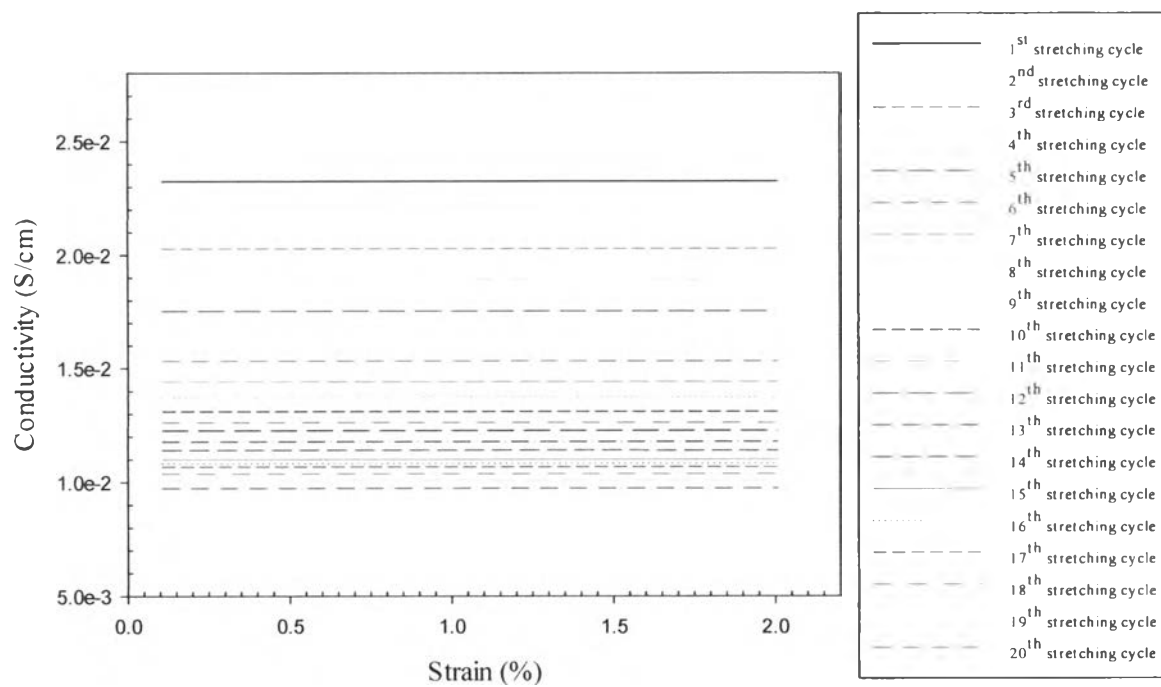


Figure H11 Conductivity for 20 stretching cycles of 20.0%v/v graphene/NR composite as measured by the melt rheometer in the tension mode with a strain rate of 0.01s^{-1} , temperature of 300 K, and applied electric field of 5 volt.

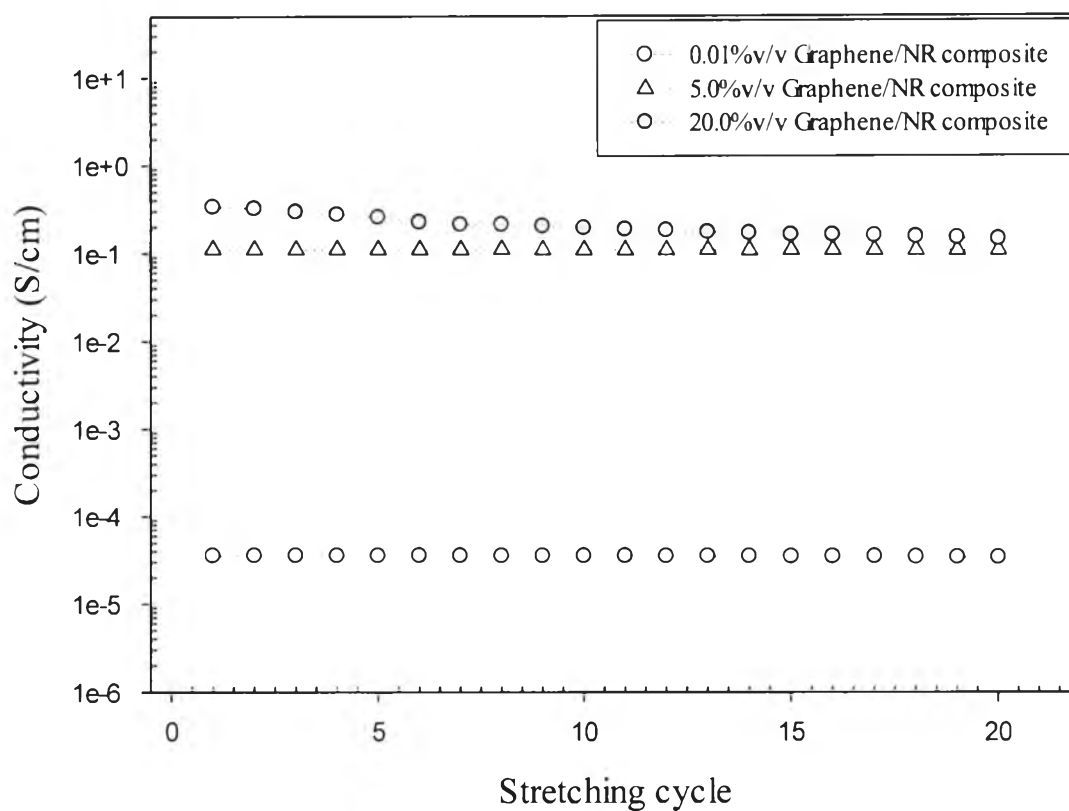


Figure H12 Conductivity versus stretching cycles of the composites at fixed strain 1% as measured by the melt rheometer in the tension mode with a strain rate of 0.01s^{-1} , temperature of 300 K, and applied electric field of 5 volt.

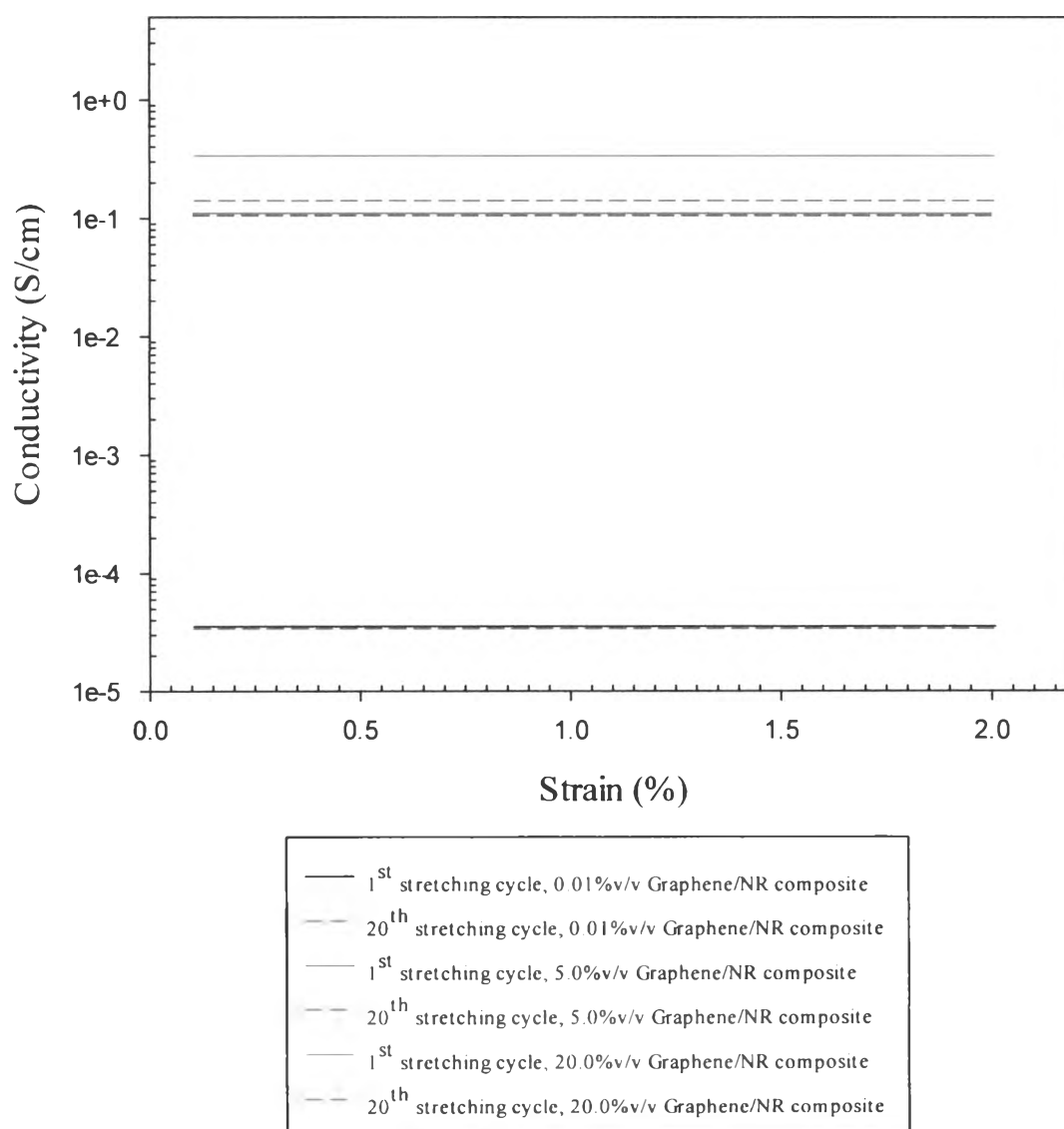


Figure H13 Conductivity of composites as a function of strain as measured by the melt rheometer in the tension mode with a strain rate of 0.01s^{-1} , temperature of 300 K, and applied electric field of 5 volt.

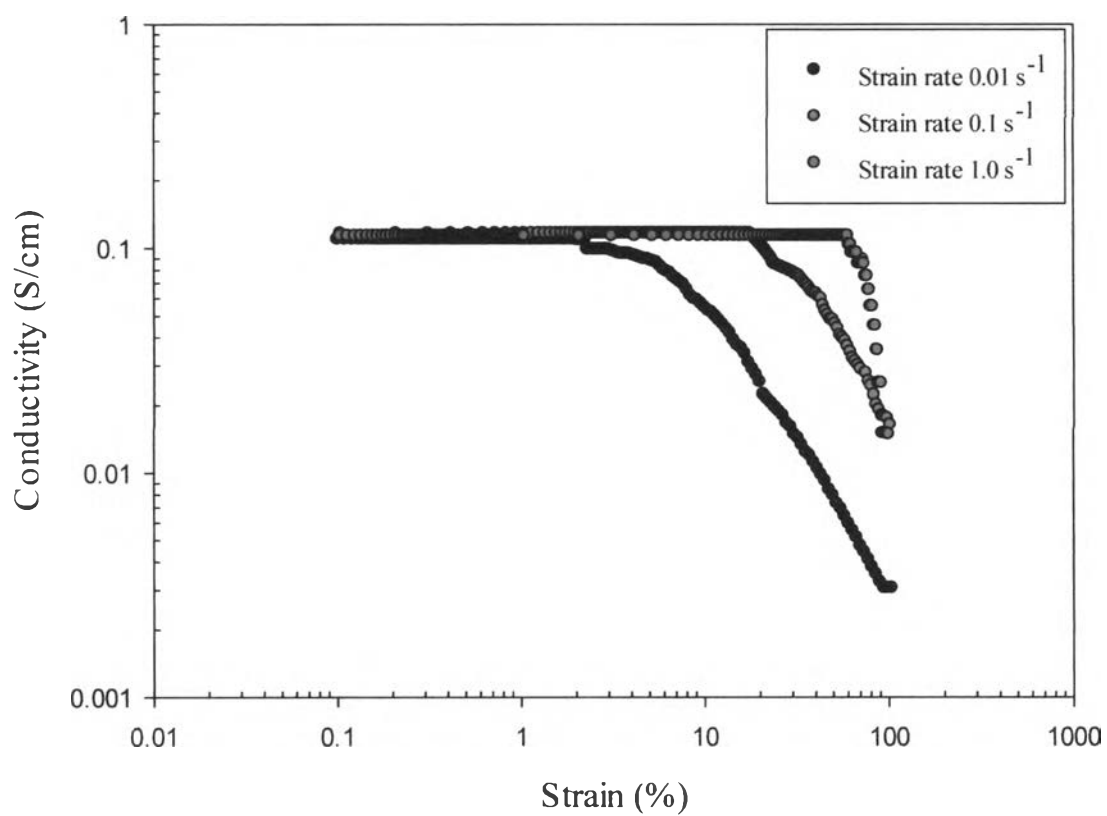


Figure H14 Conductivity of 5 %v/v graphene/NR composites as a function of strain rate as measured by the melt rheometer in the tension mode with a strain rate of 0.01s⁻¹, temperature of 300 K, and applied electric field of 5 volt.

Supplementary data of trial experiment

Composite data with fixed concentration of surfactant

Table 1 Preparation conditions of graphene/NR composites

| Graphene content (%v/v) | TWEEN80 (surfactant) (%v/v) | Natural rubber latex (ml) | Water (ml) | TWEEN80/graphene volume ratio | Remark |
|-------------------------|-----------------------------|---------------------------|------------|-------------------------------|-------------|
| 0.0 | - | 20 | - | - | - |
| 0.01 | 1 | 20 | 20 | 100 | - |
| 0.1 | 1 | 20 | 20 | 10 | - |
| 1.0 | 1 | 20 | 20 | 1 | - |
| 5.0 | 1 | 20 | 20 | 0.2 | - |
| 10.0 | 1 | 20 | 20 | 0.1 | Agglomerate |
| 20.0 | 1 | 20 | 20 | 0.05 | Agglomerate |

*Crosslink under UV irradiation time of 7 minute and crosslink concentration of 5.0

%v/v

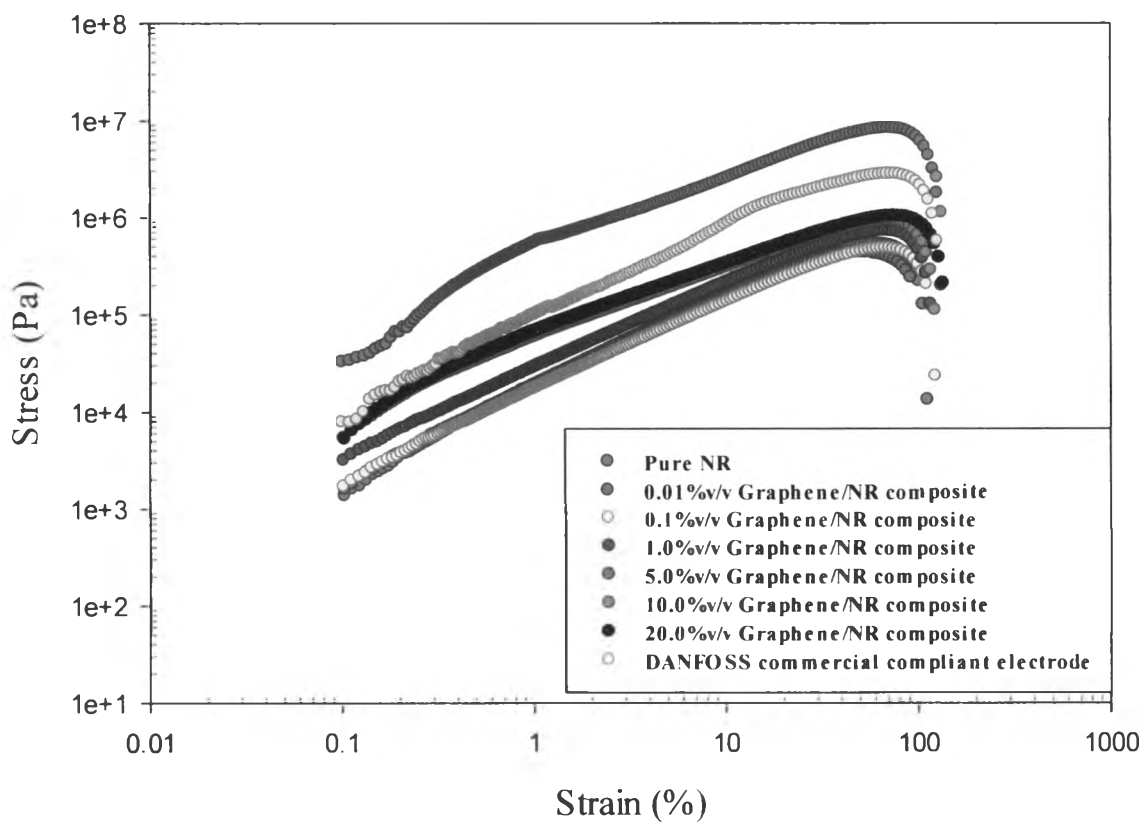


Figure 1 Stress-strain curve of graphene/NR composites at various concentrations of the graphene multilayers as measured by the melt rheometer in the tension mode with a strain rate of 0.01s^{-1} , temperature of 300 K, and applied electric field of 5 volt.

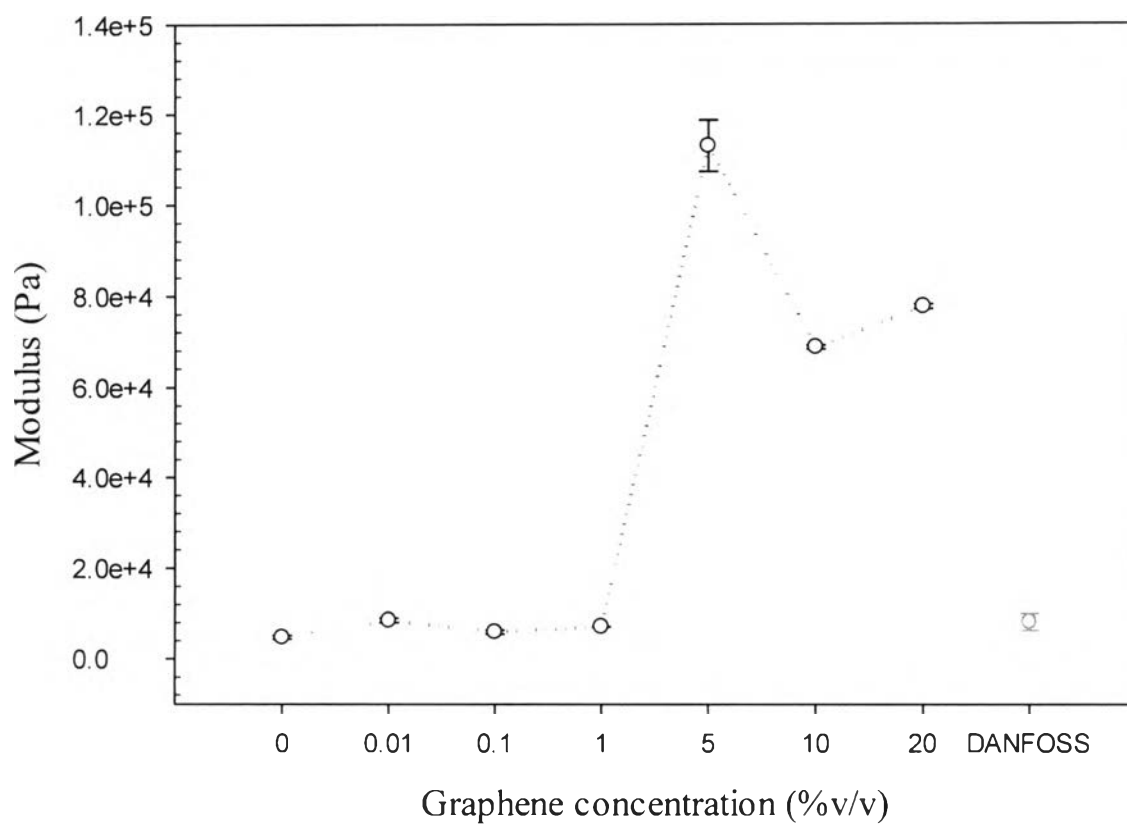


Figure 2 Modulus of graphene/NR composites at various concentrations of the graphene multilayers as measured by the melt rheometer in the tension mode with a strain rate of 0.01 s^{-1} , temperature of 300 K, and applied electric field of 5 volt.

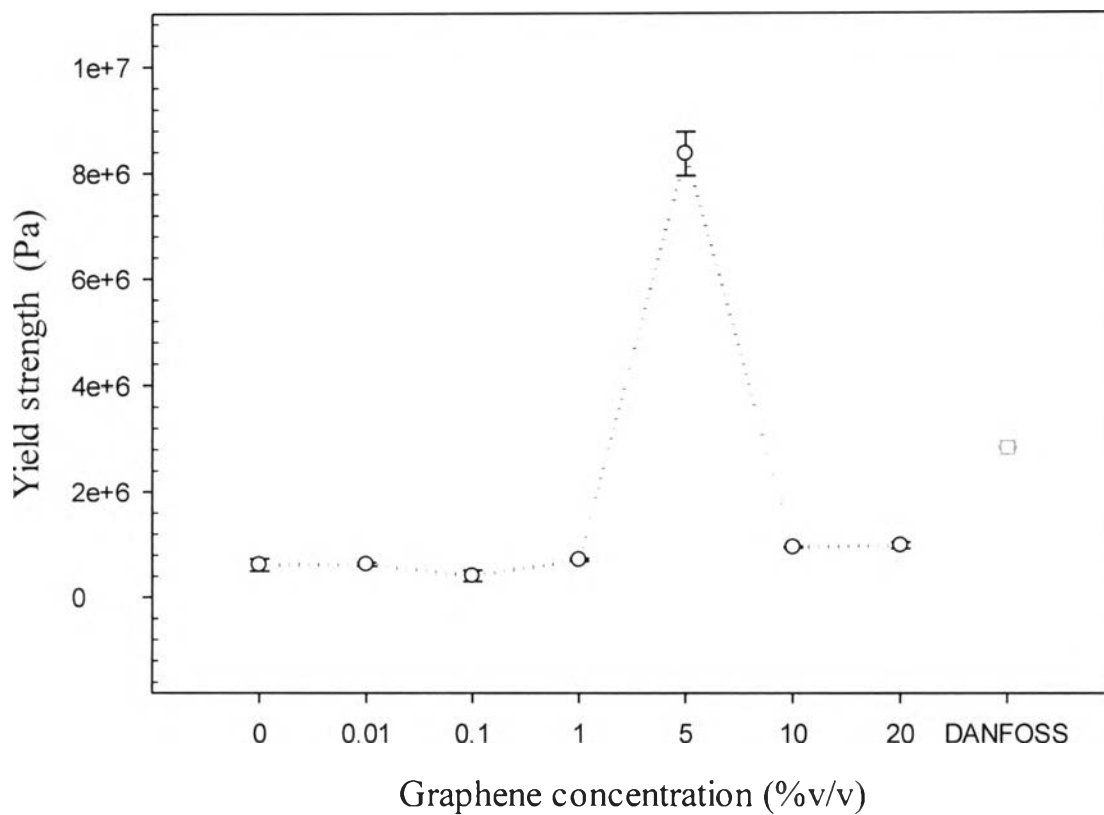


Figure 3 Yield strength of graphene/NR composites at various concentrations of the graphene multilayers measured by the melt rheometer in the tension mode with a strain rate of 0.01 s^{-1} , temperature of 300 K, and applied electric field of 5 volt.

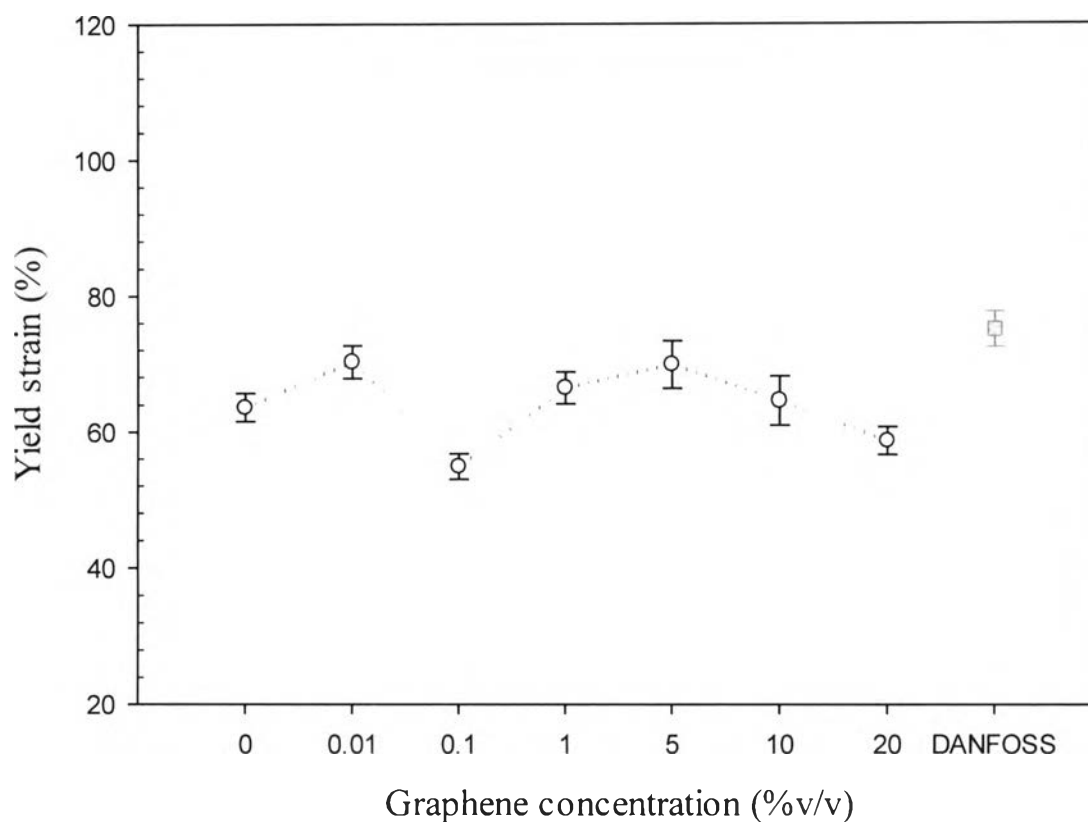


Figure 4 Yield strain of graphene/NR composites at various concentrations of the graphene multilayers as measured by the melt rheometer in the tension mode with a strain rate of 0.01 s^{-1} , temperature of 300 K, and applied electric field of 5 volt.

Table 2 Mechanical properties of graphene/NR composites at various concentrations of the graphene multilayers measured by the melt rheometer in the tension mode with a strain rate of 0.01 s^{-1} , temperature of 300 K, and applied electric field of 5 volt

| Graphene concentration (%v/v) | Yield strength (Pa) | Yield strain (%) | Modulus (Pa) |
|-------------------------------|-------------------------------------|------------------|------------------------------|
| 0.0 | $6.14\text{E}+5 \pm 1.18\text{E}+5$ | 63.60 ± 2.04 | $4.75\text{E}+4 \pm 399.45$ |
| 0.01 | $6.26\text{E}+5 \pm 3.28\text{E}+4$ | 70.23 ± 2.42 | $8.48\text{E}+3 \pm 497.65$ |
| 0.1 | $4.07\text{E}+5 \pm 1.04\text{E}+5$ | 54.87 ± 1.88 | $5.95\text{E}+3 \pm 401.56$ |
| 1.0 | $7.11\text{E}+5 \pm 2.76\text{E}+4$ | 66.46 ± 2.29 | $7.12\text{E}+3 \pm 32.10$ |
| 5.0 | $8.36\text{E}+6 \pm 4.18\text{E}+5$ | 69.86 ± 3.49 | $1.13\text{E}+5 \pm 5670.71$ |
| 10.0 | $9.52\text{E}+5 \pm 1.29\text{E}+4$ | 64.56 ± 3.58 | $6.88\text{E}+4 \pm 437.64$ |
| 20.0 | $9.88\text{E}+5 \pm 5.74\text{E}+3$ | 58.67 ± 2.06 | $7.77\text{E}+4 \pm 546.60$ |
| DANFOSS | $2.84\text{E}+6 \pm 1.78\text{E}+4$ | 75.12 ± 2.60 | $8.15\text{E}+3 \pm 1893.50$ |

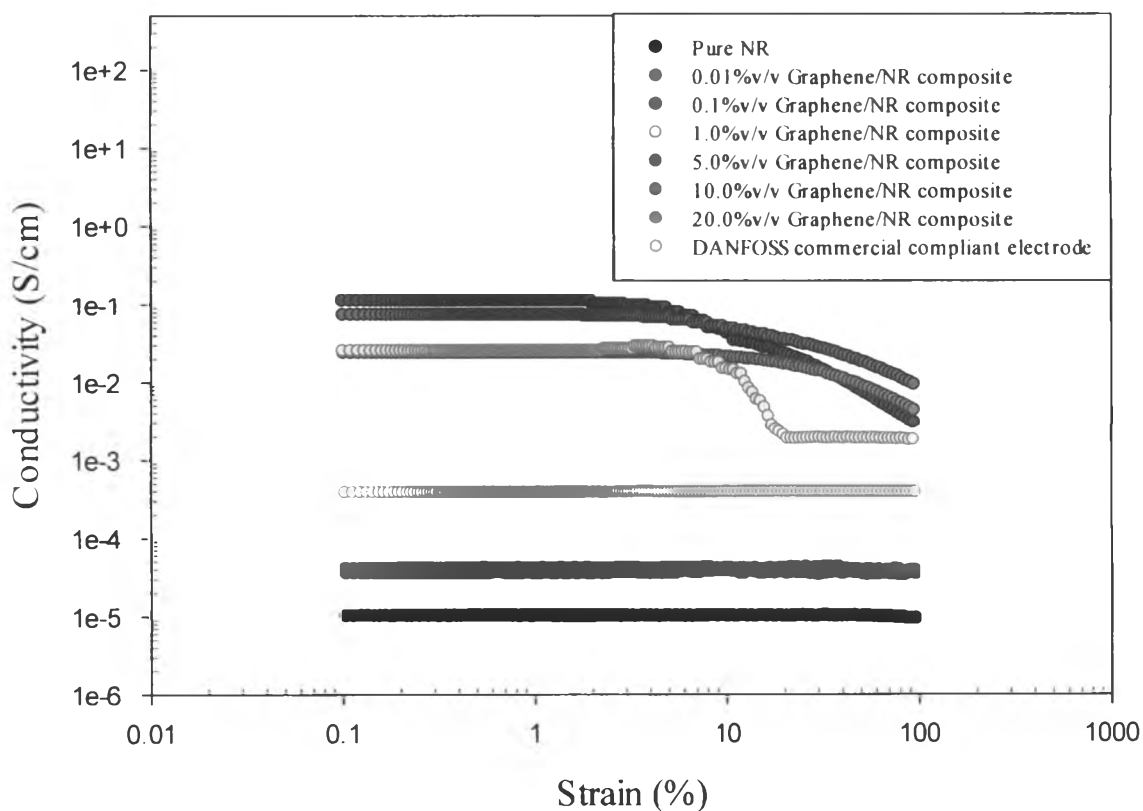


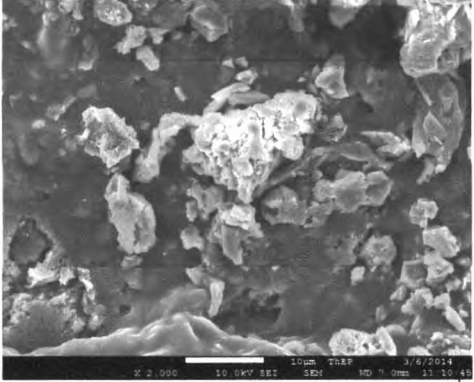
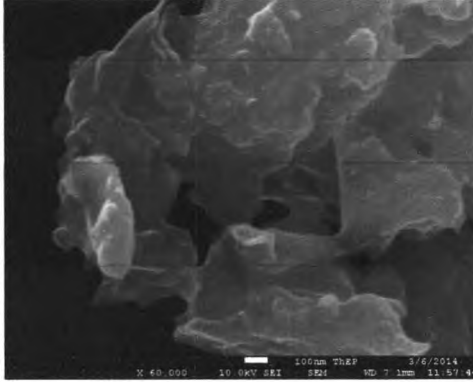
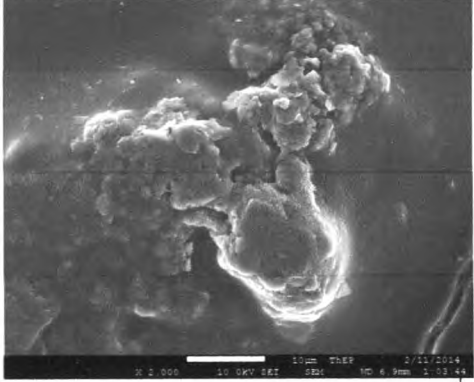
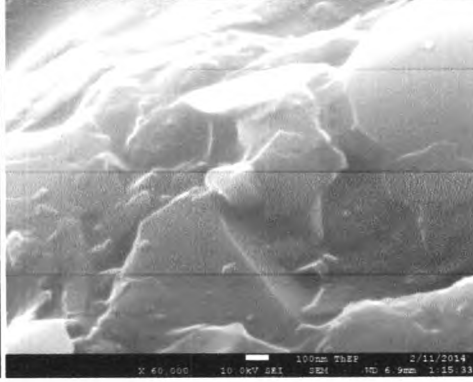
Figure 5 Conductivity of graphene/NR composites at various concentrations of the graphene multilayers as measured by the melt rheometer in the tension mode with a strain rate of 0.01 s^{-1} , temperature of 300 K, and applied electric field of 5 volt.

Table 3 Electrical conductivity of graphene/NR composites at various concentrations of the graphene multilayers as measured by the melt rheometer in the tension mode with a strain rate of 0.01 s^{-1} , temperature of 300 K, and applied electric field of 5 volt

| Graphene concentration (%v/v) | Conductivity before stretching (S/cm) | Critical strain* (%) |
|----------------------------------|--|----------------------|
| 0.0 | $1.41\text{E-}5 \pm 5.47\text{E-}6$ | > 100 |
| 0.01 | $3.55\text{E-}5 \pm 1.77\text{E-}6$ | > 100 |
| 0.1 | $4.05\text{E-}5 \pm 2.03\text{E-}6$ | > 100 |
| 1.0 | $3.84\text{E-}4 \pm 2.23\text{E-}4$ | > 100 |
| 5.0 | $1.10\text{E-}1 \pm 5.50\text{E-}3$ | 2.01 ± 0.11 |
| 10.0 | $7.28\text{E-}2 \pm 5.07\text{E-}2$ | 3.75 ± 0.94 |
| 20.0 | $2.34\text{E-}2 \pm 1.90\text{E-}2$ | 6.20 ± 0.43 |
| DANFOSS | $2.54\text{E-}2 \pm 1.27\text{E-}3$ | 6.45 ± 0.32 |

* Critical strain refers to 5% conductivity drop. Beyond this critical strain point, the material's behavior is non-linear and the conductivity declines.

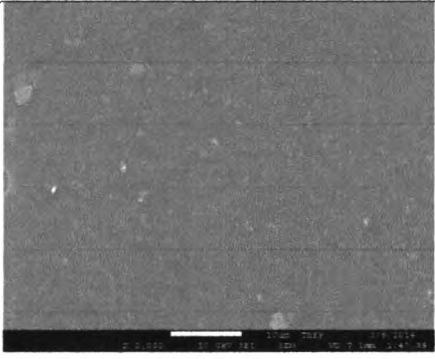
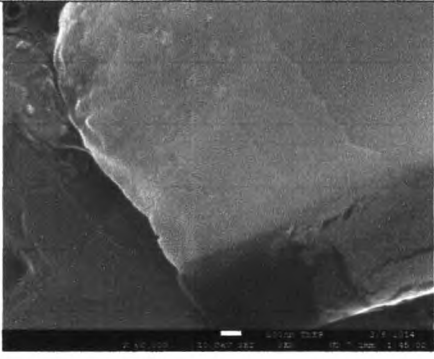
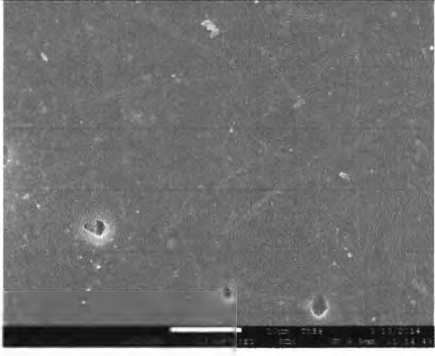
Table 4 SEM images of composites at 10.0 %v/v and 20.0 %v/v graphene concentration with magnifications of 2 kX and 60 kX

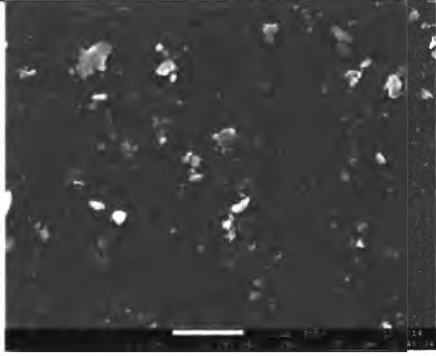
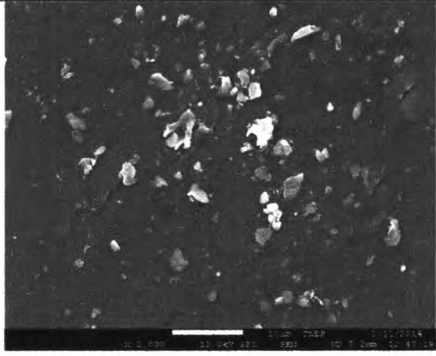
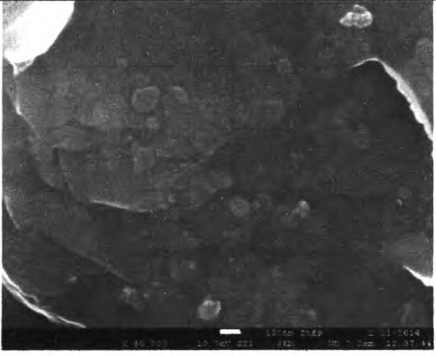
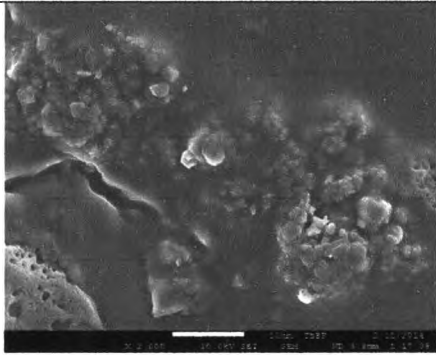
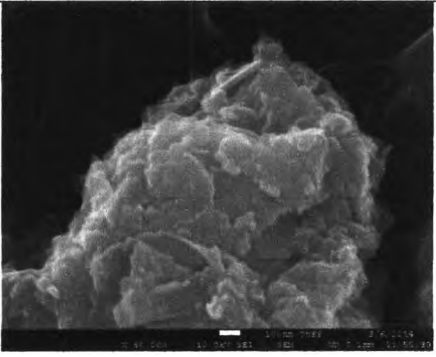
| Composites | Magnification | |
|---------------------------------------|---|--|
| | 2 kX | 60 kX |
| 10.0 %v/v graphene/NR composite |  |  |
| 20.0 %v/v graphene/NR composite |  |  |

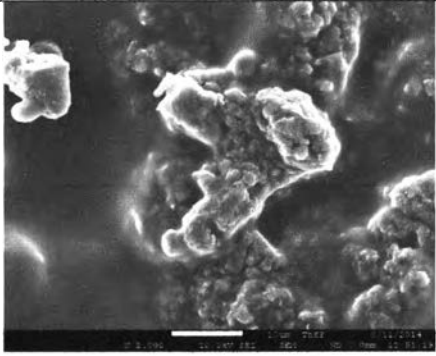
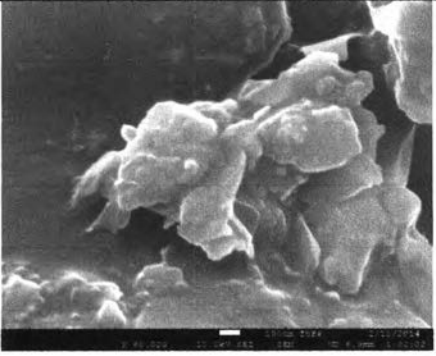
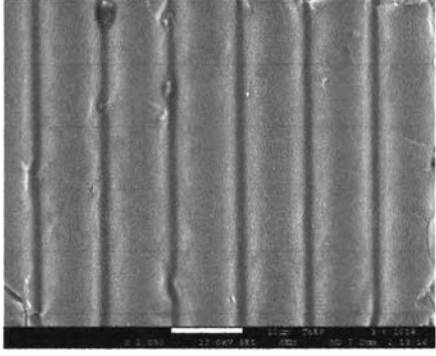
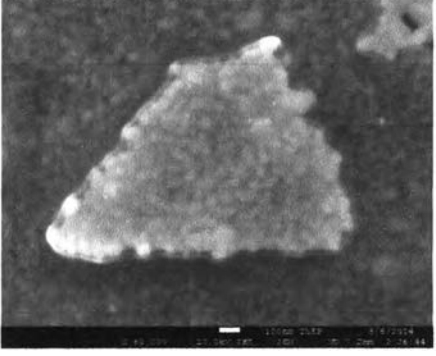
Appendix I FE-SEM Images of The Graphene/NR Composite Film

A field-emission scanning electron microscope (FE-SEM, JSM-7001F) was used to examine the morphological structure and to determine the dispersion of the graphene in the NR matrix. The film was placed on the holder with an adhesive tape and coated with a thin layer of gold using an ion sputtering device for 100 sec prior to observation under FE-SEM. The scanning electron images were investigated by using an acceleration voltage of 20 kV with a magnification in the range of 2k and 60k times.

Table II Summary of FE-SEM images of the graphene/NR composites and DANFOSS commercial compliant electrode at magnifications of 2 kX and 60 kX.

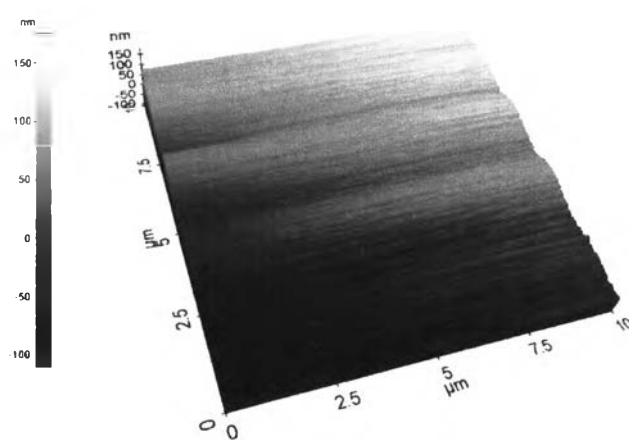
| Composites | Magnification | |
|---------------------------------------|---|--|
| | 2 kX | 60 kX |
| 0.01 %v/v graphene/NR composite |  |  |
| 0.1 %v/v graphene/NR composite |  |  |

| Composites | Magnification | |
|---------------------------------------|---|--|
| | 2 kX | 60 kX |
| 1.0 %v/v graphene/NR composite |  |  |
| 5.0%v/v graphene/NR composite |  |  |
| 10.0 %v/v graphene/NR composite |  |  |

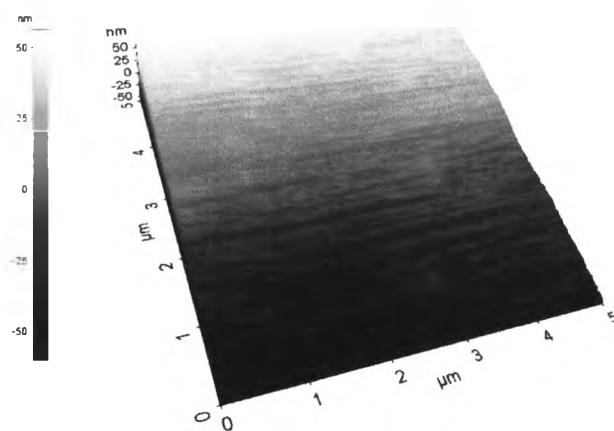
| Composites | Magnification | |
|---|--|---|
| | 2 kX | 60 kX |
| 20.0 %v/v graphene/NR composite |  |  |
| DANFOSS commercial compliant electrode |  |  |

Appendix J AFM Images of The Graphene/NR Composite Film

The topology of the composite was obtained by using the atomic force microscope (AFM, Park System, XE-100) in air under ambient conditions. For the conventional AFM, the non-contact mode was operated with the cantilever (NSC36) tapping at scan rate of 0.5 Hz and applied Z-servo gain of 10. The micro-scale dispersion of graphene in the NR matrix can be observed from the topology.

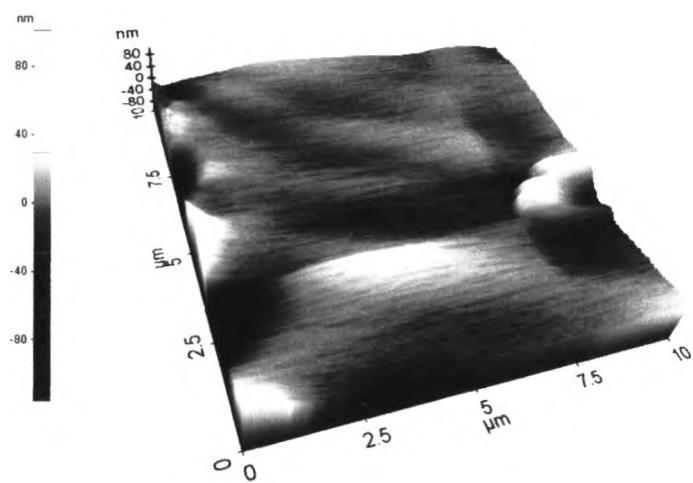


(a)

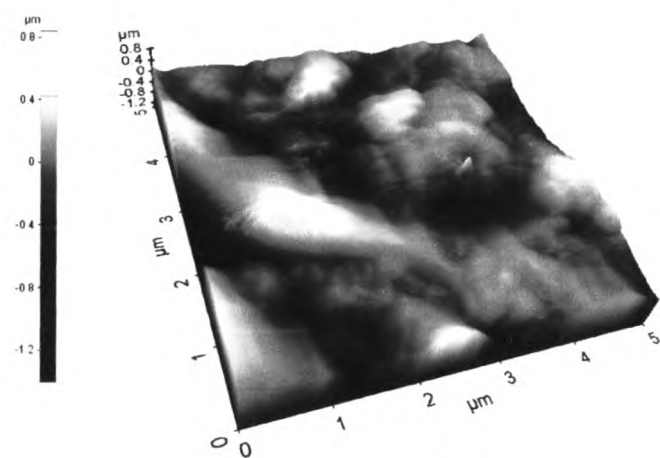


(b)

Figure J1 AFM image of pure natural rubber with scanned area of: (a) $10 \mu\text{m}^2$; (b) $5 \mu\text{m}^2$.

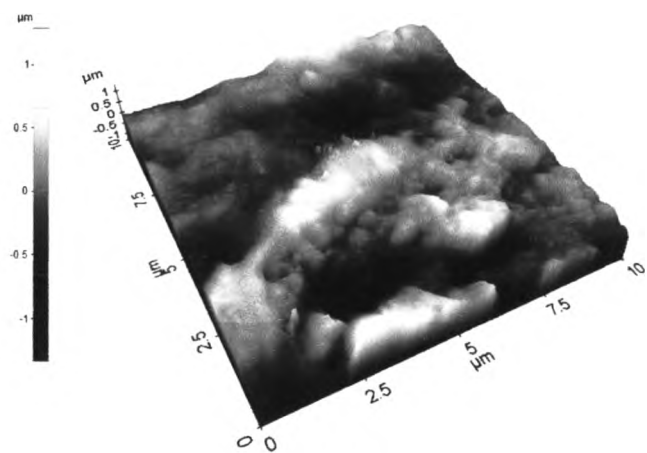


(a)

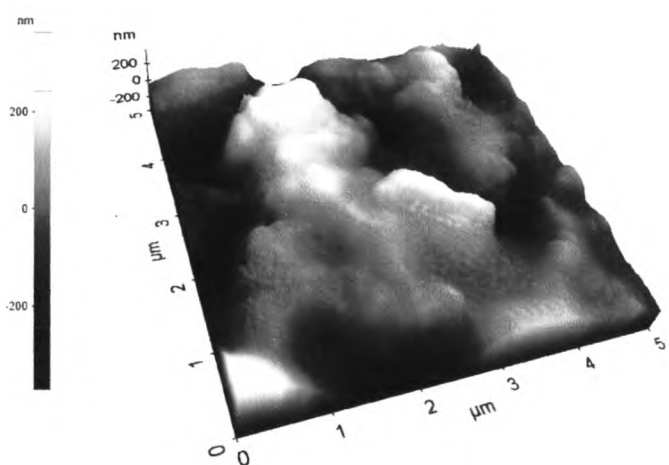


(b)

Figure J2 AFM image of 1.0%v/v graphene/NR composite with scanned area of: (a) 10 μm^2 ; (b) 5 μm^2 .

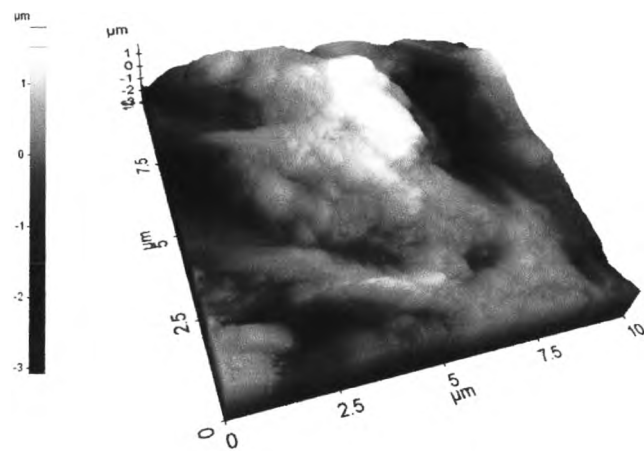


(a)

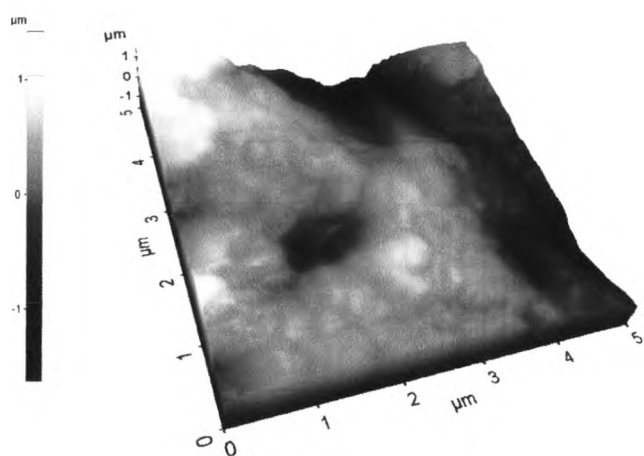


(b)

Figure J3 AFM image of 5.0%v/v graphene/NR composite with scanned area of: (a) $10 \mu\text{m}^2$; (b) $5 \mu\text{m}^2$.

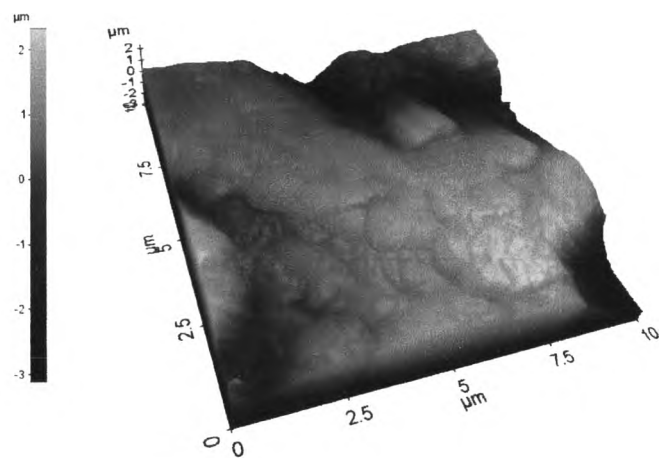


(a)

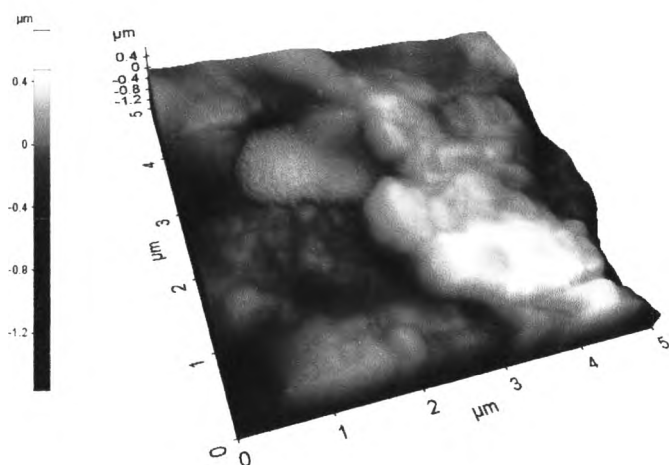


(b)

Figure J4 AFM image of 10.0%v/v graphene/NR composite with scanned area of: (a) $10 \mu\text{m}^2$; (b) $5 \mu\text{m}^2$.

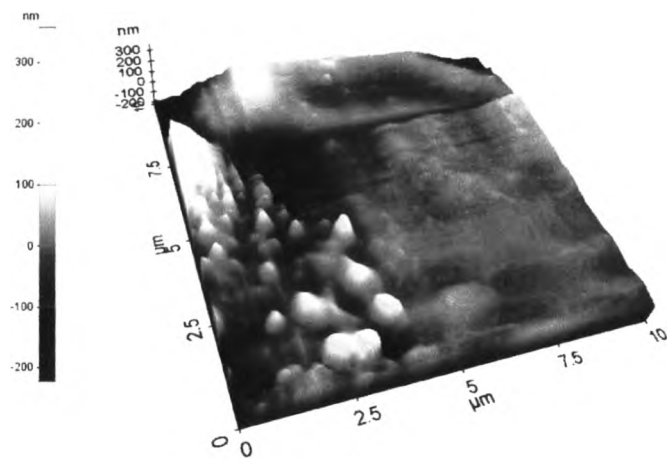


(a)

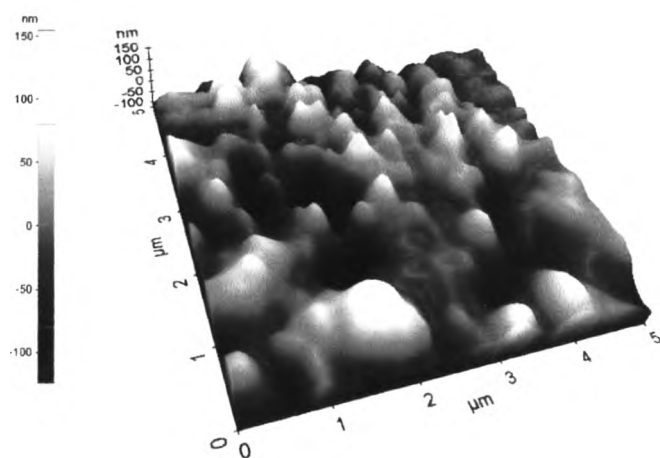


(b)

Figure J5 AFM image of 20.0%v/v graphene/NR composite with scanned area of: (a) $10 \mu\text{m}^2$; (b) $5 \mu\text{m}^2$.



(a)



(b)

Figure J6 AFM image of DANFOSS commercial compliant electrode with scanned area of: (a) $10 \mu\text{m}^2$; (b) $5 \mu\text{m}^2$.

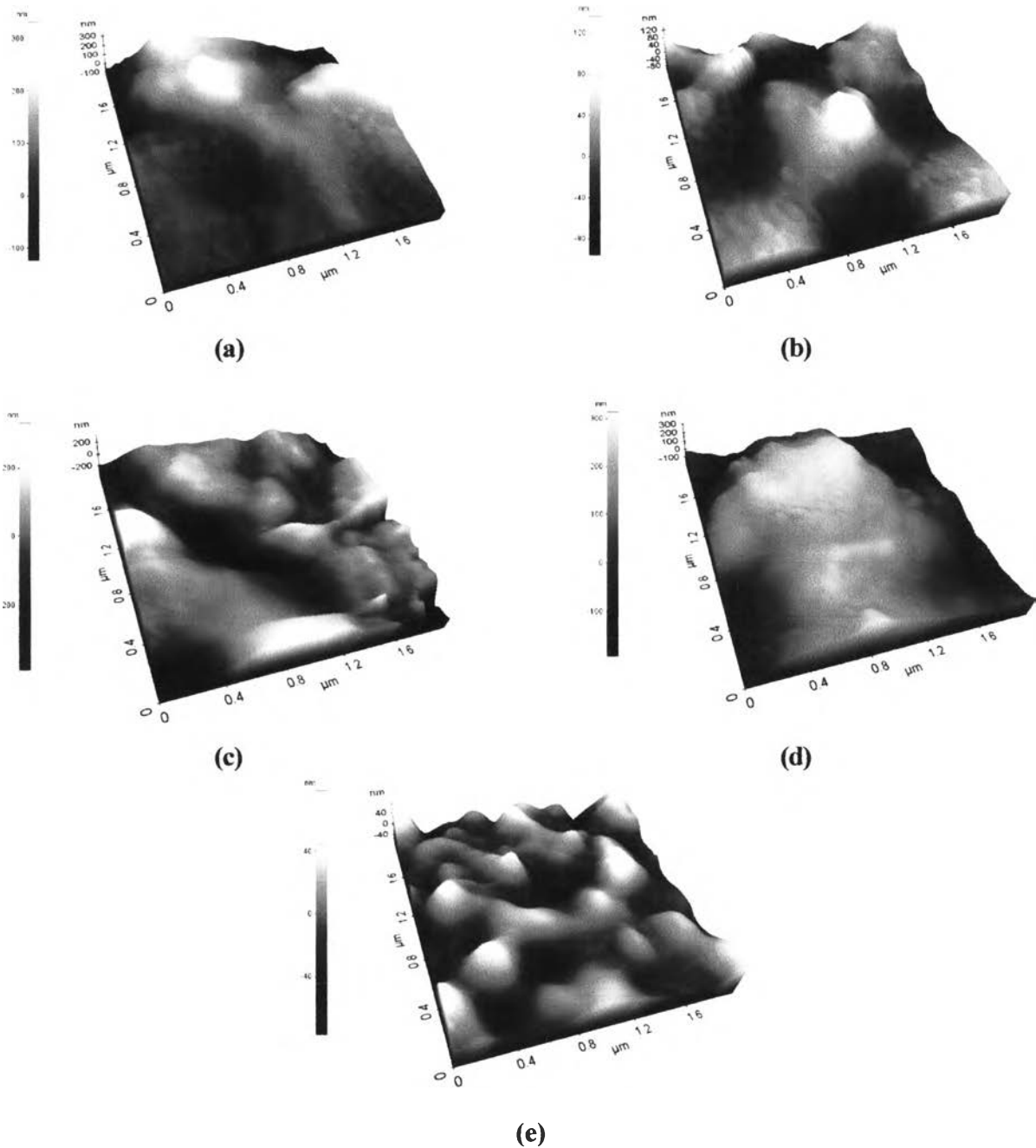


Figure J7 Distribution in micro-scale of composite in the area of $2 \mu\text{m}^2$: (a) 1.0%v/v graphene/NR composite; (b) 5.0%v/v graphene/NR composite; (c) 10.0%v/v graphene/NR composite; (d) 20.0%v/v graphene/NR composite; and (e) DANFOSS commercial compliant electrode.

Appendix K Electrical Conductivity Measurement of The Graphene Multilayers

An electrometer (Keithley, 6517A), with a custom-built two-point probe, was used to measure the electrical conductivity which is the inversion of specific resistivity (ρ) that indicates the ability of material to transport electrical charge. The meter consisted of a probe making contact on the surface of the sample in a disc shape. This probe was connected to a power supplier source for a constant source and for reading current. The applied voltage was plotted versus the resultant current to determine the linear Ohmic regime of each sample based on the Van der Pauw method. The applied voltage and the current in the linear Ohmic regime were converted to the electrical conductivity of the sample using equation (K1) as follow:

$$\sigma = \frac{1}{\rho} = \frac{1}{R_s \times t} = \frac{I}{K \times V \times t} = \frac{\text{slope}}{K \times t} \quad (\text{K1})$$

where σ is the specific conductivity (S/cm), ρ is the specific resistivity ($\Omega \cdot \text{cm}$), R_s is the sheet resistivity (Ω), I is the resultant current (A), K is the geometric correction factor, V is the applied voltage (V), and t is the thickness of the disc sample (cm).

The geometrical correction factor was taken into account of geometric effects, depending on the configuration and probe tip spacing and was determined by using standard materials where specific resistivity values were known; we used silicon wafer chips (SiO_2). In our case, the sheet resistivity was measured by using the two-point probe and then the geometric correction factor was calculated by equation (K2) as follow:

$$K = \frac{\rho}{R \times t} = \frac{I \times \rho}{V \times t} = \text{slope} \times R_s \quad (\text{K2})$$

where K is the geometric correction factor ($2.147\text{E}-03$), ρ is the known resistivity of standard silicon wafer ($\Omega \cdot \text{cm}$), t is the film thickness (cm), R is the film resistance (Ω), and I is the resultant current (A).

Table K1 Summary of the specific conductivities of the raw graphite, and graphene multilayers

| Sample | Specific conductivity (S/cm) | |
|---|------------------------------|-------|
| | Average | SD |
| Raw graphite | 675.59 | 64.76 |
| Commercial graphene multilayers grade C (XG [®] science) | 283.69 | 68.49 |

Table K2 Raw data for determination of specific conductivities of the raw graphite

| Sample | Thickness (cm) | I/V | Specific conductivity (S/cm) |
|--------|----------------|-------|------------------------------|
| No.1 | 0.1479 | 0.236 | 743.21 |
| No.2 | 0.1649 | 0.237 | 669.42 |
| No.3 | 0.1805 | 0.238 | 614.14 |

Table K3 Raw data for determination of specific conductivities of the commercial graphene multilayers grade C (XG[®] science)

| Sample | Thickness (cm) | I/V | Specific conductivity (S/cm) |
|--------|----------------|-------|------------------------------|
| No.1 | 0.2024 | 0.111 | 255.44 |
| No.2 | 0.1960 | 0.099 | 235.26 |
| No.3 | 0.1739 | 0.124 | 332.12 |

Appendix L Synthesized Graphene

L1 Experimental

L1.1 Preparation of Graphene Filler from Graphite Powder

(Hummers *et al.*, 1958, Krishnamoorthy *et al.*, 2013, Su *et al.*, 2013)

L1.1.1 Preparation of graphite oxide by the modified Hummers method

2 g of graphite powder was mixed with 35 mL concentrate H_2SO_4 and stirred in an ice bath for 2 hour. KMnO_4 6 g was gradually added into the mixture within 1 h (to keep the temperature of mixture not exceeding 20 °C) and the mixture was kept stirred for 1 hour. After 30 min, temperature of mixture was heated up to 35°C within 30 min and then stirring was kept at 35 °C for 2 h. During heating up of the mixture, 90 mL deionize water (DI) was slowly added and external heat was introduced to maintain the reaction temperature at 98 °C for 30 min. Termination of the oxidation reaction and reduction of residual KMnO_4 and manganese dioxide was carried out by adding 150 mL DI water and 10 mL of 30% H_2O_2 solution. The mixture was filtered while still hot to avoid precipitation of the slightly soluble salt of mellitic acid formed as a side reaction. The resultant solid product was repeatedly washed with 5% HCl solution after that wash with DI water until pH ~6 and then dried at 80 °C 24 hour.

L1.1.2 Preparation of Graphene from Graphite Oxide

0.2 g of graphite oxide was dispersed in DI water 200 ml. Sonicate with ultrasonicater for 30 minute to obtain graphene oxide. After that, 0.2 g of graphene oxide was dispersed in DI water 200 ml and pH was adjusted to 10 by NaOH solution. Adding 2 mL of hydrazine hydrate and the mixture was sonicated for 1 hour. Ultrasound irradiation was performed for 2 hour without cooling (temperature $\approx 60 \pm 5$ °C). The obtained Graphene nanosheets was washed thoroughly with distilled water and

centrifuged at 12000 rpm for 10 min in order to remove the residuals and dry in hot air oven.

L2 Characterizations

L2.1 Raman Spectrometer (NT-MDT, NTEGRA Spectra)

Raman spectroscopy was used to verify graphite and graphene due to the ability to identify and characterize all the members of the carbon family. The characterizations were nondestructive, fast, with high resolution and give the maximum structural and electronic information. The indications of graphite raw material and synthesized graphene were measured by the Raman spectroscopy (NT-MDT, NTEGRA Spectra) with 632.8 nm excitation laser, objective lens 100x and accumulate time 60s from National Nanotechnology Center.

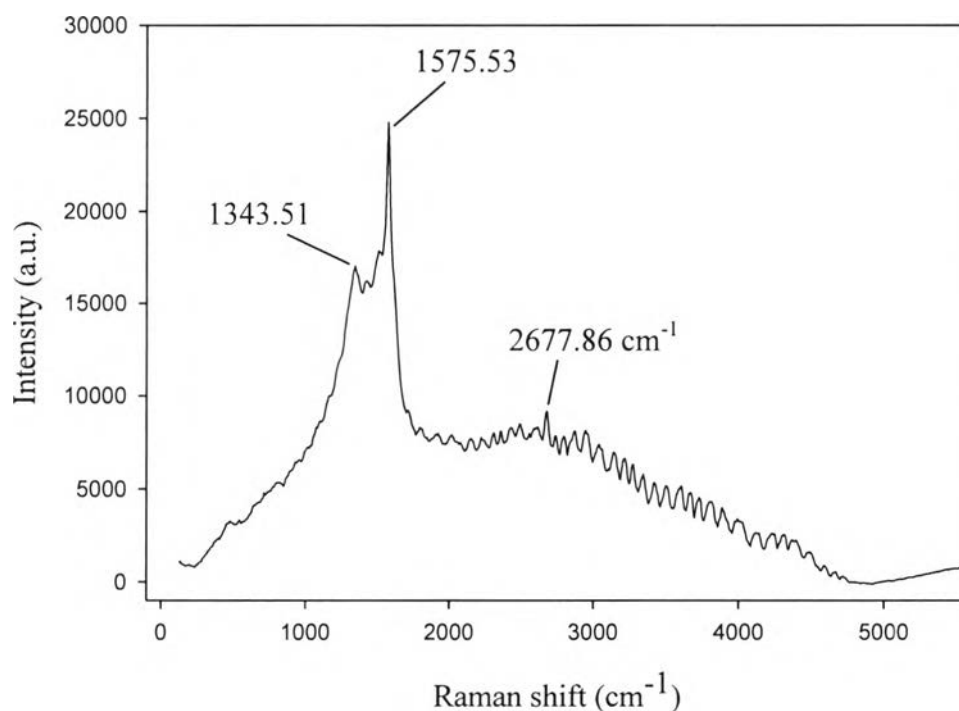


Figure L1 Raman spectrum of the synthesized graphene.

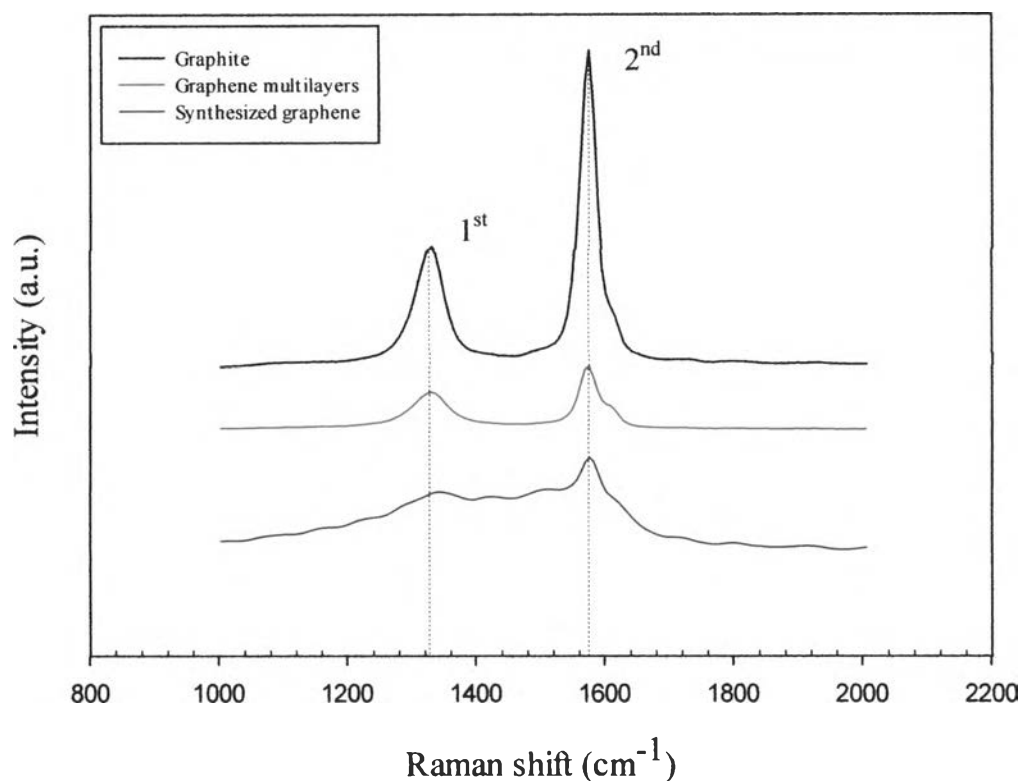


Figure L2 Raman spectra of raw graphite, commercial graphene multilayers and synthesized graphene.

Table L1 Raman shift position of Raman spectra

| sample | Raman shift position (cm^{-1}) | |
|---|---|-----------------|
| | 1 st | 2 nd |
| Raw graphite | 1329.622 | 1575.529 |
| Commercial graphene multilayers grade C (XG [®] science) | 1343.506 | 1575.529 |
| Synthesized graphene | 1329.622 | 1575.529 |

L2.2 X-ray Diffraction Spectrometer, XRD (Rigaku, DMAX 2200)

The wide angle X-ray diffraction microscope (XRD) was used to study the crystal structure below the nanometer scale. The CuK-alpha radiation source was operated at 40 kV/30 mA. K-beta filter was used to eliminate interference peak. Divergence slit and scattering slit 0.5 deg together with 0.3 mm of receiving slit were set on the instrument. The graphene powder was placed into a sample holder and the measurement was continuously run. The experiments were recorded by monitoring the diffraction appearing in the diffraction angle (2θ) range from 10 to 80 with a scan speed 5 deg/min and a scan step 0.02 deg.

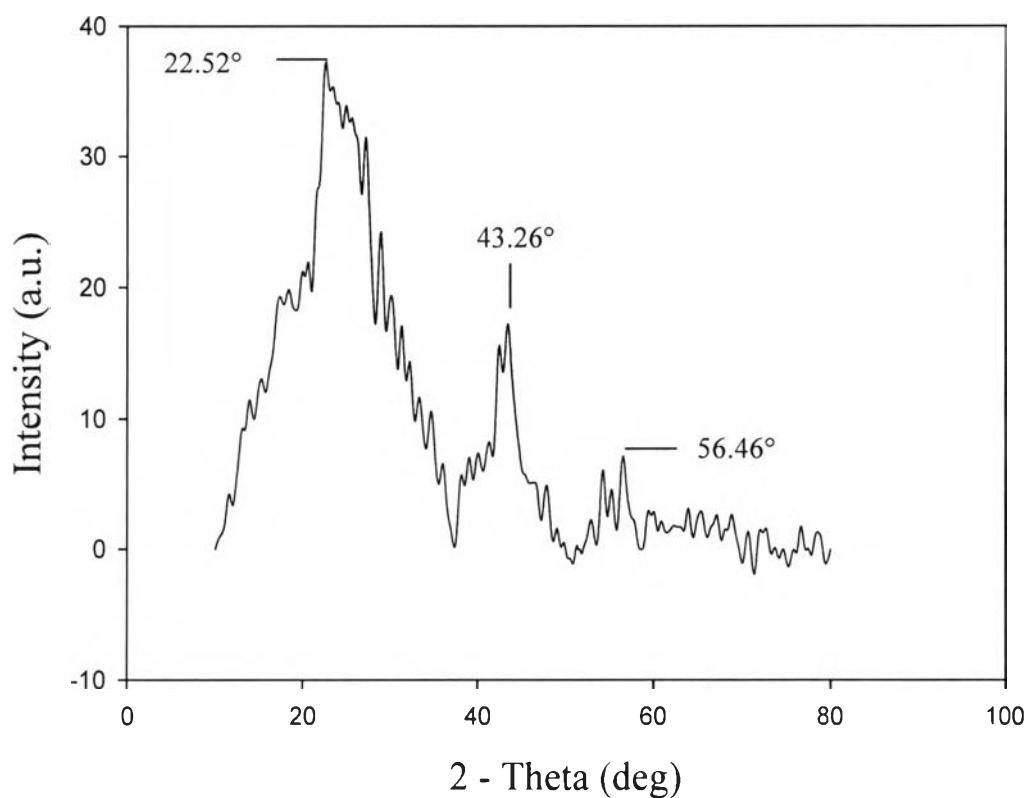


Figure L3 XRD pattern of the synthesized graphite oxide.

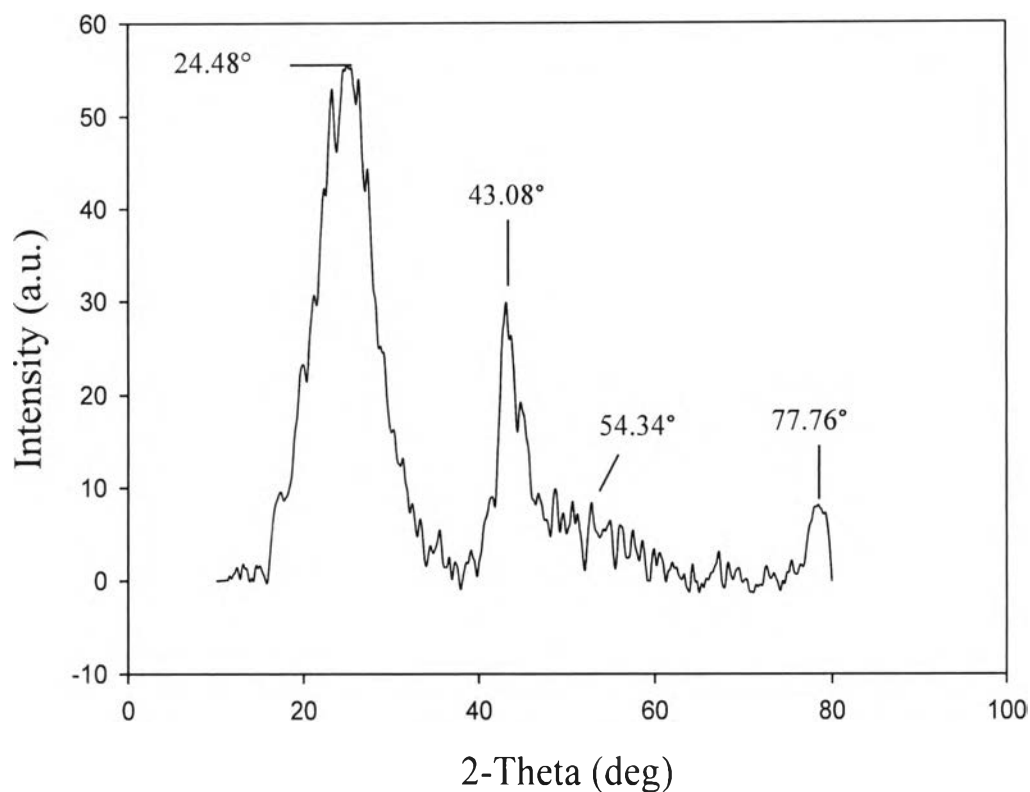


Figure L4 XRD pattern of the synthesized graphene.

Table L2 Strong peak position 2θ (deg) of synthesized graphene

| sample | Peak position 2θ (deg) | | | |
|---|-------------------------------|-----------------|-----------------|-----------------|
| | 1 st | 2 nd | 3 rd | 4 th |
| Raw graphite | 26.84 | 54.86 | - | - |
| Commercial graphene multilayers grade C (XG [®] science) | 26.44 | 43.33 | 54.38 | 77.29 |
| Synthesized graphite oxide | 22.52 | 43.26 | 56.46 | - |
| Synthesized graphene | 24.48 | 43.08 | 54.34 | 77.76 |

L2.3 Two – point probe Technique

An electrometer (Keithley, 6517A), with a custom-built two-point probe, was used to measure the electrical conductivity which is the inversion of specific resistivity (ρ) that indicates the ability of material to transport electrical charge. The meter consisted of a probe making contact on the surface of the sample in a disc shape. This probe was connected to a power supplier source for a constant source and for reading current. The applied voltage was plotted versus the resultant current to determine the linear Ohmic regime of each sample based on the Van der Pauw method. The applied voltage and the current in the linear Ohmic regime were converted to the electrical conductivity of the sample using equation (L1) as follow:

$$\sigma = \frac{1}{\rho} = \frac{1}{R_s \times t} = \frac{I}{K \times V \times t} = \frac{\text{slope}}{K \times t} \quad (\text{L1})$$

where σ is the specific conductivity (S/cm), ρ is the specific resistivity ($\Omega \cdot \text{cm}$), R_s is the sheet resistivity (Ω), I is the resultant current (A), K is the geometric correction factor, V is the applied voltage (V), and t is the thickness of the disc sample (cm).

Table L3 Summary of the specific conductivities of the raw graphite, Graphene multilayers and synthesized graphene

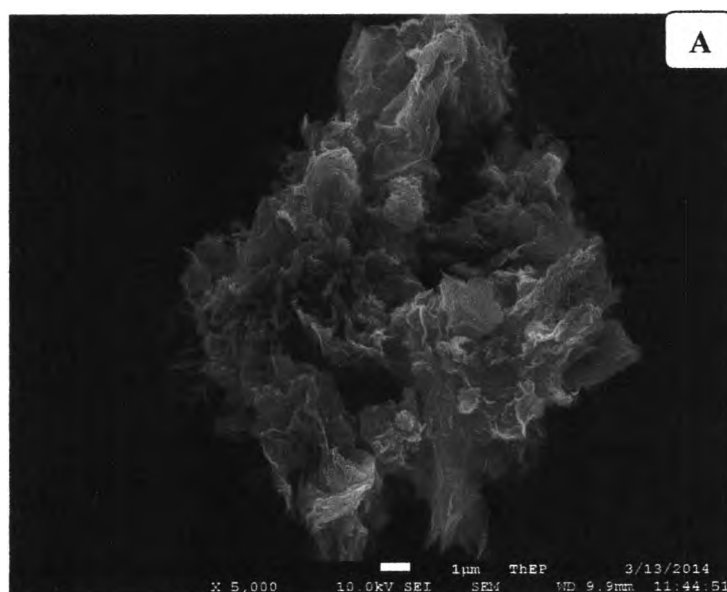
| Sample | Specific conductivity (S/cm) | |
|---|------------------------------|-------|
| | Average | SD |
| Raw graphite | 675.59 | 64.76 |
| Commercial graphene multilayers grade C (XG [®] science) | 283.69 | 68.49 |
| Synthesized graphene | 198.38 | 49.05 |

Table L4 Raw data for determination of specific conductivities of the synthesized graphene

| Sample | Thickness (cm) | I/V | Specific conductivity (S/cm) |
|--------|----------------|-------|------------------------------|
| No.1 | 0.0727 | 0.033 | 251.42 |
| No.2 | 0.0813 | 0.033 | 189.06 |
| No.3 | 0.0783 | 0.026 | 154.66 |

L2.4 SEM Image

A field-emission scanning electron microscope (FE-SEM, JSM-7001F) was used to examine the morphological structure of the synthesized graphene. The graphene powder was placed on the holder with an adhesive tape and coated with a thin layer of gold using an ion sputtering device for 100 sec prior to observation under FE-SEM. The scanning electron images were investigated by using an acceleration voltage of 20 kV with a magnification in the range of 5k and 60k times.



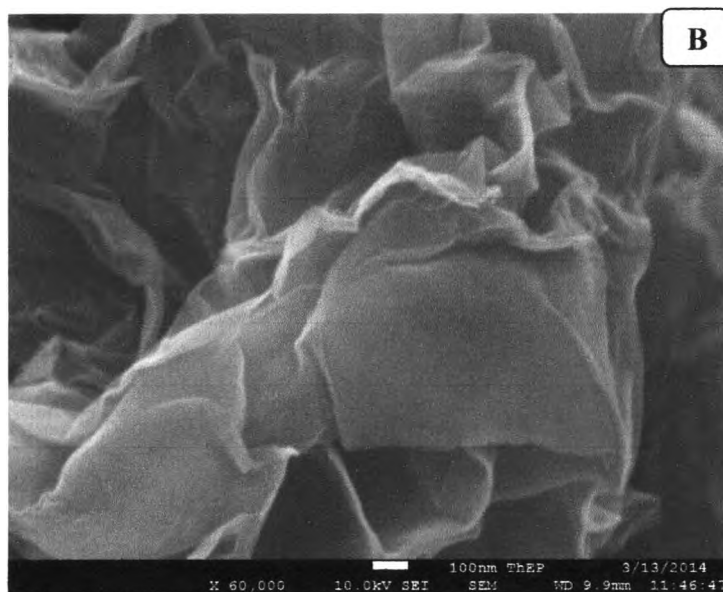


Figure L5 FE-SEM images of the synthesized graphene with magnifications of: a) 5 kX; and (b) 60 kX.

L3 Literature Reviews about the Characterizations of Graphene

L3.1 Raman Spectroscopy

Raman spectrum of graphite exhibits a band at 1580 cm^{-1} named as G band and other band at 1350 cm^{-1} named as D band. The former is due to the first order scattering of E_{2g} mode and latter associates with the defects in the graphite lattice. The Raman spectra of graphite, graphene oxide (GO) and graphene nanosheets are provided in Figure L6. The Raman spectrum of GO possesses the G band at 1595.89 cm^{-1} and D band at 1354 cm^{-1} . The increase in FWHM of the G band in the GO compared with the graphite suggests the presence of sp^3 carbon in GO. The D band in GO is broadened which was due to the reduction in size of in plane sp^2 domains by the creation of defects, vacancies and distortions of the sp^2 domains after complete oxidation. In case of

graphene, the G band is shifted towards lower wave number (1588.41 cm^{-1}) due to the recovery of hexagonal network of carbon atoms with defects.

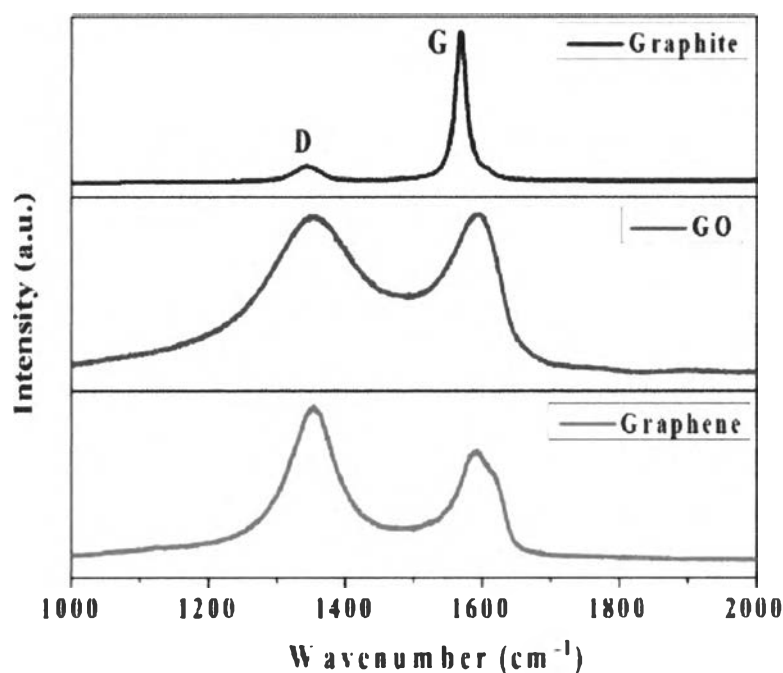


Figure L6 Raman spectra of graphite, GO and graphene nanosheets (Krishnamoorthy K. *et.al.*, 2013).

L3.2 X-ray Diffraction Spectroscopy

Graphene oxide was synthesized from graphite flakes by a modified Hummer's method. Figure L7 shows the XRD patterns of graphite and GO. Pristine graphite flakes exhibit a strong (002) reflection at 26.5° which corresponds to an interlayer distance (dspacing) of 0.34 nm. After oxidation of graphite to GO, the (002) diffraction peak shifts to a lower 2θ angle (10.8°), which corresponds to an interlayer distance of approximately 0.82 nm. This indicates the GO sheets are separated due to the covalently bonded oxygen. Hydrazine has been widely used to reduce GO to graphene and restore the conjugated sp^2 network. The deoxygenated GO by an alkaline hydrothermal process (hGO) was performed at $120\text{ }^\circ\text{C}$. The interlayer distance of the

hydrazine reduced GO (rGO) obtained from (002) reflection of the XRD pattern at 23.6° was 0.37 nm. The decrease in interlayer spacing between individual graphene sheets is attributed to the van der Waals interaction between sp^2 hybridized carbon framework that was restored during the chemical reduction. The XRD pattern of hGO also exhibits a (002) reflection at 23.9° corresponding to the interlayer spacing of 0.37 nm. The broad XRD peak of the hGO suggests these stacked graphene sheets are few layers thick.

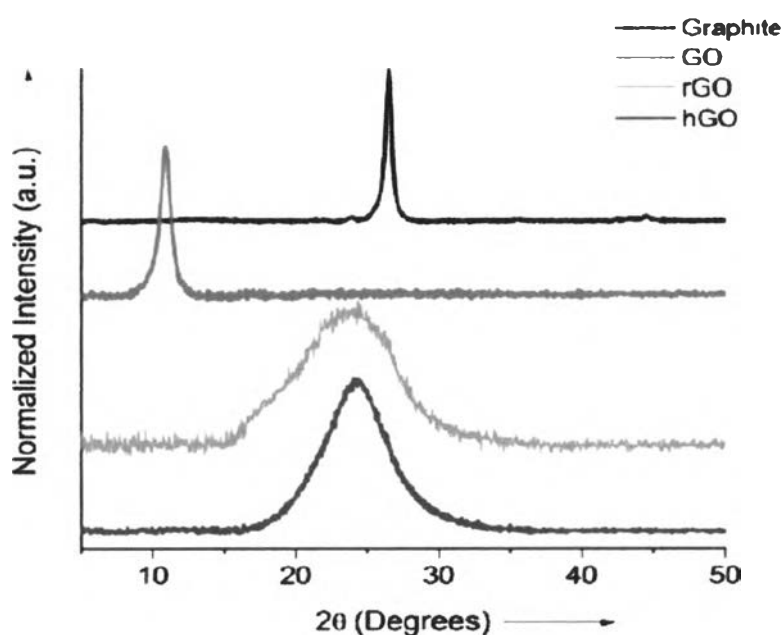


Figure L7 XRD pattern of the synthesized graphene (Sanjaya D.P. *et al.*, 2012).

References

- Hummers, W.S. and Offeman, R.E. (1958). Preparation of graphitic oxide. Journal of the American Chemical Society, 80(6), 1339-1339.
- Krishnamoorthy, K., Kim, G.-S., and Kim, S.J. (2013). Graphene nanosheets: Ultrasound assisted synthesis and characterization. Ultrasonics Sonochemistry, 20(2), 644-649.

An effective green alternative for chemically reduced graphene. Journal of Power Sources, 215, 1-10.

Su, X., Wang, G., Li, W., Bai, J., and Wang, H. (2013). A simple method for preparing graphene nano-sheets at low temperature. Advanced Powder Technology, 24(1), 317-323.

CURRICULUM VITAE

Name: Ms. Sasithorn Korattanawittaya

Date of Birth: June 29, 1989

Nationality: Thai

University Education:

2006–2009 Bachelor Degree in Materials Science and Technology,
Faculty of Science, Prince of Songkla University, Songkhla, Thailand

Proceedings:

1. Korattanawittaya, S.; and Sirivat, A. (2014, April 22). Preparation of Graphenen/Natural Rubber Composite for Compliant Electrode Applications. Proceedings of the 5th Research Symposium on Petrochemical, and Materials Technology and the 20th PPC Symposium on Petroleum, Petrochemicals, and Polymers. Bangkok, Thailand.

Presentation:

1. Korattanawittaya, S.; and Sirivat, A. (2014, April 22). Preparation of Graphenen/Natural Rubber Composite for Compliant Electrode Applications. Poster presented at of the 5th Research Symposium on Petrochemical, and Materials Technology and the 20th PPC Symposium on Petroleum, Petrochemicals, and Polymers. Bangkok, Thailand.